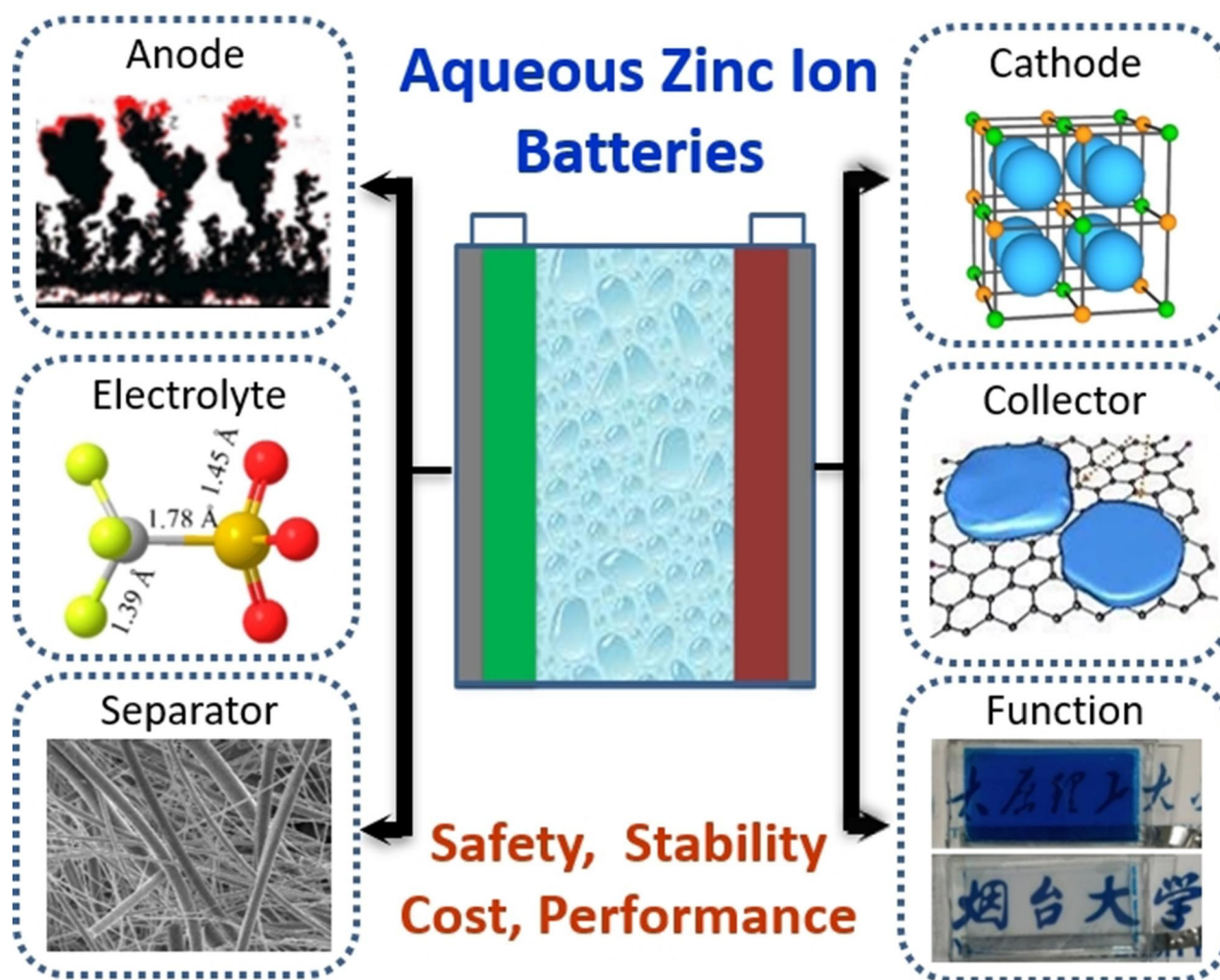


Rechargeable Aqueous Zinc-Ion Batteries with Mild Electrolytes: A Comprehensive Review

Litao Kang⁺, *^[a] Mangwei Cui⁺, ^[b] Zhongtao Zhang, ^[c] and Fuyi Jiang^[a]



Different from the contrary-old alkaline Zn-based batteries, aqueous zinc-ion batteries (ZIBs) refer to a series of safe, long-life and low-cost secondary batteries with divalent Zn^{2+} working as charge carriers. Compared to market dominant lithium ion batteries (LIBs) and Pb-acid batteries, aqueous ZIBs feature a precious balance between safety, cost, lifetime, environmental benignity and energy/power density, due to their unique chemistry. The high performances of these batteries stem from the high-capacities and large redox potential differences of cathodes/anodes, along with the swift redox reactions in the high ionic conductive aqueous electrolytes. With all components being intrinsically safe, stable, low cost and non-corrosive, aqueous ZIBs hold promising prospects in application fields

ranging from large scale energy storage systems to wearable electronics. In this paper, we comprehensively reviewed significant advances in aqueous ZIBs since their innovation in 1986, regarding the Zn^{2+} -storage mechanisms/design of cathodes, side reactions/stabilizing strategies of anodes/electrolytes, and especially the influence/optimization of current collectors and separators. Finally, a conclusion and outlook on current challenges and research trends of ZIBs is provided. This review attempts to present a general picture of the exploration and evolution of aqueous ZIBs, and to provide some guides for the further development of these energetic yet safe energy storage devices.

1. Introduction

With the fast development of portable electronics and electric vehicles, lithium ion batteries (LIBs) have become the most shining star of the battery ball, because of their competitive advantages of high energy density and long lifetime. However, LIBs are still facing some issues regarding fire risk, cost, and environmental concerns, due to the organic electrolyte design and the use of toxic/expensive elements (e.g., F in electrolytes, Li and Co in electrodes).^[1]

Different from LIBs, aqueous rechargeable batteries (ARBs) employed cheap, safe, yet highly ionic conductive aqueous solutions as electrolytes, and therefore are virtually fire risk free. Currently, the market dominant ARBs are Pb-acid batteries, which provide the cheapest energy storage ability among popular batteries and occupy 50% of the global battery market.^[2] Nevertheless, Pb-acid batteries suffer seriously from low energy density ($30\sim40\text{ Wh kg}^{-1}$), short lifetime ($300\sim800$ cycles), and the uneasy concerns on Pb pollution. Therefore, numerous efforts have been made to establish cheap, green, and high-performance ARBs.^[3] Indeed, high-performance ARBs are particularly important for scale energy storage system, where cost and safety are top priorities over energy density.^[4] In addition, ARBs are also potential choices of power sources for wearable electronics, due to their human friendly design and low package requirement.^[5]

In all ARBs, Zn aqueous rechargeable batteries (Zn-ARBs) attract considerable attentions due to their unique

advantages.^[6,7] Firstly, Zn is a cost efficient (the second cheapest metal, USD \$2 kg⁻¹)^[8] non-toxic^[9] metal anodes (negative electrodes) with large electric conductivity^[10] and high theoretical capacity (819 mAh g^{-1})^[11]. Secondly, Zn metal anodes show a desirable balance between low redox potential (-0.76 V vs. standard hydrogen electrode, SHE) and chemical stability, because of its high over-potential for hydrogen evolution.^[12-15] In fact, traditional Zn alkaline batteries (i.e., Zn|KOH|MnO₂ batteries) perform admirably as primary (or non-rechargeable) batteries, and once created a \$10-billion per year market before the rise of rechargeable batteries.^[13,16]

Encouraged by the success of Zn-MnO₂ primary batteries, design of Zn-MnO₂ ARBs has been a hot topic for decades. In as early as 1960s, evident rechargeability had been detected in alkaline Zn|KOH|MnO₂ ARBs.^[17] However, these batteries can only run in a very shallow depth of discharge (DOD, $\sim 10\%$) and therefore deliver very limited capacity, due to the instability of both the cathode and the anode in alkaline electrolyte.^[13,18,19] During cycling, Zn anode irreversibly forms Zn(OH)₂ and ZnO in alkaline electrolyte due to Zn corrosion, besides dendrite growth.^[2,20] On the MnO₂ cathode side, the poor rechargeability relates to the irreversible dissolution of discharge product MnOOH into electrolytes as Mn²⁺.^[21] Recent works indicate that the rechargeability of the Zn alkaline batteries can be remarkably improved by high stable cathodes and micro-structured Zn anodes. One can refer to related literature if interested.^[11,20,22,23]

The birth of zinc ion batteries (ZIBs) stems from the adoption of mild electrolytes (for example: ZnSO₄, ZnCl₂, Zn(NO₃)₂, Zn(BF₄)₂, ZnSiF₆, etc.) in 1980s, which aims to improve the rechargeability of Zn-ARBs.^[17,24] According to the Pourbaix diagram of Zn metal (Figure 1a),^[25] electrochemical reaction on Zn anodes is the dissolution/deposition (i.e., striping/plating) of Zn²⁺ when pH < 10. Therefore, in the mild Zn-ARBs, Zn²⁺ ions are the charge carriers that migrate between anodes and cathodes,^[6,7] instead of OH⁻ in alkaline ARBs. The anodic reaction of ZIBs can be straightforwardly expressed as [Eq. (1)]:



[a] L. Kang,[†] F. Jiang
College of Environment and Materials Engineering, Yantai University, Yantai, Shandong 264005, China
E-mail: kangltxy@163.com

[b] M. Cui^{*}
Songshan Lake Laboratory of Materials Science, Dongguan, Guangdong 523808, China

[c] Z. Zhang
School of Materials Science and Engineering, Zhengzhou University, Zhengzhou, Henan 450001, China

[†] These authors contribute equally to this paper, and should be considered as co-first authors.

 Supporting information for this article is available on the WWW under <https://doi.org/10.1002/batt.202000060>

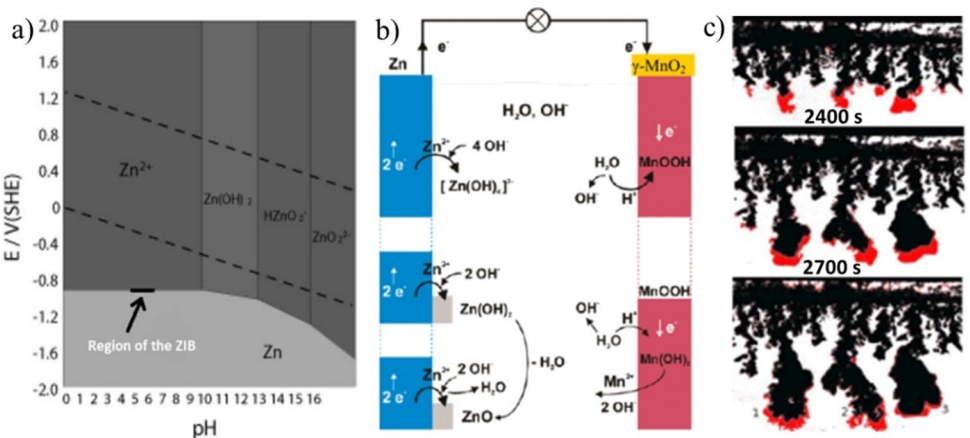
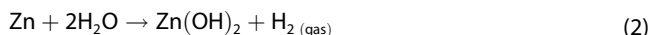


Figure 1. a) Diagram of potential-pH value (Pourbaix diagram) of Zn in aqueous solutions. Reproduced with permission from Ref. [25]. Copyright 2015, Wiley-VCH. b) Discharge mechanism of a Zn–MnO₂ alkaline battery depicting main side reactions on both electrodes. Reproduced with permission from Ref. [16]. Copyright 2004, American Chemical Society. c) In situ images of electro-plated zinc deposits in a 0.3 cm s⁻¹ flowing KOH aqueous electrolyte at deposition potential of −2.55 V. The red parts highlight new Zn deposits growing during the time intervals. Reproduced with permission from Ref. [27]. Copyright 2010, the Electrochemical Society.

The remarkable advantage of mild electrolytes over their alkaline counterparts can be partially explained by the Pourbaix diagram. As shown in Figure 1, the electrochemical reaction of Zn anodes in the alkaline electrolytes is a complex process with different species as Zn(OH)^{3−}, HZnO₂[−] or ZnO₂²⁺. In this condition, passivation products (such as Zn(OH)₂ and ZnO, Figure 1b) always form irreversibly on Zn anode surface due to following side reactions [Eqs. (2), (3)]:^[25,26]



Besides the formation of passivation products, detrimental dendritic Zn deposition on the Zn anode surfaces is also prevalent in alkaline electrolytes (Figure 1c), leading to dramatic increase of polarization or even quick internal-shorting (i.e., short circuit) failure in the batteries.^[27,28] In mild electrolytes, the electrochemical striping/plating reactions of Zn are less interfered by side reactions, making the anode reactions much more reversible.^[8] As a result, Zn anodes show much better cycling stability in mild electrolytes than in alkaline electrolytes.^[2,13] The employment of mild electrolytes also improves the cycling stability of the MnO₂ cathode, by depressing the formation of irreversible byproducts (such as



Prof. Litao Kang was awarded his Ph.D. degree in Materials Chemistry and Physics from Shanghai Institute of Ceramics, Chinese Academy of Sciences (SICCAS) in 2011. He worked as a research fellow in SICCAS till 2012, postdoctoral researcher and assistant professor at Taiyuan University of Technology during 2013–2018. Afterwards, he joined the Department of Environment and Materials Engineering, Yantai University as an associate professor. His research interest mainly focuses on aqueous batteries and energy efficient windows. Dr. Kang has published near 70 peer-reviewed papers, and has filed 15 patents.



Mangwei Cui received his B.S. and M.S. degree in Materials Science and Engineering from Taiyuan University of Technology. Now, he is an assistant engineer at the Flexible Battery Group of Songshan Lake Materials Laboratory. His research mainly focuses on high-performance aqueous multi-valence batteries with metal anodes, and flexible aqueous multi-valence battery devices.



Prof. Zongtao Zhang is an associate professor at School of Materials Science and Engineering, Zhengzhou University. He obtained his Ph.D. degree from Shanghai Institute of Ceramics, Chinese Academy of Science in 2012. Currently, His research focuses on energy conversion and management materials, especially on optical/thermal modulation materials and their applications.



Prof. Fuyi Jiang obtained his B.S. and Ph.D. degree from Zhejiang and Shandong University in 1990 and 2007, respectively. He is the former dean and also a full professor of the Department of Environment and Materials Engineering, Yantai University. Prof. Jiang's research focuses on energy storage devices, including lithium, sodium, and zinc ion batteries, which are supported by NSFC and major basic research projects of Shandong natural science foundations.

$\text{Mn}(\text{OH})_2$, Mn_3O_4 , and Mn_2O_3) that quickly appear in the alkaline electrolyte.^[28]

2. Chemistry and Advantages of Mild ZIBs

As a typical secondary batteries, ZIBs consist of a series of functional components, including cathode, anode, electrolyte, separator, and current collectors. All these parts show specific and profound influences on the kinetics and performances of ZIBs. Figure 2 graphically illustrates the key topics and main research content relating with these components, which we hope can give some guide for the further development of high performance ZIBs.

While almost all ZIBs use Zn metal (powder^[29] or foil)^[13,30] as their anodes, the choices of cathode materials are considerably diverse. To simplify the discussion, we first take one kind of the most important ZIBs, $\text{Zn}|\text{ZnSO}_4|\text{MnO}_2$ batteries, as an example to explain the chemistry of ZIBs.^[13] The chemistry schematic of $\text{Zn}|\text{ZnSO}_4|\text{MnO}_2$ ZIBs can be graphically demonstrated as Figure 3a, according to the outstanding work by Xu and Kang et al.^[13] In $\text{Zn}|\text{ZnSO}_4|\text{MnO}_2$ ZIBs, MnO_2 , Zn, and ZnSO_4 aqueous solution are employed as cathode, anode, and electrolyte, respectively.^[2,13] The cathode and anode are totally apart from each other with an electrically insulating yet ionic conductive separator (for instance, electrolyte permeate glass fiber fabric, or cation/anion exchanging membranes^[24]), in order to void electrical short circuits while allowing the migration of charge carriers Zn^{2+} . Once assembled, these ZIBs are in their charged

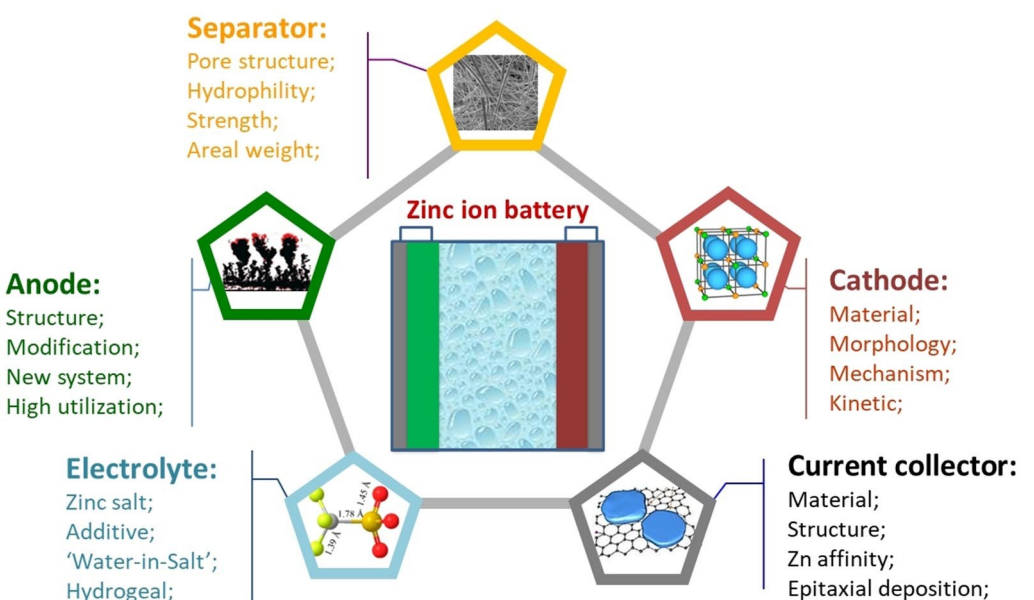


Figure 2. Main components and research topics relating to ZIBs.

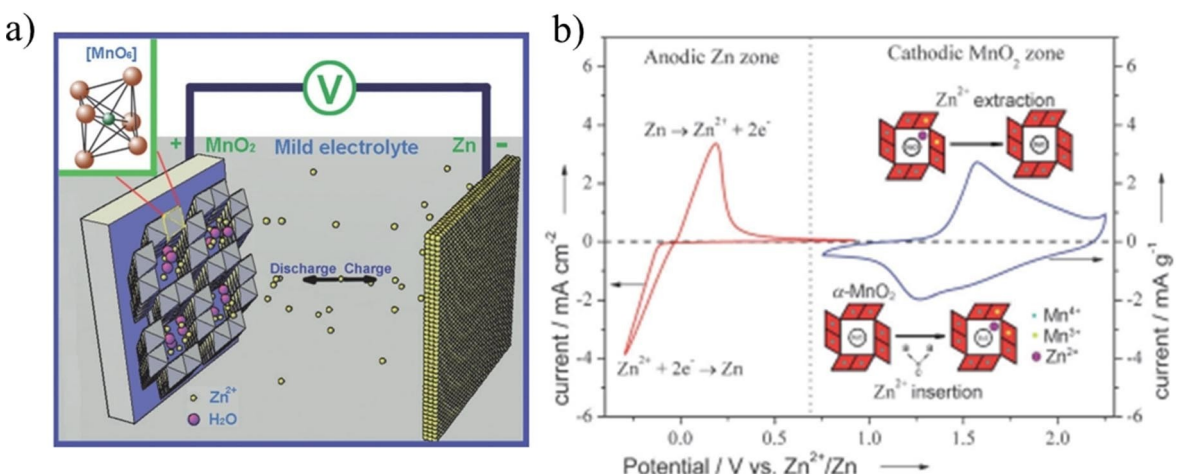


Figure 3. a) Schematic and b) CV curves of a typical mild ZIBs, $\text{Zn}|\text{ZnSO}_4|\text{MnO}_2$ battery. Reproduced with permission from Ref. [13]. Copyright 2012, Wiley-VCH.

state, delivering an average discharging and charging voltages of around 1.30 and 1.55 V, respectively (Figure 3b).

During discharging, Zn^{2+} ions in the electrolytes are migrating and stored in the cathode side, by intercalation,^[13,18,28] chemical conversion,^[2,18] or dissolution-deposition reaction^[31] according to different mechanisms. Meanwhile, the Zn metal anode is electrochemically stripped into Zn^{2+} ions to compensate the Zn^{2+} consumption caused by the cathodic reaction. During charging, reverse reactions occur on both cathode and anode sides with the assistance of external voltages, i.e., Zn^{2+} ions are released from the cathode and electrochemical plated (deposited) on the surface of the Zn metal anode. Thanks to the improved reaction reversibility in both electrodes, these $Zn|ZnSO_4|MnO_2$ ZIBs achieve much better deep-discharging rechargeability compared to alkaline $Zn|KOH|MnO_2$ batteries.^[2] Besides deep-discharging ability, $Zn|ZnSO_4|MnO_2$ ZIBs also exhibit several desirable intrinsic merits:

- a) These batteries are highly safe with literally no fire risks, and need not rigorous manufacturing and packaging conditions,^[32] due to the aqueous electrolyte design and ambient stability of electrolyte/electrolyte materials.
- b) All components of $Zn|ZnSO_4|MnO_2$ ZIBs are abundant and cheap. Therefore, the cost of $Zn|ZnSO_4|MnO_2$ ZIBs should be quite affordable for various applications. At the same time, these ZIBs are more environment benign than mainstream ARBs that use either strongly alkaline (such as $Zn-MnO_2$, $Ni-Cd$, or $Ni-MH$ batteries), or acidic (Pb -acid) electrolytes.^[13]
- c) These $Zn|ZnSO_4|MnO_2$ ZIBs show high energy density (~320 Wh kg⁻¹, based on the weight of cathode and theoretically needed anode^[33]), thanks to high theoretical capacities of both cathode and anode (819 mAh g⁻¹^[12-14], 5851 mAh mL⁻¹ for Zn, 308 mAh g⁻¹ for MnO_2 ^[15]) as well as the high working voltage (~1.3 V^[14]).
- d) The high ionic-conductivity of aqueous electrolytes (ca. 1 S cm⁻¹, about 2 order of magnitude larger than their organic counterparts^[15,34]) and the kinetically fast cathodic and anodic reactions^[2,12-14] endow the batteries excellent rate capacities (up to 12 kW kg⁻¹, based on the total weight of cathode and theoretically needed anode active materials^[33]). Due to above-mentioned outstanding advantages, ZIBs have been identified as one of the most viable batteries to replace lead acid batteries and conventional LIBs in niche areas.^[32]

3. Cathode Materials for ZIBs

The cathode materials of ZIBs should be able to electrochemically switch between at least two stable oxidation states during charge storage.^[35] Therefore, the cathode materials contain electrovalence-changeable cations, for example transition metal elements. Although the radius of Zn^{2+} ions (0.74 Å) is almost the same as that of Li^+ ions (0.76 Å), the larger atomic mass, stronger positive polarity and thicker solvation shell result in poor transport kinetics, high voltage hysteresis, and lower solid-state solubility in bulk electrode.^[36,37] Thus, most of the

electrode materials that can accommodate reversible Li^+ insertion/extraction are not suitable for ZIBs.^[4]

Recently, many cathodes beyond MnO_2 have been investigated as ZIBs' cathode, including manganese oxides (Mn_2O_3 ,^[38] $ZnMn_2O_4$,^[12] $LiMn_2O_4$,^[39] $Na_{0.95}MnO_2$,^[40] layered V_2O_5 derivatives ($Zn_{0.25}V_2O_5 \cdot nH_2O$,^[8] $Na_2V_6O_{16} \cdot 1.63H_2O$,^[41] $Na_{0.33}V_2O_5$,^[42] $Ca_{0.25}V_2O_5 \cdot nH_2O$,^[15]), layered VS_2 ,^[43] $Na_3V_2(PO_4)_3$, Prussian blue analogues ($Fe[Fe(CN)_6]$,^[44] $Zn_3[Fe(CN)_6]_2 \cdot xH_2O$,^[45,46] $Cu_3[Fe(CN)_6]_2$,^[25]), etc. Typical performances of these materials have been summarized in Table 1. It is found that MnO_2 delivers much higher capacity than a majority of the other cathode materials. However, the low electrical conductivity of MnO_2 is a big obstacle for their practical application, since it will dramatically depress the practical capacities of this material at high rate or high mass loading. On the other hand, even though V_2O_5 -based cathodes exhibit comparable or even superior capacities and rate capability compared to MnO_2 , their low discharge voltage and toxic nature are very disadvantageous.^[9,47] In our opinion, these two materials are currently the most promising candidate cathode materials for ZIBs.

3.1. Manganese Oxides

Among various ZIBs' cathode materials, MnO_2 attracts intensive attentions due to its low cost, natural abundance, non-toxic nature, and high theoretical capacity (for one-electron reaction of Mn^{4+} to Mn^{3+} , the theoretical capacity is 308 mA g⁻¹). In as early as 1865, MnO_2 had been used as cathode materials of primary $Zn-MnO_2$ batteries.^[48] In 1980s, commercial γ - MnO_2 had been proved to have reversible charge storage ability in a variety of zinc salt aqueous electrolytes, such as $ZnSO_4$, $ZnCl_2$, $Zn(NO_3)_2$, $Zn(BF_4)_2$, $ZnSiF_6$, etc.^[17,24] Nowadays, MnO_2 seems revived as one of the most important cathode materials of ZIBs. Figure 4 exhibits the quite different crystallographic structures of typical MnO_2 polymorphs.^[49] All MnO_2 polymorphs can be regarded as frameworks of $[MnO_6]$ octahedral subunits sharing corners or edges. Significantly, different MnO_2 polymorphs possess quite different tunnels, from (3×3) of todorokite-type MnO_2 to (1×1) of β - MnO_2 ,^[49,50] which may remarkably influence their charge storage performances.^[33,49] Up to date, a variety of MnO_2 polymorphs (e.g., α -,^[13,33] β -,^[18] γ -,^[17,24,33] δ -,^[33] todorokite-like^[50]) have been verified to be active for charge storage in mild Zn^{2+} -aqueous electrolytes. For Zn^{2+} ,^[13] (as well as Ni^{2+} ,^[33]) storage, Xu's comparison experiments suggest that α - MnO_2 holds the highest capacity due to its stable and large (2×2) tunnels. Very recently, Zhi^[51] and Choi^[52] show that pre-intercalation of Na^+ and crystal water into layered δ - MnO_2 can effectively mitigate their structural degradation towards λ -phase^[53] and improve its ionic conductivity,^[54] turning this material into an attractive cathode candidate for ZIBs. Also, many reports also indicated that microstructures, besides crystallographic structures of MnO_2 polymorphs, influence also the charge storage performances of MnO_2 .^[18] Currently, most of the research focuses on understanding the Zn^{2+} -storage

Table 1. Summary of electrochemical performances of typical cathode materials of ZIBs.

Cathode	Electrolyte	Capacity [mAh g ⁻¹] @ current density [mA g ⁻¹]	Capacity Retention @ cycle number	Voltage window [V]	Mass loading [mg cm ⁻²]	Energy density [Wh kg ⁻¹] @ power density [W kg ⁻¹] ^[a]	Ref.
α -MnO ₂ nano-fiber	2 M ZnSO ₄ + 0.1 M ZnSO ₄	260 @ 308 161 @ 1540	~100% @ 60 92% @ 5000	1.0–1.8	1.0–5.0	~170 (electrode + electrolyte)	[2]
α -MnO ₂ nano-particle	1 M ZnSO ₄ or 1 M Zn(NO ₃) ₂	210 @ 105 100 @ 600 68 @ 8568	~100% @ 100	1.0–1.9	5.0 mg (area unknown)	–	[13]
α -MnO ₂ nano-rod CNT/ α -MnO ₂ composite	1 M ZnSO ₄ 2 M ZnSO ₄ + 0.5 M MnSO ₄	205 @ 10 120 @ 1000	– 333% @ 300	0.7–2.0 1.0–1.9	5.0 –	–	[32] [29]
α -MnO ₂ nano-rod β -MnO ₂ nano-rod	3 M Zn(CF ₃ SO ₃) ₂ + 0.1 M Mn (CF ₃ SO ₃) ₂	250 @ 200 260 @ 200 151 @ 2000	~70% @ 100 ~80% @ 150 94% @ 2000	0.8–1.9	~2.0	– 254 @ 197 110 @ 5910	[18]
Commercial β -MnO ₂		~120 @ 200	110% @ 200			–	
γ -MnO ₂ nano-rod		~230 @ 200	~83% @ 100			–	
β -MnO ₂ nano-rod	3 M ZnSO ₄ + 0.1 M MnSO ₄	110 @ 200	~170% @ 150	0.8–1.9	~2.0	–	[18]
Commercial γ -MnO ₂	2 M ZnSO ₄	150 @ 50	~100% @ 30 (failed at 30 ± 4 cycles)	0.9–1.7	13.0	44 (cathode + electrolyte)	[17, 24]
Meso-porous γ -MnO ₂	1 M ZnSO ₄	219 @ 0.5 mA cm ⁻²	63% @ 40	0.8–1.8	–	–	[48]
δ -MnO ₂ nano-flake δ -MnO ₂ nano-flake	2 M ZnSO ₄ + 0.1 M MnSO ₄	122 @ 83 300 @ 184	45% @ 100 ~100% @ 120	1.0–1.8 1.0–1.9	– 5.0–10.0	– –	[53] [21]
MnO ₂ Todorokite Spinel-ZnMn ₂ O ₄	1 M ZnSO ₄ 3 M Zn(CF ₃ SO ₃) ₂	98 @ 50 150 @ 50 ~85 @ 500	89% @ 50 – 94% @ 500	0.7–2.0 0.8–1.9 2.0	~2.0 202	– –	[50] [12]
Mn ₂ O ₃ Zn _{0.25} V ₂ O ₅ · nH ₂ O Ca _{0.25} V ₂ O ₅ · nH ₂ O	2 M ZnSO ₄ 1 M ZnSO ₄ 1 M ZnSO ₄	148 @ 100 300 @ 300 340 @ 0.2 C	87% @ 30 80 @ 1000 96% @ 3000	1.0–1.9 0.5–1.4 0.6–1.6	– 5.0–7.0 ~5.7	– ~450 Wh/l 267 @ 53.4	[38] [8] [15]
Zn ₃ V ₂ O ₇ (OH) ₂ · 2H ₂ O	1 M ZnSO ₄	213 @ 50 76 @ 5000	68% @ 300	0.2–1.8	4–5	–	[9]
Na _{0.33} V ₂ O ₅ Na ₂ V ₆ O ₁₆ · 1.63H ₂ O	3 M Zn(CF ₃ SO ₃) ₂ Zn(CF ₃ SO ₃) ₂	367.1 @ 100 296 @ 100 158 @ 5000	93% @ 1000 78% @ 100 90% @ 6000	0.2–1.6 0.2–1.6	1.0–2.0 –	– –	[42] [41]
Layered VS ₂	1 M ZnSO ₄	193 @ 50 112 @ 500	98% @ 200	0.4–1.0	–	123	[43]
Co _{0.247} V ₂ O ₅ · 0.944H ₂ O	20 M LiTFSI + 1 M Zn(TFSI) ₂ PAM hydrogel	432 @ 100 163 @ 10 ⁴	90% @ 7500	0.6–2.0	1–3	485.7	[89]
NASICON structured Na ₃ V ₂ (PO ₄) ₃ /C NASICON structured Na ₃ V ₂ (PO ₄) ₂ F ₃ @C	0.5 M Zn(OAc) ₂ 2 M Zn(CF ₃ SO ₃) ₂	97 @ 50	74% @ 100	0.8–1.7	–	–	[10]
Fe[Fe(CN) ₆]	1.0 M Zn(OAc) ₂ / ([Ch]OAc + 30 wt % water)	122 @ 10	94% @ 10	0.8–2.0	5.0	–	[44]
Cu ₃ [Fe(CN) ₆] ₂	20 mM ZnSO ₄	52 @ 60	96% @ 100	1.3–2.2	–	45.7 @ 52.5 33.8 @ 477	[25]
Zn ₃ [Fe(CN) ₆] ₂	1 M ZnSO ₄	65 @ 60 60 @ 120	81% @ 100 76% @ 100	0.8–1.9	8.0	100 @ 100 46 @ 1700	[110]
Co(III)-rich Co ₃ O ₄	4 M ZnSO ₄ + 0.2 M CoSO ₄ in PAM hydrogel	202 @ 500 105 @ 4000	98% @ 600 95% @ 4000	0.8–2.2	1.05	360.8	[128]
Mn ₃ O ₄ H ₂ V ₅ O ₈ NW/graphene	3 M Zn(CF ₃ SO ₃) ₂	394 @ 100 270 @ 6000	92% @ 5000	0.2–1.6	1	168 @ 34 89 @ 2215 (cathode + theoretically required Zn)	[68] [4]
Pyrene-4,5,9,10-tetraone	2 M ZnSO ₄	336 @ 40 162 @ 5000 113 @ 20k	~70% @ 1000	0.36–1.46	4–6	186.7 @ 22.1 12 @ 15.3 (cathode + consumed Zn)	[160]
Polyaniline	2 M ZnCl ₂ + 3 M NH ₄ Cl	204 @ 500 119 @ 16k	100% @ 1000	0.7–1.7	0.8	175.1 @ 430 90.1 @ 12100	[88]

Table 1. continued

Cathode	Electrolyte	Capacity [mAh g ⁻¹] @ current density [mA g ⁻¹]	Capacity Retention @ cycle number	Voltage window [V]	Mass loading [mg cm ⁻²]	Energy density [Wh kg ⁻¹] @ power density [W kg ⁻¹] ^[a]	Ref.
Quinone	3 M Zn(CF ₃ SO ₃) ₂ (impregnated in Nafion separators)	335 @ 20 197 @ 500	87 % @ 1000	0.8–1.3	2.5–10	220 based on cathode + theoretically required Zn 80 based on full cell	[150]

[a] Based on the weight of active materials if no special declaration is given.

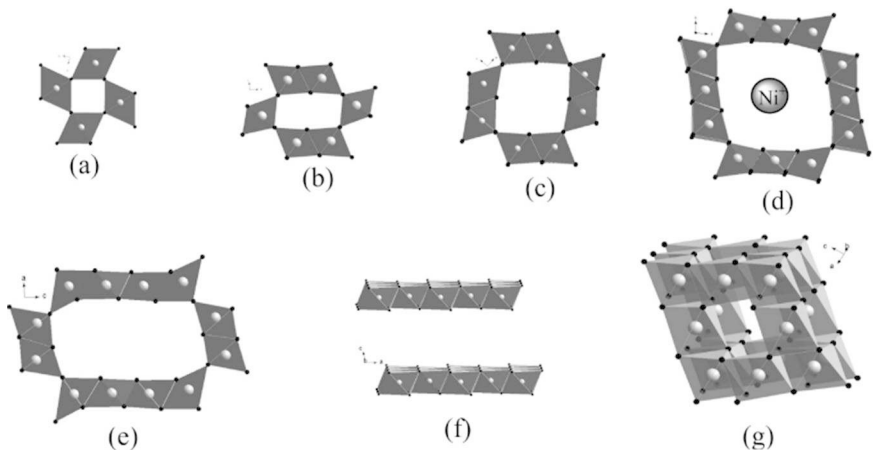


Figure 4. Crystallographic structures of MnO₂ pyrolusite (β -phase, a), ramsdellite (γ -phase, b), cryptomelane (α -phase, c), Ni-todorokite (d), OMS-5 (e), birnessite (δ -phase, f), and spinel (λ -phase, g). Reproduced with permission from Ref. [49]. Copyright 2009, American Chemical Society.

mechanisms, as well as the preparation of high performance MnO₂ cathode materials.

3.1.1. Charge Storage Mechanisms of MnO₂

Zn²⁺-intercalation mechanism in ZnSO₄ aqueous electrolyte: Due to their very different structures, it is easy to speculate that MnO₂ polymorphs hold different charge storage mechanisms. For α -MnO₂, their large 2×2 tunnels can be inserted by mono-/bi-valence ions in nature.^[33] In as early as 2009, Xu and Kang et al. proposed a Zn²⁺-intercalation mechanism to explain the reversible charge storage ability of α -MnO₂ nano-particles (Figure 3), based on XPS and XRD analyses.^[13] According to their theory, the cathodic reactions of α -MnO₂ in ZIBs can be expressed as [Eq. (4)]:



Therefore, combining the anodic and cathodic reactions gives an overall Zn–MnO₂ ZIBs reaction as [Eq. (5)]:



However, the XRD fitting results of the discharged (i.e., Zn²⁺-inserted) state MnO₂ were not completely satisfied, e.g., there seems no standard peaks can match the quite strong

measure peaks at $\sim 12^\circ$ and 60° . Meanwhile, this mechanism conflicts the fact that water is indispensable for the charge storage process of MnO₂ cathode.^[2,55] Even though the proposed mechanism seems not perfect,^[2,28,32] this work successfully aroused research interests on mild ZIBs after around 20-years research dormancy.^[13,17]

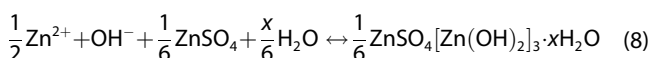
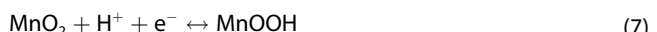
Conversion reaction mechanism in ZnSO₄ aqueous electrolyte: Different from the abovementioned theory, Lee et al.^[32] argued that the charge storage reactions of α -MnO₂ involve a reversible phase transition between tunneled α -MnO₂ and layered Zn-birnessite MnO₂ (δ -MnO₂ with Zn²⁺ insertion), based on XRD, HRTEM and EDX analyses. This theory implies that a δ -MnO₂ cathode should remain its structure during discharging. However, different researchers detected impure XRD peaks in discharged δ -MnO₂ cathodes, which on the other hand can be well indexed to ZnSO₄[Zn(OH)₂]₃·xH₂O.^[21,53] Indeed, even in Lee's work, the XRD patterns of 5th–10th discharged cathode contain several XRD peaks far different from Zn-birnessite MnO₂.^[32] Therefore, it is very possible that the reactions are much more complicated than a phase transformation between α -MnO₂ and Zn-birnessite MnO₂.

For meso-porous γ -MnO₂, Alfaruqi et al.^[48] proposed another chemical reaction mechanism for its charge storage ability, based on *in situ* synchrotron XANS and XRD studies. They believed that the discharged tunnel-type parent γ -MnO₂ underwent a reversible structural transformation to spinel-type ZnMn₂O₄ (Zn²⁺ inserted λ -MnO₂) and two new intermediary Mn

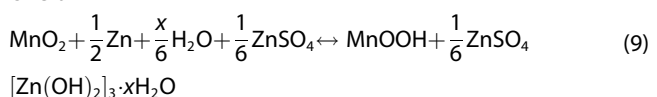
(II) phases, namely tunnel-type $\gamma\text{-Zn}_x\text{MnO}_2$ and layered-typed L-Zn_xMnO₂ (Figure 5a). Again, the new XRD peaks of discharged cathodes can also be indexed to ZnSO₄[Zn(OH)₂]₃·xH₂O.^[2] In addition, it is also difficult to explain why the final discharged cathodes contain three phases, rather than a single final discharge phase.

Recently, Pan and Liu et al. present a quite different chemical conversion reaction mechanism for the charge storage ability of $\alpha\text{-MnO}_2$.^[2] In their works, homogeneous $\alpha\text{-MnO}_2$ nano-fibers (preferred orientation =[220] axis) were deliberately selected as cathodes, in order to clearly ex situ observe the cathode's morphology and composition evolution during charge-discharge cycling. During cycling, the authors detected several important features of the Zn–MnO₂ ZIBs: 1) the Zn–MnO₂ ZIBs showed rather different charge-discharge curves for the initial two cycles; 2) in the initial cycle, a nontrivial over-potential of ~300 mV is observed; 3) the $\alpha\text{-MnO}_2$ underwent a dramatic morphology transformation from nano-fibers into short nano-rods and nano-particles in the first discharge process down to 1 V; 4) the short nano-rods and nano-particles accommodated Zn²⁺ rather than the nanowires. All these features are rarely seen in intercalation electrode materials.

By means of HRTEM, XRD, STEM-EDS, and ¹H NMR studies, the author detected MnOOH and ZnSO₄[Zn(OH)₂]₃·xH₂O in the discharged cathodes. Combining this finding together, a conversion reaction-based mechanism is extracted for the charge storage ability of MnO₂ [Eqs (6)–(9)]:



Overall :



According to this mechanism, H₂O is indispensable for the charge storage reactions of Zn–MnO₂ ZIBs. Indeed, in H₂O-free organic Zn²⁺-based electrolytes, Zn–MnO₂ ZIBs deliver very limited capacity, confirming that H₂O participates in the charge storage reactions of MnO₂ cathodes. According to this mechanism, protons (H⁺) in the weakly acidic ZnSO₄ electrolyte insert into MnO₂ cathode during discharge, leading to the formation of MnOOH. Meanwhile, Zn²⁺ ions are stored as ZnSO₄[Zn(OH)₂]₃·xH₂O by coupling with the residual OH⁻ near the cathode surface.^[21] This mechanism can explain the very similar charge-discharge curves of different MnO₂ polymorphs as ZIBs' cathodes, since the insertion of H⁺ into all MnO₂ polymorphs is kinetically easy.

However, this theory involves only an one-electron reaction between Mn⁴⁺ and Mn³⁺, and seems difficult to explain the double-plateau discharge curves and the bimodal CV curves of

MnO₂ cathodes (Figure 3b).^[56] For this issue, some authors suggest that the cathodic reactions of MnO₂ cathodes involve the transition of Mn⁴⁺↔Mn²⁺.^[21,29] Indeed, a battery comprising a Zn anode and a $\alpha\text{-Mn}_2\text{O}_3$ cathode outputs still an initial discharge voltage of ~1.05 V and a discharge capacity of ~80 mAh g⁻¹, suggesting the reduction of Mn³⁺ into Mn²⁺.^[38] After the 1st discharge, the Zn–Mn₂O₃ ZIBs charge-discharge curves became very similar with that of MnO₂ cathode, implying the oxidization of Mn²⁺ back into Mn⁴⁺.^[38] These results indicate that Mn²⁺ ions in the MnSO₄-containing electrolytes can also be electrically oxidized into MnO₂ by charging, causing gradual capacity increase during cycling (α -,[29,56,57] β -,[18] δ -[53] and $\gamma\text{-Mn}_2\text{O}_3$).^[48] As a result, the dynamic dissolution-deposition balance of Mn⁴⁺ and Mn²⁺ is an important impact factor for ZIBs lifetime.^[2,21] After repeated charge-discharge cycles, the re-deposited MnO₂ could even become dominant over the pristine MnO₂.^[31,32] Obviously, this phenomenon is also elusive according to the mechanism described in Equations (4)–(7). Therefore, Zhou and Liang et al.^[31] further proposed a dissolution/deposition mechanism for the Zn²⁺ storage ability of MnO₂ in mild electrolytes, which believe that dissolution/deposition reactions are the major attributor to the capacity. The discharge side product ZnSO₄[Zn(OH)₂]₃·xH₂O that covers on cathode, on the other hand, is a kinetic limitation for the further discharge of residual MnO₂. Depressing the pH of electrolytes by adding acids can prohibit the formation of ZnSO₄[Zn(OH)₂]₃·xH₂O, and therefore effectively boost the capacity of MnO₂ cathodes.^[58–61] However, a low pH volume will remarkably accelerate the corrosion of Zn anodes and deteriorate the cycling stability of ZIBs.^[21] Commonly, the pH of mild ZIBs' electrolytes is higher than 3.

H⁺ and Zn²⁺ co-insertion mechanism in ZnSO₄ aqueous electrolyte: To explain the double-plateau discharge curves and the bimodal CV curves of Zn–MnO₂ ZIBs, Sun, Zhu and Wang et al.^[28] proposed an H⁺ and Zn²⁺ successive co-insertion chemistry after systematical electrochemical and structural analyses. In their battery, the nano-flake MnO₂ cathode (akhtenskite phase, JCPDS 30-0820) was directly in situ electrodeposited on carbon fiber paper (CFP) in mild acidic ZnSO₄+MnSO₄ electrolyte, in order to mimic the state of a long-cycled MnO₂ cathode that has undergone much times dissolution-deposition processes. The electrodeposited cathode consists of sub-10-nm MnO₂ grains, providing abundant electrode/electrolyte contact interfaces to reduce ion diffusion distance. These structural features ensure the reactions with slow electrochemical kinetics to happen, delivering an excellent cycling performance with a low capacity decay rate of 0.007% per cycle for 10000 cycles at a high rate of 6.5 C. This binder- and conductive-agent-free cathode can effectively simplify the mechanism analysis process.

Analogous to other Zn–MnO₂ ZIBs, the battery demonstrated two plateaus (Region I and II) in its discharge curves (Figure 5b). Surprisingly, these two plateaus demonstrate quite different rate capability. With increasing discharge rate, the voltage and capacity of the Region I plateau drops very slowly compared to the one in Region II, indicating a faster reaction kinetic. At a high rate of 6.5 C, the Region II plateau only

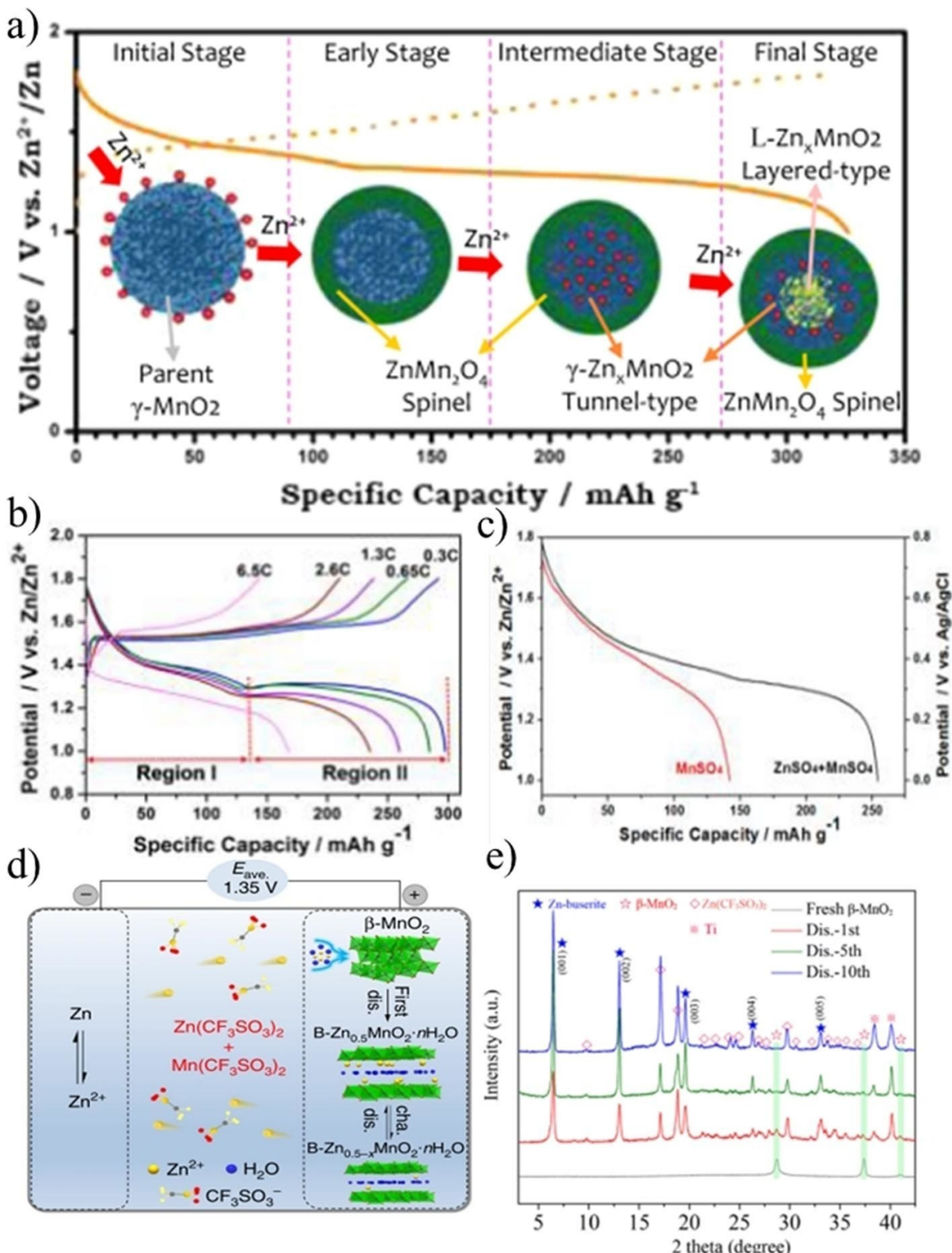


Figure 5. a) Schematic illustration of the reaction pathway of Zn-insertion in the prepared γ -MnO₂ cathode. Reproduced with permission from Ref. [48]. Copyright 2015, American Chemical Society. b–c) Charge-discharge curves of electrodeposited MnO₂ cathode in 2 M $ZnSO_4$ + 0.2 M $MnSO_4$ electrolyte (b) and 0.2 M $MnSO_4$ electrolyte. Reproduced with permission from Ref. [28]. Copyright 2017, American Chemical Society. d) Schematic illustration of the electrochemistry of β -MnO₂ in $Zn(CF_3SO_3)_2 + Mn(CF_3SO_3)_2$ aqueous electrolyte, e) XRD patterns of the β -MnO₂ cathodes after 1st, 5th and 10th cycles in the $CF_3SO_3^-$ -based electrolyte. The characteristic peaks of initial β -MnO₂ became discernable after 10 cycles. Reproduced with permission from Ref. [18]. Copyright 2017, The Authors.

contributes less than 20% of the total capacity. GITT and EIS results also suggest similar kinetic difference between these two regions, manifesting their distinct reaction mechanisms. With the assistance of further comparison experiment and XRD characterization, the Region I and II discharge voltage plateaus are assigned to H^+ and Zn^{2+} insertion reactions, respectively (Figure 5c). This mechanism can also explain the reason why H_2O is necessary to activate the high capacities of MnO_2 cathodes.^[2,28] In layered δ - MnO_2 system, similar H^+ and Zn^{2+} co-insertion mechanism is also detected.^[51]

Conversion reaction mechanism in $Zn(CF_3SO_3)_2$ aqueous electrolyte: In $ZnSO_4$ -based electrolyte, the charge storage mechanisms relating the formation of $ZnSO_4[Zn(OH)_2]_3 \cdot xH_2O$ sounds reasonably for MnO_2 cathode, but this mechanism is not necessarily right in other aqueous electrolytes. In $Zn(CF_3SO_3)_2 + Mn(CF_3SO_3)_2$ aqueous electrolyte, Zhang and Chen et al. symmetrically analyzed the structural evolution of α -, β -, and γ - MnO_2 nano-rods by using quite a number of advanced characteristic technologies.^[18] Experimental results indicate similar phase transformation from pristine MnO_2 to layered Zn-buserite MnO_2 during the first discharge, regardless of the polymorphs (Figure 5d). In following charge-discharge cycles, reversible Zn^{2+} insertion/extraction occurred in the resulting Zn-buserite MnO_2 (Figure 5e). Interestingly, the variation of Mn valence in MnO_2 cathodes is very small compared to the charge-discharge capacities. The authors postulate that such unexpected phenomenon stems from the disproportional dissolution of Mn^{3+} species ($Mn^{3+} \rightarrow Mn^{4+}(\text{solid}) + Mn^{2+}(\text{aq})$). Dissolution loss of Mn from MnO_2 cathodes should be a feasible attribution to the noticeable capacity loss on cycling.^[21]

3.1.2. Performances of MnO_2 Cathode Materials

Similar to other electrode materials, the charge-storage capacities of MnO_2 polymorphs depend not only on their crystallographic-/micro-structures^[13,18] and defects,^[62] but also on the preparation and measurement conditions of the electrodes, including kind/amount of electrolytes,^[2,18,21] binder and conductive agents,^[21] mass loading of active materials,^[2] charge-discharge current densities (rate capability), etc. Since the electrode preparation and measurement conditions are considerably diverse among literature, we can only give a relatively rough performance comparison in Table 1.

For the practical application of Zn – MnO_2 ZIBs, low-cost and high-performed MnO_2 cathode materials are essentially needed. It should be ideal if some commercial MnO_2 products perform well as cathodes of ZIBs. In as early as 1980s, the charge-storage performances of commercial γ - MnO_2 micro-particles had been tested in several aqueous solutions of inorganic zinc salts.^[17,24] In 2 M $ZnSO_4$ electrolyte, commercial γ - MnO_2 micro-particles delivered a reversible charge-storage capacity of $\sim 150 \text{ mAh g}^{-1}$ at a current density of 50 mA g^{-1} and a high loading mass of 30 mg cm^{-2} .^[17] This performance seems significantly lower than that of meso-porous γ - MnO_2 (215 mAh g^{-1} at 0.5 mA cm^{-2}) with a high specific-surface-area ($148 \text{ m}^2 \text{ g}^{-1}$).^[48] In the case of β - MnO_2 , the higher capacities of nano-particles than

micro-particles have also been reported.^[18] These performance differences imply that rational design of MnO_2 microstructure is important for the fast and smooth occurrence of Zn^{2+} -storage reactions.

Considering the poor electrical conductivity of MnO_2 , a composite materials of MnO_2 with conducting materials (e.g., carbon materials) should be very favorable for performance enhancement.^[63–65] In 2014, Xu and Li et al. prepared a composite cathode material of α - MnO_2 nano-rods (diameter $\sim 10 \text{ nm}$; length $\sim 50 \sim 120 \text{ nm}$) and acid-treated CNTs (carbon nanotubes) via a co-precipitation method.^[29] Thanks to the small size of the MnO_2 and the high conductivity of the CNTs, this composite achieves both excellent capacity ($\sim 400 \text{ mAh g}^{-1}$ at 1 Ag^{-1}) and cycling stability ($\sim 100\%$ Coulombic efficiency after 500 charge/discharge cycles). In 2018, Wu, Yan and Mai et al. reported a reduced graphene oxide (rGO) scroll-coated α - MnO_2 for ZIBs, achieving a high capacity (382 mAh g^{-1} at 0.3 Ag^{-1}) along with good long term cycling stability (94% capacity retention after 3000 cycles at 3 Ag^{-1}).^[66] Moreover, depositing MnO_2 onto 3D networks of CNTs or graphenes^[65,67] is also an effective way to build well-performance ZIBs' cathodes. However, directly carbon coating MnO_2 through wet chemical process seems difficult, because of the oxide's poor thermal stability.^[68,69] During carbonization process, MnO_2 will lose oxygen and transform to other low valence manganese oxide (MnO_x) when temperature $> 450^\circ\text{C}$.^[38,70] Even in the carbon coating solution, transformation from MnO_2 into $MnCO_3$ may also occur, which further forms MnO_x after calcination. Sometimes, further oxidization may implement on the obtained $MnO_x@C$, in order to elevate manganese valence and capacity of the composite.^[68] While, other works indicate that the $MnO_x@C$ can be directly used as high performance cathode materials of ZIBs.^[69]

According to the experimental results by Xu et al.,^[13] α - MnO_2 is the polymorph that holds the highest charge-storage capacity among α -, β -, γ -, δ -, and λ - MnO_2 , possibly due to its large tunnel structure. Generally, the capacities of α - MnO_2 range from 200 to 300 mAh g^{-1} at low current densities (e.g., nano-particles: 210 mAh g^{-1} @ 105 mA g^{-1} ,^[13] nano-rods: 205 mAh g^{-1} @ 10 mA g^{-1} ,^[32] nanowires: 285 mAh g^{-1} @ 103 mA g^{-1}).^[2] However, a careful survey indicates that comparable capacities have also been achieved in other polymorphs (e.g., meso-porous γ - MnO_2 : 285 or 215 mAh g^{-1} @ 0.05 or 0.5 mA cm^{-2} ,^[48] $KMnO_4$ -decomposed δ - MnO_2 : 300 mAh g^{-1} @ 184 mA g^{-1} ,^[21] β - MnO_2 nano-rods: 258 mAh g^{-1} @ 200 mA g^{-1}).^[18]

Recently, Nam and Choi et al. convincingly show the high capacity of δ - MnO_2 that contains crystal water.^[52] It is found that the interlayer crystal water in δ - MnO_2 can effectively screen the electrostatic interactions between inserted cations and the host framework to facilitate cations' diffusion. As a result, the δ - MnO_2 with high crystal water content achieves a high capacity of 350 mAh g^{-1} at 100 mA g^{-1} . Pre-intercalating δ - MnO_2 with Na^+ can also elevate the electrochemical performance of this oxide by increasing crystal water content and structure stability.^[51] The authors also argue that the layered δ - MnO_2 (interlayer distance $\sim 0.7 \text{ nm}$) is theoretically more

suitable to serve as ZIBs' cathodes than tunnel structured α -MnO₂ (tunnel diameter ~ 0.46 nm).

3.1.3. Other Manganese Oxides

Besides MnO₂ materials, manganese oxides with other Mn valences have also been tested as cathode materials of ZIBs. For example, Jiang et al. assembled ZIBs with commercial sub-micron α -Mn₂O₃ (CAS No.1317-34-6) cathode.^[38] The α -Mn₂O₃ cathode displays a reversible capacity of 148 mAh g⁻¹ (at 100 mA g⁻¹) with good rate capability and excellent cycling stability (cycling life up to 2000 times). The author believed that the pristine α -Mn₂O₃ underwent a reversible phase transition from bixbyite structure to layered-type zinc birnessite during cycling. In 2016, Wu and Chen et al. prepared a freestanding and flexible cathode of commercial spinel-phase LiMn₂O₄ and CNTs for hybrid ZIBs,^[39] achieving also excellent rate capability (72 mAh g⁻¹ @ 2400 mA g⁻¹) in Li₂SO₄+ZnSO₄ electrolyte.

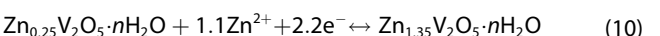
In the same year, Zhang, Cheng and Chen et al. reported a facile and scalable co-precipitation approach to prepare spinel ZnMn₂O₄/C composite cathode for ZIBs in Zn(CF₃SO₃)₂ electrolyte.^[12] The ZnMn₂O₄ gains were only 15 nm in size, and contained considerable amount of Mn vacancies. The Mn-vacancy-rich ZnMn₂O₄ allows easier Zn-ion diffusion by lowering electrostatic barrier, leading to higher Zn²⁺ diffusion coefficient and improved electrochemical performance. In 2018, Ma, Jiang and Li et al. reported a rechargeable ZIBs with a highly active Mn₃O₄@C nanowire cathode and Zn/C composite anode.^[68] The Mn₃O₄@C nanowires were prepared through a three-step method. Firstly, MnO₂ nanowires were hydrothermally synthesized, which then were coated with polydopamine (MnO₂@PDA) and transformed into MnO@C after thermal carbonization. Finally, the MnO@C was oxidized into Mn₃O₄@C by H₂O₂ and heating. It is believed that Mn₃O₄ are highly active for redox reactions, due to its special polymorphism, as well as the coexistence of mixed-valence states.^[71,72] While the in situ evolved carbon shells can well disperse the Mn₃O₄ active material and maintain high geometrical stability against bulky aggregating by acting as a robust 'nano-reactor', besides boost the overall electrical conductivity. Moreover, the 1D structure of the Mn₃O₄@C can accommodate volume change and facilitate rapid electron transfer. As a result, this cathode material delivered an impressive capacity of 237 mAh g⁻¹ @ 120 mA g⁻¹ (or ~ 107 mAh g⁻¹ @ 6000 mA g⁻¹). The cycling stability of this battery is also desirable (capacity retention $\sim 80\%$ after over 2000 cycles).

3.2. Layered V₂O₅ Derivatives and Vanadium Oxides

Besides manganese oxides, layered vanadium oxides are also one promising kind of cathode material candidate for ZIBs, owing to their large interlayer distance, high theoretical capacity, abundant resource, and low cost.^[4] The layered structure providing an easy intercalation channel for cations

including doubly charged Zn²⁺ ions. Therefore, even a commercial bulky V₂O₅ cathode can easily achieve a high capacity of 200–470 mAh g⁻¹ in 3 M Zn(CF₃SO₃)₂ electrolyte.^[47] During charge/discharge cycling, the V₂O₅ bulk quickly cleaved into nano-sheets, because of the weak interlayer interaction. To void structural instability during charge/discharge cycling, a variety of strategies has been developed, aiming to enhance the interlayer-bonding strength of layered vanadium-oxides.^[4,8,15]

In 2016, Kundu and Nazar et al.^[8] first reported excellent electrochemical charge-storage properties of vanadium oxide bronze cathode (Zn_{0.25}V₂O₅·nH₂O) nano-ribbons in ZnSO₄ aqueous electrolyte, a derivative of layered δ -V₂O₅ containing intercalated Zn²⁺ and crystal water (Figure 6a). The highly crystallized Zn_{0.25}V₂O₅·nH₂O ultra-long ribbons were prepared via a rapid microwave hydrothermal method (tens of microns in length and 100–150 nm in width). Careful characterizations assign the reversible charge-storage process of Zn_{0.25}V₂O₅·nH₂O (as well as other layered vanadium oxides) to Zn²⁺ intercalation/de-intercalation reactions within the host material.^[4,8,15,47] In discharge process, the framework enclosing intersecting paths in the interlayers of Zn_{0.25}V₂O₅·nH₂O electrochemically accommodates Zn²⁺ and water (Figure 6b), while the Zn anode side undergoes a striping reaction. In charge process, Zn²⁺ ions are de-intercalated from the cathode material, and plated back onto the Zn anode. The overall chemistry of this battery can be expressed as Equation (10):



This Zn_{0.25}V₂O₅·nH₂O nano-ribbons deliver high capacities and rate capability (223 and 183 mAh g⁻¹ at 15 and 20 C, C = 300 mA g⁻¹, Figure 6c), as well as excellent cycling stability ($> 81\%$ capacity retention after 1000 cycles.). According to the authors, the excellent electrochemical performance of Zn_{0.25}V₂O₅·nH₂O can be ascribed into following features:

- 1) This cathode material possesses an open-framework layered structure with expanded interlayer spacing by crystal/structural water and [ZnO₆] octahedra (or pillars), which not only ensures smooth cation migration, but also enhances cycling stability by pinning the layered structure (Figure 6b).^[8]
- 2) The multiple oxidation states of vanadium give this material a high theoretical capacity.^[8,15]
- 3) The charge shield effect of the crystal/structural water reduces the electrostatic repulsion between Zn²⁺ and the host framework, and thus enhances the capacity and rate performance (analogous to the case of layered δ -MnO₂).^[73,74]
- 4) The high specific surface area and *b*-axis long growth direction shorten the Zn²⁺ and electron migration length during charge/discharge, facilitating the reaction kinetics of the (de)intercalation reactions.^[8]
- 5) Diffusion coefficient of Zn²⁺ in Zn_{0.25}V₂O₅·nH₂O ($\sim 10^{-9}$ – 10^{-10} cm² S⁻¹^[8]) is quite high compared to common electrode materials (e.g., 10³–10⁴ higher than LiFePO₄,^[75] 100-fold higher than Li₄Ti₅O₁₂,^[76] comparable to the commercial LiCoO₂^[77])

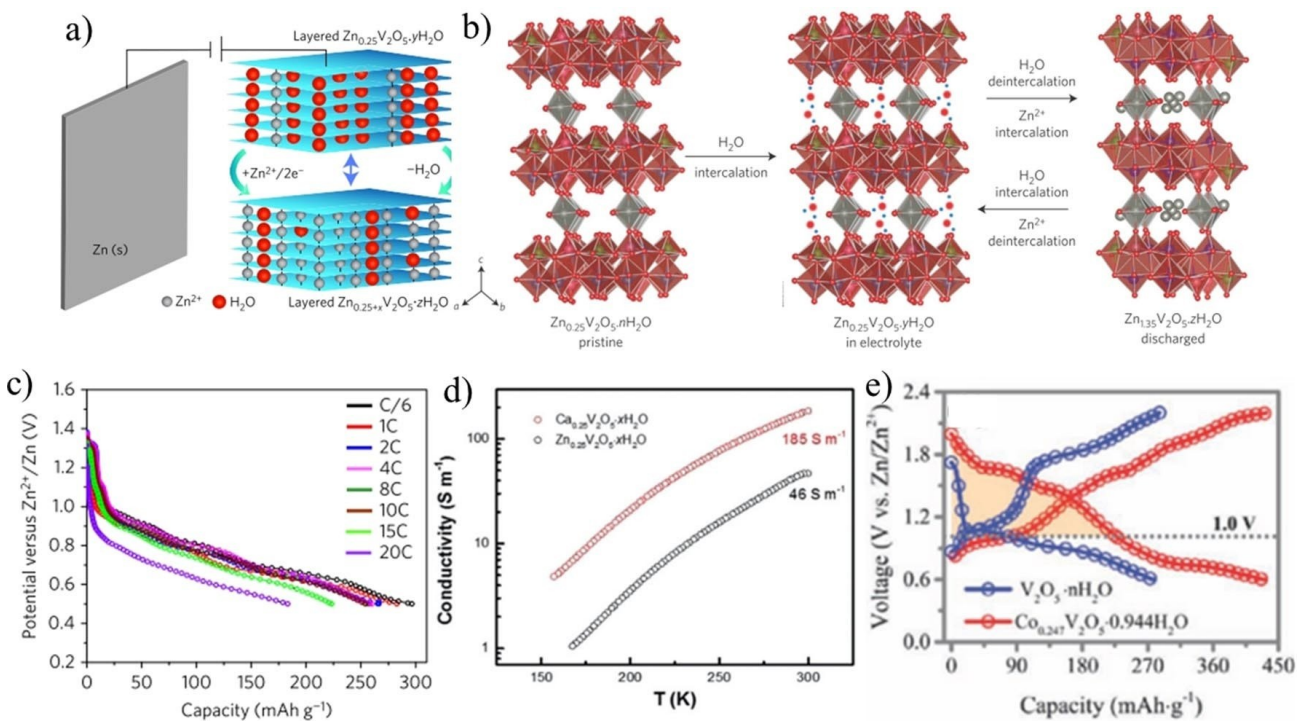


Figure 6. a) Schematic of the Zn metal/ $Zn_{0.25}V_2O_5$ cell on discharge in aqueous 1 M $ZnSO_4$. b) Scheme showing reversible water intercalation into $Zn_{0.25}V_2O_5 \cdot nH_2O$ immersed in electrolyte/ H_2O , and the water de-intercalation accompanying Zn^{2+} intercalation upon electrochemical discharge. The red and blue spheres represent O and H, respectively. c) Galvanostatic discharge profiles at C/6 to 20 C rates (1 C = 300 mAh g^{-1}). Reproduced with permission from Ref. [8]. Copyright 2016, Springer Nature. d) Electricity conductivities of individual $Ca_{0.25}V_2O_5 \cdot nH_2O$ and $Zn_{0.25}V_2O_5 \cdot nH_2O$ nano-belts. Reproduced with permission from Ref. [15]. Copyright 2018, Wiley-VCH. e) Galvanostatic charge/discharge curves of $Co_{0.247}V_2O_5 \cdot 0.944H_2O$ and V_2O_5 cathodes. Reproduced with permission from Ref. [89]. Copyright 2019, Wiley-VCH.

After the pioneering work of Kundu and Nazar et al., a variety of well-performed layered V_2O_5 and its derivatives have been explored as cathode materials of ZIBs, including $Ca_{0.25}V_2O_5 \cdot nH_2O$,^[15] LiV_3O_8 ,^[78] $H_2V_3O_8$ /graphene,^[4] V_2O_5 ,^[34,47] $V_2O_5 \cdot nH_2O$,^[74] $Na_2V_6O_{16} \cdot 1.63H_2O$,^[41] $Zn_3V_2O_7(OH)_2 \cdot 2H_2O$,^[9] $VO_{1.52}(OH)_{0.77}$,^[79] VO_2 /graphene,^[80] VS_2 ,^[43] and $FeVO_4 \cdot nH_2O$.^[81] In most of these works, foreign cations and crystal water are introduced into the vanadium oxide systems to enforce the interlayer connection and increase electric conductivity. For example, Xia and Alshareef^[15] argued that double-layered calcium vanadium oxide bronze ($Ca_{0.25}V_2O_5 \cdot nH_2O$) is a more suitable cathode materials for ZIBs. Even sharing similar layered δ -type crystallographic structures with $Zn_{0.25}V_2O_5 \cdot nH_2O$, the replacement of Zn^{2+} by Ca^{2+} can introduce following merits:

- 1) $Ca_{0.25}V_2O_5 \cdot nH_2O$ shows a larger interlayer distance than $Zn_{0.25}V_2O_5 \cdot nH_2O$, very favorable for the diffusion of intercalated Zn^{2+} in the host lattice (GITT-determined diffusion coefficient: $Ca_{0.25}V_2O_5 \cdot nH_2O \sim 10^{-8} \text{--} 10^{-9} \text{ cm}^2 \text{ s}^{-1}$,^[15] one magnitude higher than that of $Zn_{0.25}V_2O_5 \cdot nH_2O$);^[8]
- 2) The lower molecular weight and density of $Ca_{0.25}V_2O_5 \cdot nH_2O$ are favorable for achieving higher gravimetric and volumetric capacity;
- 3) $Ca_{0.25}V_2O_5 \cdot nH_2O$ offer fourfold higher electrical conductivity than $Zn_{0.25}V_2O_5 \cdot nH_2O$ (Figure 6d).

Thanks to these features, the $Ca_{0.25}V_2O_5 \cdot nH_2O$ delivers impressive capacities of 340 and 289 mAh g^{-1} at 0.2 and 1 C, respectively. When cycled at 80 C, the $Ca_{0.25}V_2O_5 \cdot nH_2O$ cathode

retains ca. 96 % and ca. 78 % of its initial capacity after 3000 and 5000 cycles, respectively,^[15] outperforming the $Zn_{0.25}V_2O_5 \cdot nH_2O$. Beside foreign cations, Zhou and Mai et al. disclosed that the existence of structural water could also contribute a great improvement of electrochemical performance,^[41] analogous to the case of layered δ - MnO_2 .^[52] These works clearly suggest that crystal structural modulation is an effective way for performance optimization of ZIBs' cathodes.

Besides crystal structure modification, combining vanadium oxides with conductive agents (e.g., carbon nanotubes or graphene) can also improve their electrochemical performances by ensuring fast electron transport. For example, Wei and Wang et al.^[4] reported a composite cathode material consisting of $H_2V_3O_8$ (or $V_3O_7 \cdot H_2O$) nano-wires (3–5 μm lengths and 50–100 nm diameters) wrapped by graphene sheets. The $H_2V_3O_8$ is packed by V_3O_8 layers interconnected by hydrogen bonds.^[82] Compared to other layered vanadium oxides held by weaker van der Waals force (for example V_2O_5), the hydrogen bonds in $H_2V_3O_8$ could offer better structural integrity and stability during charge/discharge process (like roles played by $[ZnO_6]$ octahedra in $Zn_{0.25}V_2O_5 \cdot nH_2O$,^[8] or $[CaO_7]$ polyhedra in $Ca_{0.25}V_2O_5 \cdot nH_2O$).^[15] Also, the co-existence of V^{5+} and V^{4+} offers the $H_2V_3O_8$ nano-wires a higher electronic conductivity,^[83] the high average valence of vanadium (4.67) contributes more active redox sites and larger specific capacity. When prepared into nanostructured materials, especially combined with gra-

phene, the large electrode/electrolyte and $\text{H}_2\text{V}_3\text{O}_8$ /graphene contact area ensures fast electron and ion transport within $\text{H}_2\text{V}_3\text{O}_8$. Above-mentioned features endow the $\text{H}_2\text{V}_3\text{O}_8$ nanowire/graphene composite with a high capacity (394 and 270 mAh g^{-1} at 0.1 and 6 A g^{-1}), and excellent cycling stability (capacity retention = 87% after 2000 cycles). Based on the weight of $\text{H}_2\text{V}_3\text{O}_8$ /graphene composite and the theoretically required Zn, the battery offers a high energy density of 168 Wh kg^{-1} (or 34 Wh kg^{-1}) at a power density of 89 W kg^{-1} (2215 W kg^{-1}).

Taking advantages of the flexibility of graphene, Dai and Niu et al.^[80] further designed a freestanding rGO/VO₂ composite cathode for high rate ZIBs. In the composite cathode, rGO forms continuous and porous network, which can not only enhance ion and electron mobilization, but also effectively accommodate the repeated volume changes of VO₂ caused by charging and discharging (or Zn²⁺ extraction/insertion) cycles. In contrast to layered V₂O₅ derivatives, the VO₂ adopts a shear-type structure, very helpful to resist lattice shearing during Zn²⁺ insertion/extraction.^[84,85] As a result, a high energy density of 65 Wh kg^{-1} even at a high power density of 7800 W kg^{-1} is achieved in this ZIB. This device delivers also an excellent cycling stability with 99% capacity retention after 1000 cycles. The simultaneously achievement of high energy/power density and long cycling lifetime in these ZIBs suggested can probably bridge the gap between conventional batteries and supercapacitors, opening new opportunities for rationally powering portable electronic devices and hybrid electric vehicles. Taking good use of the flexibility of the cathode, Zn anode, and solid-state electrolyte, flexible soft-packaged ZIBs can also be assembled.^[51,86–88] One can refer to the instructive review article by Yu and Lu for systematic discussion on the topic of flexible ZIBs.^[5]

As discussed above, vanadium oxides always deliver high capacity ($> 300 \text{ mAh g}^{-1}$) and excellent rate capability, owing to their open layered structure and multiple oxidations. However, a majority of the capacity (over 80%) is distributed $< 1.0 \text{ V}$, leading to a low energy density regarding their high capacity. To overcome this problem, Ma and Zhi et al.^[89] introduced cobalt ions and water molecules into V₂O₅ as interlayer pillars, and successfully developed a novel high-voltage and long-lifespan cobalt vanadium bronze (Co_{0.247}V₂O₅·0.944H₂O). The pre-intercalation of cobalt ions remarkably increased the absorption energy of Zn²⁺, promoting the operational voltage of ZIBs up to 1.7 V, with 227 of 432 mAh g^{-1} discharge capacity located above 1.0 V (Figure 6e). This work gives a new approach for high performance vanadium oxide cathodes.

3.3. Sulfides

Molybdenum disulfide (MoS₂) is another important layered compound that holds possibility to develop into versatile intercalation electrode materials for secondary batteries. In ordinary, the via van der Waals bonded MoS₂ layers show a large interlayer distance of 0.62 nm (i.e., the distance between the two intermediate MoS₂ layers = 0.31 nm), permitting the

intercalation and transport of various ions, especially the alkaline ions.^[90] The application of MoS₂ as electrode materials of LIBs,^[91] sodium ion batteries,^[92] and potassium ion batteries^[93] has been widely reported. However, the reversible Zn²⁺ intercalation into MoS₂ is more difficult, due to the large size of hydrated Zn²⁺ (0.55 nm), the strong Coulombic ion-lattice interaction, and the low inherent conductivity of this material. Calculation shows that the Zn²⁺ intercalation into MoS₂ must be accompanied by the break of Zn²⁺-H₂O bonds and input of considerable energy, which can explain the low capacity and sluggish kinetics of reaction.^[94]

Implementation of crystallographic, defect, hydrophilicity engineering can effectively modify physical and chemical properties of this material, and boost the Zn²⁺-storage performances. In 2019, Li and Zhi et al.^[95] reported an expanded MoS₂ (E-MoS₂, 2H phase) vertically aligning on carbon fiber cloth (CC) as a promising cathode candidate for rechargeable and flexible ZIBs (Figure 7a–d). The expansion of interlayer spacing in this E-MoS₂ (from 0.62 nm of traditional bulky MoS₂ to 0.70 nm) could be ascribed to the intercalation of hydrated Na⁺ and NH₄⁺ during hydrothermal synthesis, which is very helpful to reduce the resistance/energy barrier of Zn²⁺ intercalation and diffusion. Furthermore, the hierarchical nanostructure of this freestanding E-MoS₂@CC composite shortens the Zn²⁺ diffusion pathways while enhancing the interfacial contact between E-MoS₂ and the electrolyte. This rational design achieves a noteworthy capacity of 202.6 mAh g^{-1} (mainly from capacitive process) in 2 M ZnSO₄ electrolyte. On the other hand, the ordinary commercially available MoS₂ only shows a capacity of 60 mAh g^{-1} under the same discharge condition.

DFT calculation indicates that the edges and sulfur vacancies in the 2H MoS₂ are primary adsorption sites attracting the preferential insertion of Zn²⁺, while the defect-free basal planes are inert. Inspired by this understanding, Xu and Wang et al.^[90] developed defect engineered MoS_{2-x} nano-sheets with rich sulfur vacancies as cathode of ZIBs. The defect-rich MoS₂ nano-sheets were prepared by a facile hydrothermal + heating method. Also, the defects and stacking faults cause an expanded interlayer spacing up to 0.66~0.68 nm, favorable for the intercalation and diffusion of Zn²⁺ ions to the active sites. The treatment can boost the capacity by one order of magnitude (e.g., from 5 to 100 mAh g^{-1}), apart from the enhancement of cycling stability.

DFT calculation also suggests the twin advantages of O-incorporation on 2H MoS₂.^[94] Firstly, only 5% oxygen incorporation can dramatically widen the MoS₂ interlayer spacing from 6.2 to 0.95 nm. Secondly, oxygen incorporation shows effectiveness on improving the hydrophilicity of this material. Therefore, Liang and Alshareef et al. deliberately reduced the hydrothermal temperature of CS(NH₂)₂ + (NH₄)₆Mo₇O₂₄·4H₂O solution down to 180 °C, at which the molybdate precursor might not completely decompose and the remaining Mo–O bonds can react with CS(NH₂)₂ to form the oxygen-incorporated MoS₂ (MoS₂–O, Figure 7e–f).^[96] The oxygen incorporation strategy can boost the Zn²⁺ diffusivity by 3 orders of magnitude and the Zn²⁺-storage capacity by 10 times (21 vs. 232 mAh g^{-1} ,

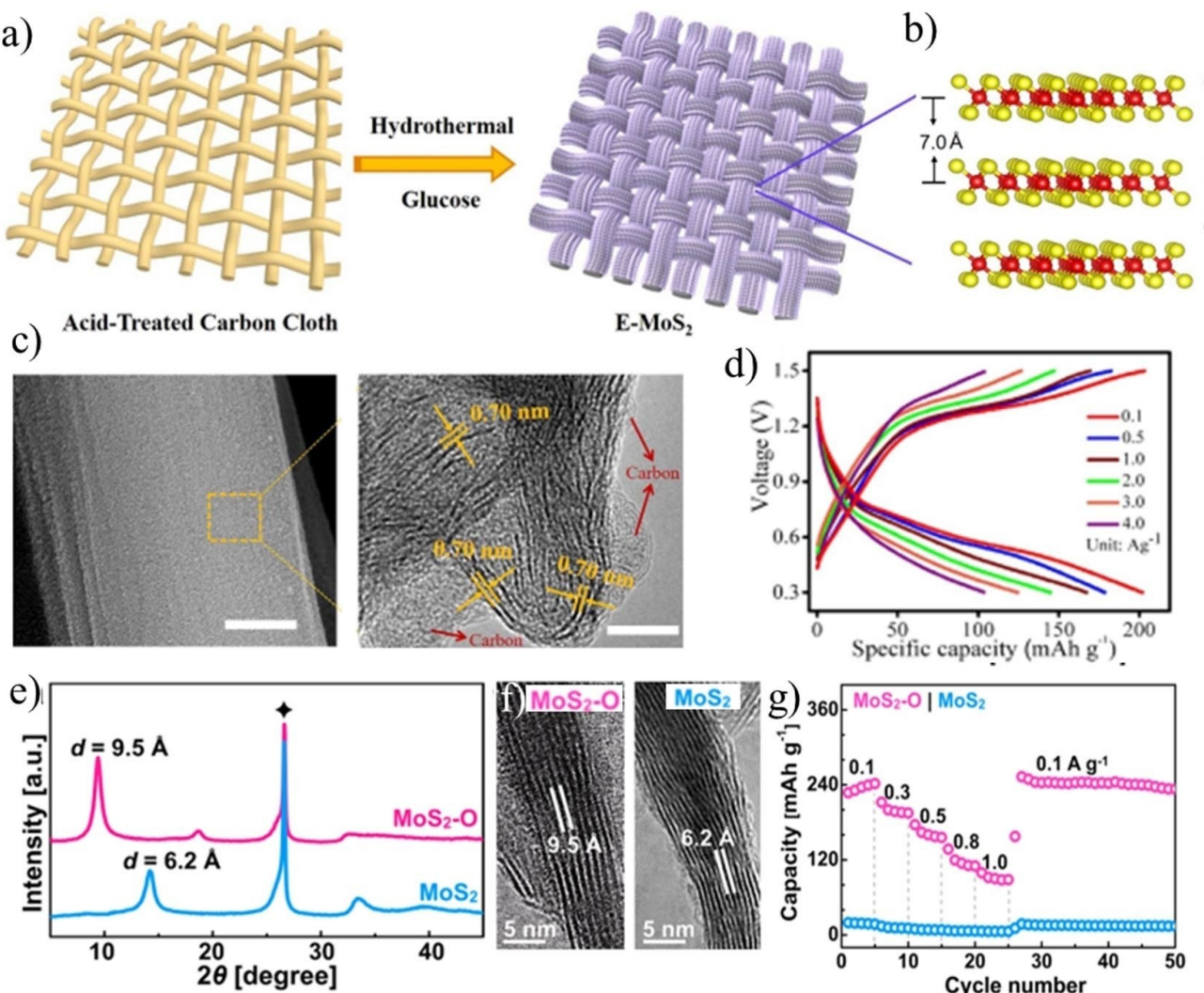


Figure 7. Hydrothermal preparation of E-MoS₂ cathode: a) fabrication schematic diagram, c) atomic structure, b) SEM images (Scale bars: 1 μm and 20 nm, respectively), and d) galvanostatic charge/discharge curves at various current densities. Reproduced with permission from Ref. [95]. Copyright 2019, Elsevier. Comparison of MoS₂-O with MoS₂: e) XRD patterns, f) TEM images, g) cycling stability under different current densities. Reproduced with permission from Ref. [94]. Copyright 2019, American Chemical Society.

Figure 7g).^[94] During Zn²⁺ intercalation, the layered structure of MoS₂-O was expanded but not exfoliated or damaged. Meanwhile, a phase transition from 2H to 1T polymorph occurred, suggesting the high reaction activity of this material.

Promising layered cathode candidates for batteries including also VS₂,^[43,97] VS₄,^[98] and Bi₂S₃.^[99] In 2017, An and Mai et al.^[43] first explored the Zn²⁺-storage behaviors of hydrothermally prepared 1T VS₂ nano-sheets (e.g., hexagonal metallic phase, interlayer spacing 0.576 nm^[97]), which achieved an impressive capacity of 190.3 mAh g⁻¹ in ZnSO₄ electrolyte, along with a long-term cycling stability. Furthermore, Zhi and Zhang et al.^[97] deposited hierarchical 1T VS₂ onto a stainless steel mesh, and developed a binder-free and freestanding cathode, VS₂@SS. Due to the close interconnection between the active material and current collector, this electrode exhibited an excellent Zn²⁺-storage capacity of 198 mAh g⁻¹ and stable cycling performance. Significantly, the electrode worked still well at a very high mass loading of ~11 mg cm⁻², a level competing with the

commercial batteries. Characterizations indicate that this material undergoes two electrochemical processes, a reversible intercalation/de-intercalation processes at ~0.7 V vs. Zn/Zn²⁺,^[43] and a conversion process between Zn²⁺-inserted VS₂ and V₃S₄ at ~0.6 V.^[97]

Patronite vanadium sulfide (VS₄), an analogue of VS₂, is a remarkable host material for cations, including Li⁺, Na⁺, Al³⁺. The charge storage process of VS₄ involves an anionic redox mechanism from pristine S₂²⁻ dimer to S²⁻. Recently, Qin et al. demonstrated a patronite VS₄ anchored on reduced graphene oxide (VS₄@rGO) as high performance cathode of ZIBs.^[98] The hydrothermally prepared VS₄@rGO can deliver a decent capacity of 180 mAh g⁻¹ in 1 M Zn(CF₃SO₃)₂ electrolyte. Interestingly, a synergistic reaction mechanism composed of intercalation and conversion seems responsible for the Zn²⁺-storage process in this material, alike the case of LIBs.^[100]

Furthermore, Xiong and Xue et al.^[99] also proposed a Bi₂S₃ cathode for ZIBs. The Bi₂S₃ nano-particles were synthesized by a

precipitation + low temperature process. In this sulfate material, the highly anisotropic layer structure bonded by weak van der Waals interaction provides sufficient pathway for foreign ions to intercalate into and diffusion (i.e., giving a high ionic conductivity). Therefore, a capacity of 161 mAh g^{-1} at 0.2 A g^{-1} and an excellent cycling stability can be readily achieved in ZnSO_4 electrolyte. The capacity stems mainly from capacitive process, accompanied by a small fraction of contribution from intercalation/de-intercalation process. While demonstrating encouraging capacities ($160 \sim 240 \text{ mAh g}^{-1}$), all these sulfate cathode materials quite suffer from low average discharge voltages ($0.6 \sim 0.7 \text{ V}$), a major disadvantage for the achievement high energy density.

3.4. Metal Hexacyanoferrates (Prussian Blue Analogues)

To establish a primary impression on Prussian blue analogues, the crystal structure of a cubic nickel hexacyanoferrate (Ni-HCFs for short, a typical metal hexacyanoferrate or Metal-HCF) is showed in Figure 8a,^[36] which shares the same cubic open framework structure with Prussian blue.^[44] In this crystal, the Fe^{3+} and Ni^{2+} ions form an ordered arrangement on the B sites, which are coordinated by C and N, respectively.^[101] The triple-bonded $-\text{C}\equiv\text{N}-$ ligands increase the separation between Fe^{3+} and Ni^{2+} ions to open up large cage structures (A sites, 3.2 \AA), making them high accessible for cation and small molecule insertion. Putting different metal ions on the B sites results in a rich Metal-HCF (or Prussian blue analogues) family that shares a general formula of $\text{A}_x\text{M}_1[\text{M}_2(\text{CN})_6] \cdot n\text{H}_2\text{O}$ (M_1 and M_2 =divalent and trivalent metal ions, A=inserted/mobile metal ions, $x=0$ to 2 with corresponding changes in the oxidation states of M_1

and M_2 ions).^[36,102] In general, Metal-HCFs are non-toxic, inexpensive, and easy to synthesize.^[44]

Because of the interesting structures, Metal-HCFs have garnered much attention as intercalation-type cathodes for secondary batteries.^[103] In this kind of open-framework structures, the large channels along A sites provide large enough spaces for cation diffusion and insertion,^[36] while the high-valence Fe^{3+} can neutralize the positive charges of the inserted cations by switching into Fe^{2+} .^[25] At the beginning, researches were focused on the reversible storage of alkaline metal ions (such as Li^+ , Na^+ and K^+) in the cubic Metal-HCFs hosts.^[104,105] In particular, Ni-HCFs and Cu-HCFs demonstrate an excellent cycle life and high-rate capability for reversible insertion of K^+ and Na^+ cations.^[101] In aqueous electrolyte, the water molecules in the solvated shells of charge-carrying cations interchange with zeolitic water on the A sites in Metal-HCFs.^[101,106,107] These water molecules can also partially shield electrostatic interactions between the charge-carrying cations and the host crystal, facilitating ion insertion into the host material (like the water assisting insertion process of Mg^{2+} into V_2O_5 electrodes).^[36,108] Ferricyanide vacancies ($\sim 5 \text{ \AA}$ in diameter) may provide additional diffusion paths for ions' insertion.^[109]

The success of monovalent ion insertion has motivated researchers to explore these materials for divalent insertion. In 2013, Cui's group reported the reversible insertion of divalent alkaline earth cations (i.e., Mg^{2+} , Ca^{2+} , Sr^{2+} and Ba^{2+}) in the cubic Ni-HCFs.^[36] Ex situ XRD spectra of the Ni-HCFs electrodes indicate that the crystal increases by only 1.3, 1.1, and 0.9% in strain during full insertion of K^+ , Mg^{2+} , and Ba^{2+} , respectively. The low lattice expansion ($\sim 1\%$) indicates that the A sites of the open-framework Metal-HCFs are large enough for stable and reversible storage of a verity of cations. Recently, Zhang,^[110]

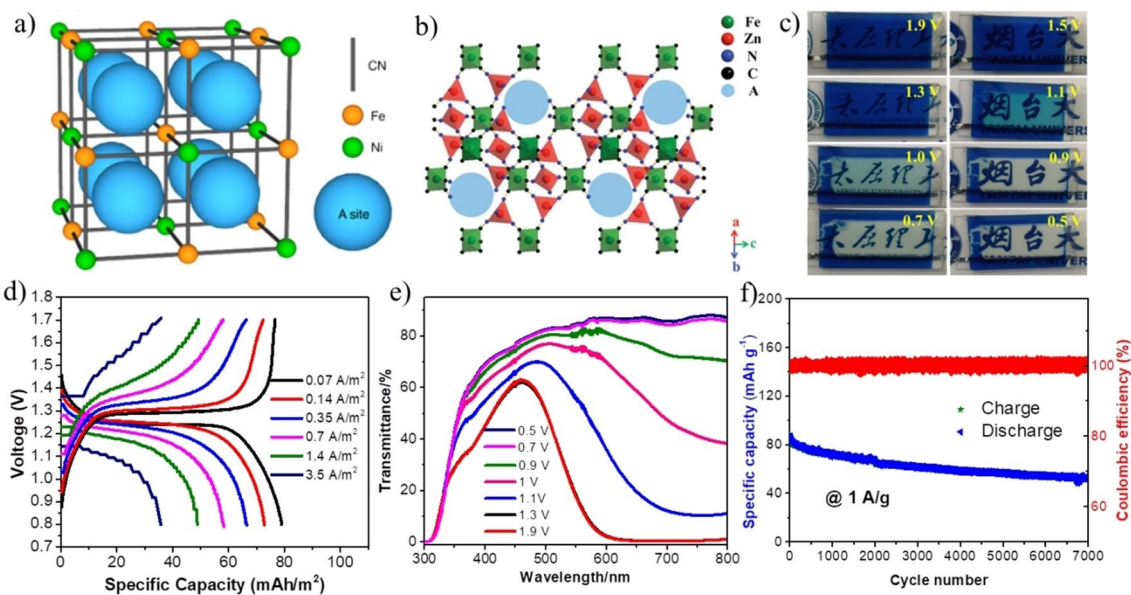
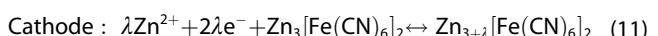


Figure 8. The crystal structure of a) cubic Ni-HCF. Reproduced with permission from Ref. [36]. Copyright 2019, American Chemical Society and b) rhombohedral Zn-HCF. Reproduced with permission from Ref. [110]. Copyright 2015, Wiley-VCH. Photographs (c), galvanostatic charge-discharge (GCD) curves (d), transmittance spectra (e), cycling stability (f) of a Zn-Fe-HCF battery in a $0.9 \text{ M KCl} + 0.1 \text{ M } \text{Zn}(\text{CH}_3\text{COO})_2$ dual-cation electrolyte. Reproduced with permission from Ref. [113]. Copyright 2020, Wiley-VCH.

Trócoli^[25] and Liu^[44] separately reported a rhombohedral Zn-HCF, a cubic Cu-HCF, and a cubic Fe-HCF (Prussian blue) cathode for ZIBs. The cubic Cu-HCF and Fe-HCF have very similar cubic crystal structure,^[36] implying a similar reaction kinetics for ion insertion.^[111] The rhombohedral Zn-HCF exhibits a different structure but still possesses large open sites (A sites, Figure 8b), ensuring the smooth and reversible insertion of monovalent and divalent cations (such as Na^+ , K^+ , Cs^+ and Zn^{2+}) and water molecules.^[107,112]

Electrochemical tests of the Zn-HCF in different sulfate aqueous electrolytes indicate the superior cycling stability of Zn^{2+} insertion over the Na^+ and K^+ , even though the diffusion kinetics of Zn^{2+} in Zn-HCF is slower than those of Na^+ and K^+ .^[110] Low dissociation trend of Zn-HCF in the ZnSO_4 electrolyte is in charge of the high cycling stability, resulting in a decent capacity retention of around 76~81% after 100 cycles. While, the large electrostatic interaction between divalent Zn^{2+} insertion ions and host atoms should be the main reason of the slow kinetics and the obvious capacity loss during cycling.^[36,73] At 60 mA g^{-1} , Zn^{2+} -storage capacity of the Zn-HCF reaches up to $\sim 74 \text{ mAh g}^{-1}$ in ZnSO_4 electrolyte. When coupled with a Zn metal anode, both Zn-HCF and Cu-HCF cathodes yield an average operation voltage of $\sim 1.7 \text{ V}$, a record-high volume for ZIBs at the reported time.^[25,110] Deep analyses indicate that reversible Zn^{2+} insertion is responsible for the electrochemical capacity of all Metal-HCF cathodes in the ZIBs. For the case of Zn-HCF, the chemistry of this cathode can be expressed as [Eq. (11)].^[110]



For practical applications, the limited specific capacities (40~120 mAh g^{-1} ^[4,44,110] depending on the current density), relatively poor rate capability stemming from the slow Zn^{2+} -diffusion kinetics,^[44] and the short cycle lifetime associating with the Metal-HCF dissociation^[110] are the major obstacles for Metal-HCFs. Very recently, our group developed a 0.9 M $\text{KCl} + 0.1 \text{ M Zn}(\text{CH}_3\text{COO})_2$ dual-cation electrolyte to stable not only Fe-HCF cathode but also Zn anode, achieving an ultra-long lifetime of 7,000 cycles with capacity retention of 60.7%.^[113] Pay attention that the Fe-HCF was deposited on a transparent conducting FTO glass, resulting in a bi-functional device with excellent electrochromic and energy storage ability(Figure 8c-f). This device represents an emerging class of versatile electrochromic batteries (or energy storage smart windows), which can effectively increase the energy efficiency of buildings by means of light and electric energy management.^[114-116]

From quite different point of view, Yang et al.^[46] argue that the low utilization efficiency of C coordinated Fe ($\equiv \text{C}-\text{Fe}$) should be an important reason for the poor rate performance and relatively low working voltage of Metal-HCFs. In the case of Na^+ storage in FeHCF, $\sim 68\%$ of the capacity attributes to the redox reaction of $\equiv \text{N}-\text{Fe}$ at $\sim 0.1 \text{ V}$ vs. Ag/AgCl , while the residual capacity attributed to $\equiv \text{C}-\text{Fe}$ at $\sim 0.8 \text{ V}$.^[117] Based on the above understanding, Yang et al., for the first time, established a high-voltage scanning strategy to activate $\equiv \text{C}-\text{Fe}$ and improve FeHCF's cycling stability and rate performance.^[46]

For further performance improvement, this group further proposes a Co-HCF cathode material for ZIBs.^[118] By making good use of the two-species redox reaction of $\text{Co}(\text{II})/\text{Co}(\text{III})$ and $\text{Fe}(\text{II})/\text{Fe}(\text{III})$, the materials deliver a high working voltage plateau of 1.75 V and a high capacity of 173.4 mAh g^{-1} , the highest capacity of Metal-HCF cathodes for ZIBs.

3.5. NASICON Compounds

Besides manganese, vanadium oxides and metal hexacyanoferates, NASICON polyanionic compounds (formula = $\text{AxMM}'(-\text{XO}_4)_3$, A = Li, Na, Mg, etc., M, M' = Ti, V, Cr, Fe, etc., X = P, Si, S, etc.) are also an important family of intercalation cathode materials for secondary batteries.^[10,119] An in-depth structure research by Gu et al.^[120] suggests that there are two kinds of Na sites (6b and 18e) existing in the $\text{Na}_3\text{V}_2(\text{PO}_4)_3$ lattice, according to their different coordination environments (coordination number = 8 and 6, respectively). When be charged, the two Na^+ ions on the 18e sites are extracted while the Na^+ ions on the 6b sites remain immobilized, leading to the formation of $\text{NaV}_2(\text{PO}_4)_3$ with large Na^+ -storable open sites. Due to their stable framework, large channels and rapid ionic diffusion capability, NASICON compounds have been widely investigated as long-life intercalation cathode materials of Li^+ and Na^+ storage.^[121-124]

Considering the smaller size of Zn^{2+} than Na^+ (0.74 vs. 0.99 Å), Huang et al. firstly realized and confirmed the reversible storage ability of Zn^{2+} in a graphene-like carbon wrapped $\text{Na}_3\text{V}_2(\text{PO}_4)_3$ (NVP@C, Figure 9a).^[10] The NVP@C, which was prepared through a two-step "hydrothermal + post-annealing" approach, consists of ~100 nm NVP nano-particles wrapped by carbon nano-sheets. The carbon shells provide a continuous 3D network for fast electron transport, while the nano-scale dimensions of the NVP particles effectively shorten the migration distance of Zn^{2+} within the host material. With a mild $\text{Zn}(\text{CH}_3\text{COO})_2$ electrolyte to depress the H^+ corrosion on vanadium, Huang's group designed a novel high-rate NVP@C/ $\text{Zn}(\text{CH}_3\text{COO})_2/\text{Zn}$ aqueous battery system.^[10] XPS and in situ XRD measurement indicates that the pristine $\text{Na}_3\text{V}_2(\text{PO}_4)_3$ firstly lost the two 18e-site Na^+ ions and transformed into $\text{NaV}_2(\text{PO}_4)_3$ till charge voltage $> 1.46 \text{ V}$ (Figure 9b-c). In following cycles, reversible insertion and extraction of Zn^{2+} ions into/from the $\text{NaV}_2(\text{PO}_4)_3$ matrix occurred, delivering a reversible discharge capacity of 97 mAh g^{-1} with an relatively low average discharge voltage of 1.1 V (at a current density of 50 mA g^{-1} , Figure 9b-c). In this battery, rapid capacity decay occurred within the initial 10 charge-discharge cycles, possibly caused by the lattice distortion accompanying with Zn^{2+} insertion. After 100 cycles, 74% of the initial capacity retained. Furthermore, Huang et al. also designed a $\text{Na}^+/\text{Zn}^{2+}$ dual-cation electrolyte to further optimize the kinetic and performance of this NVP@C/Zn battery (will discussed in section 3.6).^[125]

Depart from the Zn^{2+} mechanism proposed by Huang, Zhou and Mai et al.^[126] argues that the simultaneous $\text{Zn}^{2+}/\text{Na}^+$ intercalation/de-intercalation may be responsible for the capacity of $\text{Na}_3\text{V}_2(\text{PO}_4)_3@\text{reduced graphene oxide}$ (NVP@rGO) in

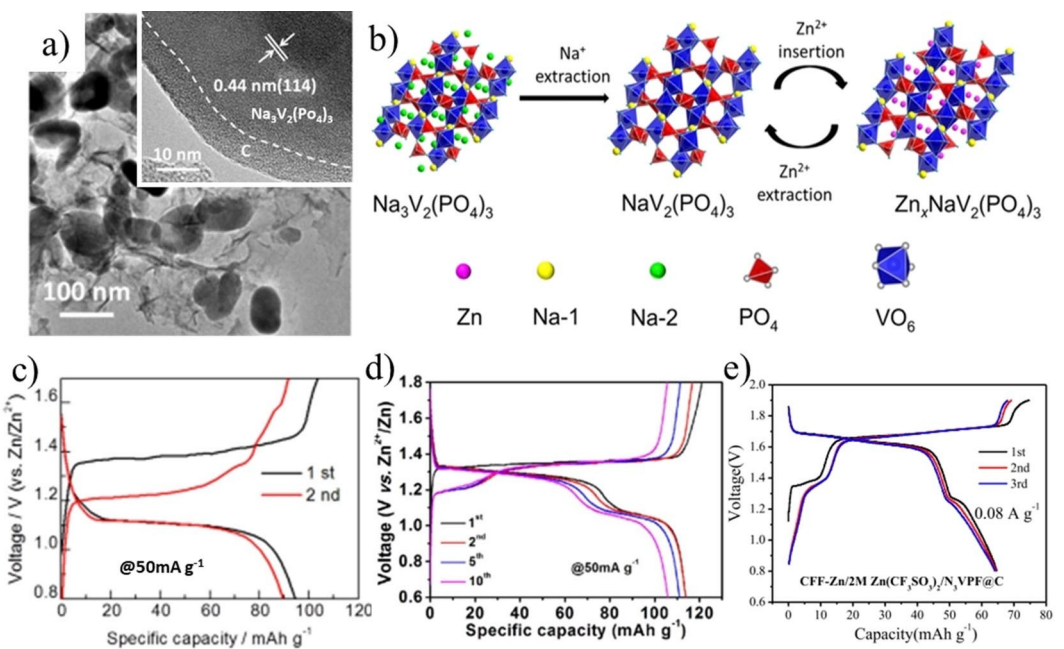


Figure 9. a) TEM images, b) schematic representation for Zn²⁺ storage mechanism, c) galvanostatic charge-discharge curves of Na₃V₂(PO₄)₃@C in 0.5 M Zn (CH₃COO)₂ electrolyte. Reproduced with permission from Ref. [10]. Copyright 2016, Elsevier. Galvanostatic charge-discharge curves of d) Na₃V₂(PO₄)₃@rGO (reproduced with permission from Ref. [126], Copyright 2019, Elsevier) and e) Na₃V₂(PO₄)₂F₃@C, in 2.0M Zn(CF₃SO₃)₂/NPF₆@C. Reproduced with permission from Ref. [119]. Copyright © 2018, Elsevier.

a 2.0M Zn(CF₃SO₃)₂ electrolyte (pH=4). Indeed, the NVP@rGO exhibits two discharge voltage plateaus and bimodal CV curves in the Zn(CF₃SO₃)₂ electrolyte,^[126] quite difference from the single voltage plateau and unimodal CV curves in the Zn (CH₃COO)₂ electrolyte (Figure 9d).^[10] The dominant reduction/oxidation plateaus/peaks at higher potentials are assigned to the Na⁺ insertion/extraction processes (the contribution of H⁺ insertion/extraction is negligible^[119]), and the secondary plateaus/peaks are the Zn²⁺ insertion/extraction processes. The Na⁺ insertion/extraction peaks gradually weaken during cycling, possible due to the trace amount of Na⁺ in the electrolyte. At the same time, the Zn²⁺ insertion/extraction processes become stronger. If Na⁺ is electrochemically pre-extracted from the Na₃V₂(PO₄)₃ (i.e., becomes Na_xV₂(PO₄)₃) before battery assembling, the resulting Na_xV₂(PO₄)₃/Zn(CF₃SO₃)₂/Zn shows only the characteristics of Zn²⁺ insertion/extraction processes, due to the totally absence of mobile Na⁺ in the electrodes. This work clearly shows the dependence of charge storage mechanism of NVP on electrolytes.

To further improve performance of ZIBs, Wang et al.^[119] examined a composite cathode material of carbon coated NASICON-typed Na₃V₂(PO₄)₂F₃ (Na₃V₂(PO₄)₂F₃@C). Due to the strong affinity of F atoms toward the neighboring cations, Na₃V₂(PO₄)₂F₃ holds higher structure stability and higher redox potential than Na₃V₂(PO₄)₃,^[127] favorable for the achievement of high voltage and long cycling stability for ZIBs. In 2.0M Zn (CF₃SO₃)₂ electrolyte, the Na₃V₂(PO₄)₂F₃@C/Zn battery delivered ~0.5 V higher working voltages than the Na₃V₂(PO₄)₃ counterpart (ca. 1.62 V, Figure 9e), very desirable for the elevation of battery's energy density. The authors also developed a carbon-coating method to alleviate the dendritic Zn deposition on the

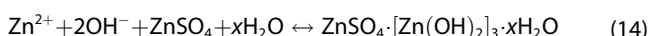
Zn anodes (will discussed in section 4), and achieved a 4000-cycle long lifetime at a current density of 1 Ag⁻¹ with 95% capacity retention. In even a flexible pouch battery configuration, its lifetime is still significant (600 cycles with 80.6% capacity retention), reflecting the promise of NASICON compound-based ZIBs for practical application.

3.6. Co₃O₄

Due to the high redox potential of Co(II)/Co(III) (1.83 V vs. SHE), Zn/Co₃O₄ batteries are one of the few aqueous electrolyte batteries with a potential > 2 V voltage (theoretical voltage = 2.59 V). However, conventional Zn/Co₃O₄ batteries are operated in alkaline electrolytes, resulting in poor cycling stability associating with the formation of ZnO, Zn(OH)₂, carbonate, as well as the dendritic Zn deposition.^[20] As discussed in section 2, replacing alkaline electrolytes with mild ones can effectively slow the detrimental side reactions on the Zn anode side. Recently, Ma and Zhi et al.^[128] initiated a high voltage, high stable and flexible Co₃O₄/Zn battery with mild aqueous electrolyte (ZnSO₄+CoSO₄) by taking full use of the redox potential difference between the Co₃O₄ cathode and the Zn anode. In this mild Co₃O₄/Zn battery, excess amount of Co(III) was intentionally introducing into the Co₃O₄ cathode material, in order to enhance its electrochemical kinetics. Experimental results indicate that a high charge voltage (up to 2.2 V), high specific capacity (205 mAh g⁻¹ at current density of 0.5 Ag⁻¹) and long-cycling lifespan (up to 5000 cycles with a capacity retention of 92%) are simultaneously achieved in this battery, thanks to the rational design of both cathode material and

electrolyte. The oxygen evolution reactions from water splitting at 2.26 V (vs. Zn/Zn²⁺) limits further widening the working voltage.

To clarify the energy storage mechanism of the Co(III) rich-Co₃O₄ cathode, the authors employed ex situ TEM, XRD and Raman techniques to monitor the structure evolution of the cathode. The ratio of Co(III)–O/Co(II)–O Raman sign decreased from 1.15 to 0.98 during discharging, and recovered back to 1.15 in the following charging process. Similar variation of the Co³⁺/Co²⁺ ratio was also detected in the XPS test (from 1.68 to 0.45 and back to 1.68 in a discharging-charging cycle). The Co (II) species in the discharged cathode materials is determined to be face-centered cubic CoO by both TEM and XRD characterization. Therefore, the author proposed a conversion reaction mechanism between CoO and Co₃O₄ for the charge-discharge reactions of the Zn/Co(III) rich-Co₃O₄ battery, which can be expressed as below [Eqs. (12)–(16)]:



Overall : < for nr = φfo16φ >

3.7. Cathodes for Dual-Cation ZIBs

In conventional mild ZIBs, Zn²⁺ cations (and sometimes also H⁺)^[28] are charge carriers for the battery chemistry. As a result, only materials with Zn²⁺/H⁺ storage ability can be used as cathodes of ZIBs. Introducing second kind of cation (foreign cation) into electrolytes makes it possible to employ intercalation cathodes of other batteries into ZIBs,^[129,130] resulting in dual-cation ZIBs or Zn hybrid batteries.^[6] During charge, Zn²⁺ ions in the electrolyte are electrochemically plated onto the Zn metal anodes. At the same time, the cathodes de-intercalate foreign cations into the electrolyte, in order to compensate the cation loss of electrolyte caused by Zn plating reactions. In discharge, reverse Zn-striping/foreign cation intercalation reactions occur on the anode/cathode sides, respectively. By this way, a variety of cathodes can be used to couple with Zn metal anodes and form diverse new hybrid ZIBs.^[130,131] The rationally designed dual-cations electrolyte may even benefit the cycling stability of the ZIBs, because of the improved reaction kinetics and sometimes also the depression of Zn dendrite growth.^[113,132] In dual-cation ZIBs, enough Zn⁺ and foreign cations must be pre-stored in the electrolyte to ensure the full use of the electrodes. This requirement may limit the energy density of batteries, if the solubility of cations' source salts is low.^[132]

Zn²⁺/Li⁺ dual-cation batteries: In as early as 2006, Kengo and Nagakazu^[129] had reported a Zn/LiMn₂O₄ rechargeable

battery with a Li₂SO₄+ZnSO₄ electrolyte, which delivers an average discharge voltage of 1.55 V and a decent capacity of ~70 mAh g⁻¹ (by the mass of LiMn₂O₄, with a very high mass loading of 50 mg cm⁻³). Despite suffering from limited cycling stability (<250 discharge/charge cycles), Kengo's battery design instigates a number of studies on this Zn²⁺/Li⁺ dual-cation battery.^[130] In fact, LiMn₂O₄ is a mechanically stable cathode material with only ~7% volume change from its lithiated (discharged) to non-lithiated (charged) state. In practice, cycling stability of LiMn₂O₄ may be limited by its dissolution into electrolyte following the disproportion reaction of 2Mn³⁺→Mn²⁺ + Mn⁴⁺, especially in acidic environment. On the other hand, a electrolyte pH<9 is also required for complete Li de-intercalation from LiMn₂O₄ before oxygen evolution.^[133] In neutral aqueous electrolytes (e.g., LiSO₄), LiMn₂O₄ cathodes in hybrid super-capacitors can demonstrate up to 3000 cycles with almost no capacity fading.^[134] By chemical doping or surface coating, the cycling stability of LiMn₂O₄ cathodes can be further prolonged.^[135]

In 2012, Yan et al. demonstrated a 1.8 V Zn–LiMn₂O₄ battery with commercial LiMn₂O₄ cathode and a ZnCl₂+LiCl electrolyte (pH=4).^[133] It is found that replacing pure LiMn₂O₄ with doped counterpart can improve the battery's capacity retention from ~90% after 1000 cycles up to 95% after 4000 cycles. In situ XRD patterns of the LiMn₂O₄ cathode clearly revealed the reversible Li⁺ insertion/extraction reactions during cycling. Recently, similar Zn/LiCl-ZnCl₂/LiFePO₄ dual-cation battery is also reported.^[131] This battery delivers flat discharge curves with an average work voltage of 1.2 V, and a capacity of 92 mAh g⁻¹ after 400 cycles at even a high current density of 1020 mA g⁻¹. In the case of aqueous batteries, the large scale application of Li⁺ intercalation cathodes maybe limited by the high cost of lithium.

Zn²⁺/Na⁺ dual-cation batteries: As discussed in section 3.4, NASICON-type Na₃V₂(PO₄)₃, as intercalation host, can accommodate both Zn²⁺ and alkaline metal cations (such as Na⁺).^[10,125] The high natural abundance of sodium makes the application of Na⁺ intercalation cathodes more cost-efficient than the Li⁺ intercalation compounds. Also, the kinetics of Na⁺ insertion into the host materials are generally faster than the Zn²⁺ intercalation reactions, because of the low charge density of Na⁺. Therefore, Na₃V₂(PO₄)₃ prefers to intercalate Na⁺ in Zn²⁺/Na⁺ dual-cation electrolytes, resulting in a better electrochemical performance. For instance, Huang et al. found that Na₃V₂(PO₄)₃@C composite delivers an average discharge voltage of 1.42 V in a CH₃COONa+Zn(CH₃COO)₂ electrolyte,^[125] obviously higher than that in a pure Zn(CH₃COO)₂ electrolyte (1.1 V, Figure 9c),^[10] clearly reflecting the advantage of this Zn²⁺/Na⁺ dual-cation electrolyte design. In fact, before Huang's work, Wen and Wu et al.^[40] had already reported a Zn–Na_{0.95}MnO₂ dual-cation battery with analogous battery chemistry. The authors firstly prepared birnessite-MnO₂ (δ-MnO₂) by a hydrothermal method, and then doped the δ-MnO₂ with Na⁺ via a solid reaction approach. The resulting rod-like Na_{0.95}MnO₂ outputs a discharge voltage of 1.4 V and a capacity retention of 92% after 1000 cycles in CH₃COONa+Zn(CH₃COO)₂ electrolyte, near to the volume of Na₃V₂(PO₄)₃.^[125]

Zn²⁺/K⁺ dual-cation batteries: Analogous to the case of NASICON-type compounds, intercalating mono-valent cations into Metal-HCFs seems kinetically smoother than divalent cations.^[103] In particular, the intercalation reaction of K⁺ into Metal-HCFs (e.g., Cu-HCF and Ni-HCF^[104]) delivers highest redox potential and best cycling stability among alkali cations, due to its small hydrated ion size.^[136] Taking this advantage into account, a Zn–Fe-HCF battery is designed with a Zn²⁺/K⁺ dual-cation electrolyte (i.e., 0.9 M KCl + 0.1 M Zn(CH₃COO)₂).^[113] Systematic analyses indicate that introducing K⁺ into electrolyte benefits the reactions on both anode and cathode sides, resulting in an ultra-long cycling life of 7000 cycles. In addition, the couple of Zn and Fe-HCF enables the battery remarkable color-changing (i.e., electrochromic) ability. That is to say, charge/discharge process can effectively modify the color of this transparent battery.^[137]

Zn²⁺/Al³⁺ dual-cation batteries: Besides the dual-cation Fe-HCF/Zn batteries, an elaborate Zn²⁺/Al⁺ dual-cation ZIBs has also been designed by Li and Elezzabi et al.,^[114] by making good use of the Al³⁺ storage in WO₃.^[138] As a famous electrochromic material, the WO₃ cathode can switch between colorless and blue color during charging/discharging in the ZnSO₄ + AlCl₃ aqueous electrolyte. Moreover, this group also developed a variety of electrochromic ZIBs.^[114–116] Wen and Wu's group have also proposed a Zn²⁺/Al⁺ dual-cation battery with a composite Al₂(SO₄)₃/Zn(CHCOO)₂ aqueous electrolyte, a Zn metal anode and an expanded graphite nano-sheet cathode.^[139] To prepare the expanded graphite nano-sheets, a graphite/NH₄NO₃/graphite symmetric cell was charged and discharged between 5 and –5 V successively. The high charge voltage oxidizes H₂O into O₂, and the discharge voltage reduces NO₃[–] into NO. These gaseous species produce large expanding force, and effectively enlarge the distance of graphitic layers.^[140] This graphite expansion process not only boosts Al³⁺ (in the form of [Al(H₂O)₆]³⁺) insertion/extraction and capacitive activity, but also reduces the charge transfer resistance due to the readily accessible structure of this electrode for the electrolyte. As a result, a 94 mAh g^{–1} discharge capacity with an average voltage of 1.0 V is achieved at 0.1 A g^{–1} in the expanded graphite nano-sheets, 37 mAh g^{–1} higher than the pristine graphite. This Zn²⁺/Al⁺ dual-cation device is attractive for large-scale stationary energy storage, since all its components are abundant, low-cost, and sustainable. Replacement of the expanded graphite nano-sheets with electric double layer electrode materials (e.g. activated carbons,^[141–143] carbon nanotubes and granophenes^[144]) gives a zinc-ion hybrid supercapacitors. In this kind of devices, dual-cation electrolytes are unnecessary, thanks to the electric double-layer charge storage mechanism of the activated carbons.^[145]

3.8. Organic Cathodes

With the ever-increasing demand for wearable electronic devices, flexible ZIBs with mild electrolyte are attracting more and more attentions, due to these non-toxic and non-corrosive natures.^[5,86,87,146] In this field, organic cathodes that are intrinsically bendable, lightweight, environmentally friendly are regarded as the sustainable alternative to conventional inorganic cathode materials.^[88,147–150] For example, electrochemical performance of Quinone compounds in aqueous electrolyte had been reported in as early as 1972, which shows that tetrachlorobenzoquinone showed a reduction potential of 0.7 V in dilute H₂SO₄ solution.^[151] Quinone- and hydroquinone-based electrochemical reactions are significant in also biological electron transport systems.^[152,153] Systematic researches indicate that quinone compounds are one kind of universal electrode for aqueous rechargeable (H⁺, Li⁺, Na⁺, K⁺, and Mg²⁺) batteries.^[154,155] Unlike in the case of organic-electrolyte batteries,^[156] quinones are barely soluble in water, which is helpful for the achievement of better cycling stability in aqueous electrolytes.^[154]

Recently, Chen et al.^[150] first reported a high performance degradable calix[4]quinone (C4Q)-cathode for aqueous ZIBs, which has an open bowl structure and eight carbonyls. Electrochemical performance comparison of several typical quinone compounds indicates that the quinone compounds with carbonyls (C=O double bond) in para-position (1,4-naphthoquinone/1,4-NQ, 9,10-anthraquinone/9,10-AQ, and C4Q) generally show higher capacity and lower charge/discharge gap (e.g., polarization) than those with carbonyls in ortho-position (1,2-naphthoquinone/1,2-NQ and 9,10-phenanthrenequinone/9,10-PQ) (Figure 10a), due to the small steric hindrance of the former compounds on Zn ion reactions. Meanwhile, it is also found that there is a direct relationship between the working potential of different quinones and the energy of their lowest unoccupied molecule orbital (LUMO). The lower LUMO energy indicates the higher discharge potential.^[157]

When coupled with a Zn metal anode, the C4Q cathode delivers a flat and safe operation voltage of 1.0 V with a high capacity of 335 mAh g^{–1} at 20 mA g^{–1} (Figure 10b), corresponding to uptake of 3 Zn²⁺ and utilization of six carbonyls (from C4Q to Zn_xC4Q). Density functional theory (DFT) calculations, ATR-FTIR and Raman analyses all indicate that the carbonyl groups (more precisely two carbonyls at the top and four carbonyls at the bottom) have low electrostatic potential (ESP) and should be the reactive sites for the uptake of Zn²⁺. Unfortunately, the discharge products of this organic cathode (i.e., Zn_xC4Q) are more soluble than the C4Q in aqueous electrolytes. The dissolved C4Q^{2x–} from Zn_xC4Q can diffuse to the Zn metal anode through conventional porous separators and cause side reaction on the anode side, resulting in quick capacity decay (in a manner very like the “shuttle effect” of polysulfides in Li/S batteries^[158,159]). Using Nafion cation-exchange separators to suppress the dissolution of the cathode, the battery simultaneously achieves low polarization (70 mV), high energy efficiency (93%) and high cycling stability (capacity retention = 87% after 1000 cycles at 500 mA g^{–1}). In this battery, the Nafion separator must be sealed strongly to prevent the “shuttle effect” of C4Q^{2x–}, imposing difficulties for their applications in flexible batteries (need to work while being bended).

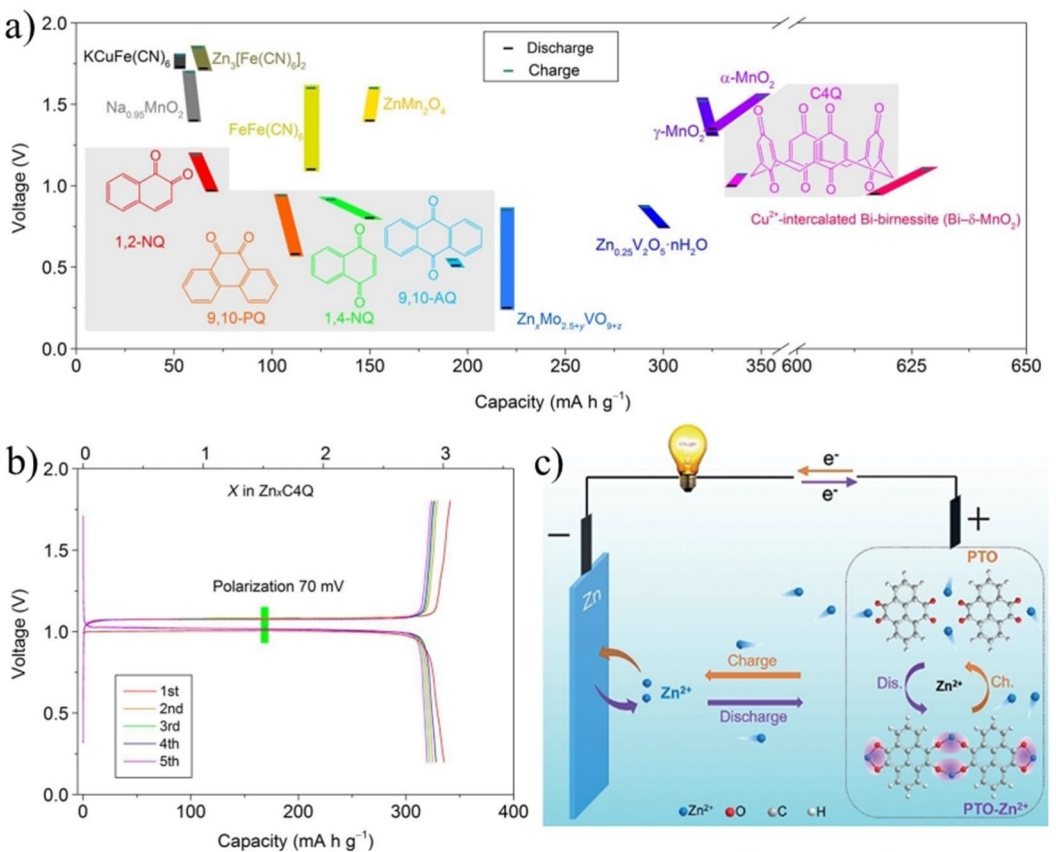


Figure 10. a) Comparison of discharge/charge voltages and capacities of the studied quinone compounds (1,2-NQ, 1,4-NQ, 9,10-PQ, 9,10-AQ, and C4Q) with typical cathodes of aqueous ZIBs. b) Galvanostatic discharge/charge curves of Zn–C4Q battery at the current density of 20 mA g⁻¹. The upper x-axis represents the uptake number of Zn ions. Reproduced with permission from Ref. [150]. Copyright 2018, American Association for the Advancement of Science. c) Illustration of the reversible reaction mechanism of the aqueous Zn-PTO battery. Reproduced with permission from Ref. [160]. Copyright 2018, Wiley-VCH.

To address this issue, Wang et al.^[160] developed a new pyrene-4,5,9,10-tetraone (PTO) cathode for aqueous ZIBs. Superior to C4Q,^[150] the PTO cathode shows inherent insoluble characteristic even in its discharge state. As a result, a low-cost glass fiber separator is enough to endow the PTO/Zn battery with a noteworthy cycling stability (~70% capacity retention after 1000 cycles). FTIR analyses show that the Zn²⁺ uptake ability of PTO originates from the coordination reactions between Zn²⁺ and the carbonyl groups (Figure 10c). This coordination/de-coordination Zn²⁺ storage mechanism introduces not only high capacity (reach up to 336 mAh g⁻¹ at 40 mA g⁻¹), but also a high super-capacitor-type rate capability (with capacity remaining at 162 and 113 mAh g⁻¹ at 5 and 20 A g⁻¹, respectively). Moreover, the PTO/Zn battery possesses excellent flexibility in a belt-shaped configuration, with almost no discernible capacity loss after folding for 80 times. For this PTO cathode, the low working potential (~0.75 V in average) is a main drawback that should be solved.

Furthermore, Liu et al.^[88] reported an integrated Zn-PANI (polyaniline) flexible battery. To prepare the flexible current collector, both sides of a filter paper (as separator) were successively coated with a cellulose nano-fiber layer and a 95 wt% graphite nano-platelet + 5 wt% cellulose nano-fiber conductive layer. Afterwards, the PANI cathode layer and the

Zn anode layer were separately coated onto different side of the treated filter paper via simple electro-deposition methods. After penetration with aqueous electrolyte (2 M ZnCl₂ + 3 M NH₄Cl), the Zn-PANI battery was completely made up. Compared with the sandwiched configuration flexible batteries assembled from isolated cathode, separator and anode, this integrative Zn-PANI battery is more tolerant of mechanical deformation (e.g., bending, folding or twisting), thanks to the close-connected interfaces. This rational structure design should also benefit achievement of excellent cycling stability and rate capability, due to the reduced interface resistance. At a current density of 0.5 A g⁻¹, the PANI cathode demonstrates a high specific capacity of 203.5 mAh g⁻¹.

More recently, Tie and Niu et al.^[161] developed a novel aqueous ZIB based on a diquinoxalino [2,3-a;2',3'-c] phenazine (HATN) cathode in 2 M ZnSO₄ aqueous electrolyte. The charge storage of the organic cathode of these ZIBs depends on fast and reversible H⁺ insertion/extractions, accompanied by highly reversible structural evolution. This is the first report on proton-storable organic cathode for mild aqueous ZIBs. The unique battery chemistry endows the Zn-HATN batteries with enhanced electrochemical performance, suggesting that organic cathodes are reliable approaches to mild aqueous ZIBs.

Table 2 summarizes the properties and challenges of different cathode materials. Among them, NASICON compounds and Metal-HCFs suffer seriously from the low practical capacities. Moreover, the implementation of NASICON compounds in ZIBs requires dual-cation electrolyte design in order to optimize the reaction kinetics, which may further depress the energy density of the resulting ZIBs. Organic cathodes exhibit superior capacities up to 300–400 mAh g⁻¹, but face also the problems of low output voltage and high prices, even though the contained elements themselves are abundant. Currently, the researches on organic ZIBs' cathodes are still in their very earlier stage.

The voltage predicament troubles also sulfate cathodes, which always need an activating treatment to boost capacity. Co-doping is an effective way to elevate the operation voltage of cathodes, due to the high redox potential of Co²⁺/Co³⁺. However, directly utilization of the expensive cobalt oxide cathodes will discount the cost advantage of ZIBs. Finally, Manganese oxides and vanadium oxides are the most studied cathode materials for high performance ZIBs. For vanadium oxides, their open layer structures give ZIBs high rate capability. However, these materials face the sever challenges of the uneasy toxicity and inadequate output voltages. Currently speaking, Manganese oxides, the oldest cathode of ZIBs, are still the prior choice for high performance ZIBs.

4. Anode Materials of ZIBs

4.1. Zn Metal Anodes

The competitiveness of ZIBs, to large extend, derives from the advantages of their Zn anodes including: 1) high theoretical capacity (820 mAh g⁻¹, or 5851 mAh mL⁻¹);^[15] 2) low price, high abundance and stable supply;^[11] 3) low redox potential (- 0.76 V vs. SHE);^[10] and 4) relative compatibility with water due to its high hydrogen evolution over-potential.^[8] However, Zn anodes seriously suffer from the growth of detrimental dendrites alike the cases of Li, Na, K, etc.,^[162,163] which not only enlarge polarization of anodes, but also cause sudden and quick cell-shorting in a unpredictable manner.^[56] The uncontrollable growth of metal dendrites is primarily triggered by the so-called “tip-effect”, which refers to a phenomenon of strong local electric field increase in the vicinity of tips and protuberances.^[164,165] During charging of ZIBs, the strong

electric field around Zn tips and protuberances will electrostatically attract Zn²⁺ ions from the electrolyte, and preferentially deposit them onto the top of these tips and protuberances, resulting in faster local Zn-plating rate. The growing tips and protuberances, in turn, enhance the tip effect and local electric field strength, forming a self-amplified vicious cycle. As a result, the tips and protuberances quickly involve into large and harmful dendrites.^[166,167]

To understand the detailed dendrite growth behaviors, Wang et al.^[168] stimulated the Zn dendrite growth using a phase-field model of COMSOL software under different deposition conditions, such as over-potential, electrolyte concentration, ion diffusion ability, ion conductivity and anisotropy strength. Their results suggest that dendrite growth is tightly related to the gathering of Zn²⁺ ions forced by the uneven distributed over-potential. The dendritic morphology would be formed at a critical over-potential typically greater than 60 mV.^[169] In a low rate and shallow charge-discharge mode, the over-potential of Zn electro-deposition is usually small.^[168] This property has been tactfully employed by Zhi et al.^[170] to develop an electro-healing methodology, which can in situ rescue Zn anodes of cycled ZIBs by eliminating the already-formed Zn dendrites.

The performances of Zn anodes are also seriously limited by the hydrogen evolution corrosion, i.e., the reduction of H⁺ in the electrolyte into H₂ bubbles by metallic Zn. This reaction not only consumes electrolytes and decreases batteries' Coulombic efficiency, but also forms insert ZnO, Zn(OH)₂ and zinc hydroxide sulfate that passivate the Zn anodes.^[171,172] The corrosion reactions between Zn metal and aqueous electrolyte (e.g., 3 M ZnSO₄) is not uniform, and the deepest corrosion pit reached upto 130 μm after a dwell time of 30 days.^[173] Even though some novel intercalation-type anodes have been suggested (such as Na_{0.14}TiS₂^[174] and Chevrel phase Zn₂Mo₆S₈),^[112,175] the majority of ZIBs still use excess-mass Zn metal as anodes (in forms of foil^[176,177] or powders)^[11,21,22,178] for ample Zn²⁺ supply. It is worth noting that Zn anodes with excess-mass (or shallow depth of discharge, DOD) will obviously depress the energy density of a fully packaged ZIBs, due to the heavy anode design with inefficient Zn utilization.^[11,179] If the DOD of Zn anode reaches to >50%, Zn–MnO₂ batteries will match or exceed the energy densities of some LIBs.

In order to depress the side reactions on Zn anodes, researchers have developed quite a number of innovative

Table 2. Comparison of various cathode materials used in ZIBs.

	Cost	Capacity [mAh g ⁻¹]	Average Volt. [V vs. Zn/Zn ²⁺]	True density [g cm ⁻³]	Toxicity
Mn-oxides	Low	150–350	~1.3	5–5.5	Low
V-oxides	Moderate	250–400	~0.8	3.3–4.3	High
Sulfides	High	150–250	0.6–0.7	VS ₂ : 2–3 MoS ₂ : ~5	Low
Metal-HCF	Moderate	40–120	1.2–1.7	~1.8	Low
NASICON	Moderate	80–120	1.1–1.6	~3.2	Moderate
Co ₃ O ₄	High	150–200	~1.9	~6.0	Moderate
Organics	High	300–400	0.6–1.0	~1.5	Low

strategies. Generally, the strategies can be categorized into three types: 1) anode modification,^[56,119,171,178] 2) development of new electrolytes^[12,21] or electrolyte additives,^[180,181] 3) construction of new current collectors.^[86,179,182,183] In this section, we mainly focus on the first strategy. The second and third strategies will be discussed in Section 5 and 6 regarding electrolytes and current collectors, respectively. Audiences can also refer to the specific review articles by Lu and Li et al.,^[177] Zhou and Liang et al.,^[184] or Zhang and Wang et al.^[185] for more information.

Zn/C composite anodes: In 2015, Li and Xu et al.^[178] prepared a composite anode of Zn powders and activated carbon for ZIBs. It is found that adding 12 wt.% activated carbon in Zn powder anode can increase capacity retention from 56.7 to 85.6% after 80 cycles. Comprehensive characterizations indicate that the pores of activated carbon can accommodate the deposited Zn dendrites. Analogously, Ma and Li et al.^[68] synthesized a 90% Zn+10% carbon black composite anode for ZIBs. This anode was prepared by annealing the mixture of Zn and carbon black powders at 500 °C for 1 h in Ar atmosphere. Afterwards, the annealed sample was grinded into fine powders for later electrode fabrications. During annealing, fused Zn can penetrate into the cavities between carbon black, and merged together with the conducting agents. ZIBs with Mn₃O₄@C nano-wire cathodes and the composite anodes show negligible capacity degradation within 2000 cycles. Sun, Liang and Jiang et al.^[186]

developed a well-designed Zn@C composite anode, by hydrothermally carbon-coating ZnO nano-particles and then electrochemically reducing the oxide into Zn metals. The anode delivers a much improved cycling stability than bare Zn anode in alkaline Zn–MnO₂ batteries with KOH electrolyte.

Other Zn-based composite anodes: Besides Zn/C composite anodes, there are also several works on other Zn-based composite anodes. In 2016, González et al.^[172] developed a layered double hydroxide (LDH, [Zn₄Al(OH)₁₀]₂(CO₃)·nH₂O/Zn composite anodes for ZIBs. The anode is made from slurry of LDH, Zn, carbon black, and PVDF binder by a hand painting method. During cycling, the control anode of Zn powder delivered growing over-potential for Zn nucleation, indicating a worsening Zn plating striping kinetics. On the contrary, the over-potential of the LDH/Zn anode decreased quickly even though it was large in the 1st cycle, due to the flatter morphologies of Zn deposits. The electro-deposition of Cd(II) and Pb(II) can also be modified by the LDH substrates.

More recently, Wang et al.^[171] pioneered a MOF-based host material for high-efficiency (~100%) and dendrite-free Zn plating and striping (Figure 11a). The host material is 500 °C annealed ZIF-8 under N₂ flow, which shows porous structure, trace amount of Zn⁰ in the framework, and high over-potential for hydrogen evolution. The Zn⁰ provides uniform nuclei for Zn plating, and the high over-potential for hydrogen evolution can reduce the undesired corrosion of Zn anodes. Pre-deposition of Zn on the annealed ZIF-8 film results in high performance Zn/

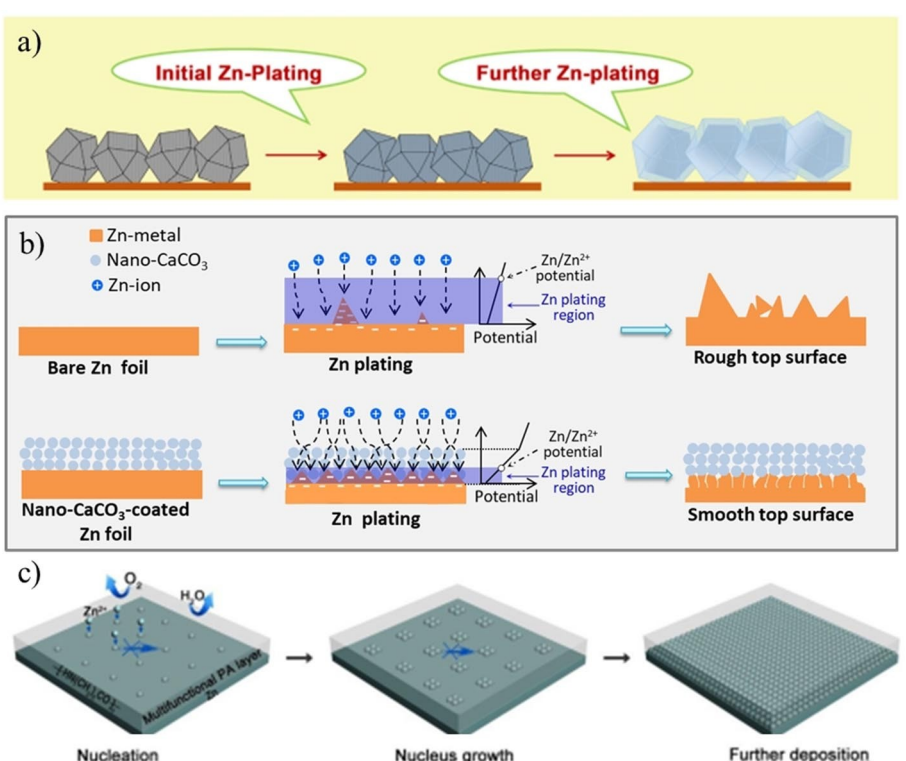


Figure 11. a) Schematic illustration of the Zn plating on the annealed ZIF-8 host. Reproduced with permission from Ref. [171]. Copyright 2019, Elsevier. b) Schematic illustrations of morphology evolution for bare and nano-CaCO₃ coated Zn foils during Zn striping/plating cycling. Reproduced with permission from Ref. [56]. Copyright 2018, Wiley-VCH. c) Schematic diagrams for Zn deposition on a polyamide/Zn(TfO)₂ composite film. Reproduced with permission from Ref. [190]. Copyright 2019, Royal Society of Chemistry.

ZIF-8 composite anodes, achieving 72% capacity retention after 20,000 cycles in the Zn-activated carbon super-capacitors.

Zn foil anodes with porous coatings: For LIBs, there is a spontaneously-formed SEI on the surface of anodes due to their low potential, which can forbidden further reactions between anodes and electrolytes while allowing smooth pass through of Li^+ . Inspired by this phenomenon, an appealing trend is emerging to design robust artificial SEI layers to depress Li dendrites and enhance the cycling stability of LIBs.^[162,165]

In ZIBs, there seem no convincing proofs showing the existence of SEI layers on most Zn anodes. Nevertheless, more and more works clearly indicate the beneficial influences of rationally designed layer on depressing Zn dendrites and stabilizing Zn anodes. In 2018, Wang and Jiang et al.^[119] proposed a carbon-coating method to improve the cycling stability of Zn anodes. The ~0.1 mm carbon film consists of 80% Super P+20% PTFE, and can effectively enhance the cycling stability of $\text{Na}_3\text{V}_2(\text{PO}_4)_2\text{F}_3@\text{C}/\text{Zn}$ batteries by inhibiting the dendritic Zn growth on anodes. At the same year, our group developed a nano-porous $\text{CaCO}_3/\text{PVDF}$ layer for highly stable Zn anodes (Figure 11b).^[56] This layer can guide an even Zn^{2+} flux within its nano-scale channels, enabling the formation of uniform, small-sized Zn nuclei with low polarization. At the same time, the insulating nature of the layer can confine the Zn plating reaction to the Zn foils' surfaces, leading to a position-selected, bottom-up deposition process of uniform Zn micro-flake array, rather than uneven, detrimental large dendrites. That is also the reason why the insulating CaCO_3 coating outperforms its conductive Super-P counterpart on stabilizing Zn anodes.

Beside CaCO_3 coatings, Liang and Zhou et al.^[187,188] confirm that coating Zn anodes with 3D nano-porous ZnO (3D-ZnO) or Kaolin architecture can also improve the Zn^{2+} transference kinetics and interface stability. The 3D-ZnO or Kaolin layers, which can effectively avoid "tip effect" and reduce the interface side-reactions and hydrogen evolution, was prepared by electro-deposition and slurry-coating process, respectively. After this modification, the anode achieved an average Coulombic efficiency of 99.55% and 1000 cycles long-time stability at a 1.3% depth of discharge. In addition, ZrO_2 coating are also effective for stabilizing Zn anodes, due to the depression of dendrite growth and corrosion reaction.^[189]

Zn foil anodes with dense coatings: In LIBs, the anodes evolve dense SEI surface layers to protect further decomposition of the electrolytes on the electrodes. It is thus reasonable to speculate that a dense surface coating should be more effective to depress the side reactions between aqueous electrolytes and Zn anodes. In 2019, Zhao and Cui et al.^[190] innovated a polyamide (PA)/zinc trifluoromethanesulfonate ($\text{Zn}(\text{TfO})_2$) composite film, representing an important breakthrough in this field (Figure 11c). This buffer layer remarkably suppresses the free water/ O_2 -induced corrosion and passivation by isolating Zn anodes from bulk electrolytes. The layer also elevates the nucleation barrier and restricts 2D diffusion of Zn^{2+} , and effectively regulates the Zn deposition behavior. With these merits, the modified Zn anode shows a 60 times longer cycling lifetime (8,000 hours) than the bare one, and can support a

reversible charge-discharge at a high DOD of 85% (corresponding to an ultrahigh areal capacity of 10 mAh cm^{-2}). The authors also clearly demonstrate the beneficial influence of this layer in $\text{Zn}-\text{MnO}_2$ full batteries.

Recently, Cai and Sun et al.^[173] reported a dense Cu top layer modification method to stabilize the Zn anodes. The top layers were prepared by a simple replacement reaction between Zn and CuCl_2 in ethanol media, which further underwent a 300 °C annealing in Ar/H₂ atmosphere (5 vol % H₂) to strengthen bonding. Due to the coverage of chemically inert Cu (redox potential = 0.34 V vs. SHE, Cu:Zn molar ratio = 1:1), the reaction speed of Zn metal anode corrosion can be effectively depressed by >80%, enabling the Zn anode a stable and low interfacial impedance and a high Coulombic efficiency (91.8 vs. 81.3%) even after a long term resting. Thanks to the increased stability of anode, the capacity retention of the $\text{Zn}-\text{MnO}_2$ batteries were increased from 27.6% after 300 cycles to 94.2% after 500 cycles. Postmortem TEM examination indicates that the Cu layer had reacted with Zn and formed Cu_5Zn_8 and Cu_2Zn_1 alloys during electrochemical cycling.

Porous Zn sponges: Besides modification of Zn anode with foreigner materials, constructing uniform Zn nanostructures with high specific surface area^[22] (or depositing Zn on nano-structured current collectors^[191]) is also proved effective for the stabilization of the anode. In 2014, Parker and Rolison et al.^[22] developed a wiring strategy to converse Zn powders into porous, monolithic, 3D aperiodic architecture, which can remarkably enhance cycling stability of the anode (Figure 12a). To prepare the sponge, the Zn powders (with 300 ppm In and Bi to suppress hydrogen evolution) were firstly mixture with binders (sodium dodecyl sulfate + carboxymethylcellulose) and solvent (water + decane) to cast monoliths after drying. The fragile monoliths were then successively heated at 409 °C for 2 h in Ar and 665 °C for 2 hour in air, to order to weld the powders by necking and wrap them with ZnO shells (Zn@ZnO sponges). To reduce the large charge-transfer resistance introduced by the semiconductor ZnO shells, the Zn@ZnO sponges were finally reduced into all-metal 3D Zn sponges by an electrochemical method. This stabilized bulk anode shows impressive performance even at deep DOD, and allows the authors to revisit a variety of Zn-based batteries (e.g., Zn-air, Zn-NiOOH, Zn-Ag).^[11] The authors further demonstrate 3D Zn-NiOOH alkaline batteries in application scenarios of: (i) >100 high-rate cycles at 40% DOD Zn at lithium-ion-commensurate specific energy, and (ii) the tens of thousands of power-demanding duty cycles required for start-stop micro-hybrid vehicles.

Zn foil with heterogeneous nucleation seeds: For crystallography point of view, the formation of a Zn dendrite is an oriented crystal growth process from a nucleation site under the driving force of "tip effect". Theoretically, uniform Zn arrays should be constructible on anodes if the nucleation sites are uniform and small enough. For instance, Chao and Fan et al.^[192] reported an electrochemically deposited Zn nano-flake array anode on 3D graphene form for high performance ZIBs. The Zn-array anode delivered notably small polarization and long cycling life due to its structural uniformity and high specific

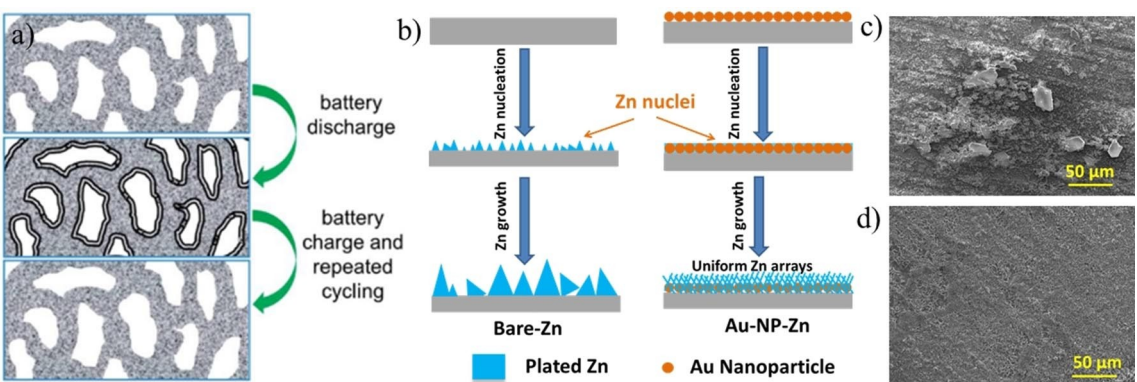


Figure 12. Schematic illustration of the Zn stripping/plating process on 3D monolithic Zn sponges (a). Reproduced with permission from Ref. [22]. Copyright 2014, Royal Society of Chemistry), bare and Au-nano-particle modified Zn (b), typical SEM images of the cycled Bare-Zn (c) and Au-NP-Zn (d). Reproduced with permission from Ref. [176]. Copyright 2019, American Chemical Society.

surface area. By making good use of Zn anodes' dendrite forming nature with pre-deposited Au nano-particles (as heterogeneous Zn nuclei), the plane surface of Zn foils could be *in situ* transformed into uniform array of Zn micro-flakes during cycling (Figure 12b-d), resulting in a profoundly improved cycling stability for both anode and full batteries.^[176] Introducing heterogeneous nuclei (such as Sn nano-particles) onto current collectors is also helpful for the achievement of high performance Zn anodes.^[193]

In situ electro-healing strategy for in-service Zn anodes: The formation of Zn dendrites are severely dependent on the charge/discharge conditions of the ZIBs.^[170] That is, the growth of Zn dendrites, as well as the degradation of ZIBs' performance, is much faster at large current densities or deep DOD. Once the Zn dendrites cause internal short circuit, in a common sense, the ZIBs can only be abandoned. To rescue the in-service ZIBs, Yang, Fan and Zhi et al.^[170] innovated an *in situ* electro-healing methodology to eliminate the already-formed Zn dendrites without de-assembling the batteries. This methodology involves only a simple switching process to a smaller current density (for example, from 7.5 to 1 mA cm⁻²). Magically, the sharp tips of zinc dendrites were gradually passivated into smooth edges and finally generate a smooth electrode surface after a short electro-healing time of several hours. As expected, the healed ZIBs delivered a much longer lifespan than the untreated ones. Pay attention that the short-circuited ZIBs cannot be rescued by this method. Therefore, the electro-healing processes should be periodically implemented to prevent ZIBs from quick failure.

At laboratory conditions, all the above mentioned strategies show positive effect on stabilizing Zn anodes. However, the practical performances of these methodologies need further systematical re-confirmation in the complex application scenarios. For real use, the rest times between charge and discharge semi-cycles are always much longer than the experimental conditions, which could substantially magnify the influence of corrosion reactions. Completely isolating Zn anodes from the aqueous electrolytes by dense coatings should be a reliable choice to depress Zn corrosion. Furthermore, the dynamic Zn striping/plating cycles can cause dramatic morphology evolu-

tion during ZIBs' service. Construction of 3D Zn-based composite anodes, in our opinion, is an attractive approach to solving this problem.

4.2. Intercalation Anode Materials

Despite tremendous progresses have been achieved to improve Zn plating striping kinetics, the practical application of metal Zn anodes is still hindered by the detrimental side reactions, unpredictable dendrite growth and poor cycling life.^[171,179] Therefore, almost all of reported ZIBs employ Zn anodes with much excess mass to ensure sufficient supply of Zn²⁺ during cycling, seriously limiting the reliability and practical energy density of ZIBs. In this aspect, Zn²⁺ (de) intercalation anodes should be an attractive alternative of Zn metal anodes for the construction of high performance ZIBs. The development of Zn²⁺-intercalation anode may also enlighten researches on other secondary batteries (e.g., Mg²⁺, K⁺, Ca²⁺, etc.).^[194]

However, development of intercalation anodes for ZIBs is far from ease, probably because of the large steric hindrance and strong electrostatic interactions between the host material and the multivalent Zn²⁺ with large hydrated ionic radius (4.04–4.30 Å). Indeed, an adequate intercalation anode should meet quite a number of requirements, including decent capacity, high Coulombic efficiency, proper redox potential, stable cycling stability, and good rate capability.^[174] The first reported Zn²⁺-intercalated anode is Chevrel-phase Mo₆S₈.^[175,195] This material can reversibly intercalate Zn²⁺ and successively transform into ZnMo₆S₈ (at 0.6–0.7 V vs. Zn²⁺/Zn) and then to Zn₂Mo₆S₈ (at 0.3–0.4 V), in both aqueous and non-aqueous electrolytes, delivering a reversible capacity of ~90 mAh g⁻¹. Besides Zn, this material is also excellent host for guest elements such as Mg, Ca, Sr, Ba, Cr, Mn, Fe, Co, Ni, etc.,^[175] thanks to its unique crystal structure and remarkable ionic and electronic transport kinetics.^[196] The potential application of this anode has been demonstrated by constructing a Mo₆S₈-ZnI₂ flow cells with a zinc-polyiodide (I⁻/I³⁻)-based catholytes.

The impressive work by Li et al.^[174] shows that a layered sulfide, TiS_2 , can be converted into an excellent interaction anode for ZIBs after being pre-sodiated (i.e., $\text{Na}_{0.14}\text{TiS}_2$). The $\text{Na}_{0.14}\text{TiS}_2$ anode can accommodate 140 mAh g^{-1} of Zn^{2+} (at $\sim 0.3 \text{ V vs. Zn}^{2+}/\text{Zn}$ and 0.05 Ag^{-1}) with high cycling stability (77% capacity retention over 5000 cycles at 0.5 Ag^{-1}), a large capacity considering the relatively high mass loading of (5.7 mg cm^{-2}). Experimental and theoretical studies indicate that the pre-sodiated treatment not only improves the structural reversibility and stability, but also enhances the ionic and electronic conductivities. Coupling this anode with a ZnMn_2O_4 cathode in $\text{Zn}(\text{CF}_3\text{SO}_3)_2$ aqueous electrolyte gives a “rocking-chair” ZIBs, outputting an average voltage of 0.95 V and a remarkable capacity of 105 mAh g^{-1} .

Considering the fact that most of the cathode materials of ZIBs are Zn^{2+} -free in their pristine states, a Zn^{2+} -containing anode is preferable for the construction of a rocking-chair type ZIB. Along this way, Kaveevivitchai and Manthiram further developed an intercalation anode $\text{Zn}_x\text{Mo}_{2.5+y}\text{VO}_{9+z}$ by chemically inserting Zn^{2+} into open-tunnel $\text{Mo}_{2.5+y}\text{VO}_{9+z}$.^[197] At ambient temperature, the material achieves a high capacity of 180 mAh g^{-1} at 20 mA g^{-1} . However, this material suffers from poor cycling stability (capacity decrease to 120 mAh g^{-1} after 30 cycles) and large polarization. The capacity fading could be attributed to the invertible Zn^{2+} trapping in small three-membered ring channels and the dissolution of active materials because of the attack of H^+ to V elements.

5. Electrolytes of ZIBs

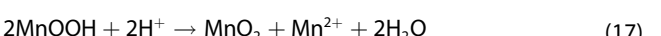
5.1. Liquid Electrolytes

Employment of mild electrolytes represents a key progress in the development of ZIBs, since it effectively depress detrimental side reactions on electrodes of traditional alkaline electrolytes, and breakthrough the rigid tradeoff between cycling stability and depth of discharge.^[13,17,26] That is to say, the mild ZIBs need not run in a shallow cycling protocol to keep their rechargeability.^[2] This design also provides a competitive power source candidate for wearable electronics, where non-corrosiveness is one of top priorities besides safety and non-toxicity.^[5,198]

The first report on ZIBs was published in 1986 by Yamamoto and Shoji,^[17] 90 years after the utilization of Zn in alkaline batteries.^[132] This research investigated the performances of $\text{Zn}-\text{MnO}_2$ (γ -phase, electrolytic) cells in a variety of mild aqueous electrolytes (including ZnSO_4 , ZnCl_2 , $\text{Zn}(\text{NO}_3)_2$, $\text{Zn}(\text{PF}_6)_2$, ZnSiF_6 , $\text{Zn}(\text{BF}_4)_2$, AlCl_3 , etc.), and confirmed the impressive cycling stability of the batteries in the ZnSO_4 electrolyte.^[17,24,199] The superior cycling stability and Coulombic efficiency enabled by ZnSO_4 electrolytes can be ascribed to the high electrochemical stability of SO_4^{2-} ,^[12] the reversible formation of discharge product $\text{ZnSO}_4[\text{Zn}(\text{OH})_2]_3 \cdot x\text{H}_2\text{O}$,^[2,200] as well as the reaction reversibility between Mn^{2+} and Mn^{4+} in this media.^[24] Within an operation voltage windows of 0.9 – 1.7 V and sufficient Zn anode, the optimized batteries showed $\sim 100\%$ Coulombic

efficiency, 1.3 V average discharge voltage and 57% MnO_2 utilization within 30 cycles. Afterwards, serious capacity fading occurred due to the corrosion and dendrite growth on Zn anodes, as well as deterioration of the cathode.^[24] The cycling stability of ZIBs can be increased, to some extent, by optimization of electrodes' manufacture process.^[13,33]

In 1998, Kim and Oh,^[21] for the first time, systematically analyzed the MnO_2 cathode failure mechanisms in ZnSO_4 electrolyte. They discovered an obvious non-faradic Mn loss process accompanied the dramatic capacity fading of ZIBs. The Mn loss stems from the disproportionation reactions of the discharged product (MnOOH) in weak acidic electrolytes, which can be described as [Eq. (17)].^[201]



Based on this understanding, the authors proposed a Mn^{2+} -containing electrolyte ($\text{MnSO}_4 + 2 \text{ M ZnSO}_4$) to balance the Mn loss. The addition of MnSO_4 also depress pH of the electrolytes and the formation of $\text{ZnSO}_4[\text{Zn}(\text{OH})_2]_3 \cdot x\text{H}_2\text{O}$, which may increase the utilization efficiency of cathode^[31] but also Zn corrosion rates. Experiments showed that, the increase of MnSO_4 concentration resulted a steadily increase of cycling stability before 0.1 M , and declined thereafter. The optimized $0.1 \text{ M MnSO}_4 + 2 \text{ M ZnSO}_4$ electrolyte enabled not only a long term cycling stability (120 cycles without significant capacity loss), but also a larger capacity. Further addition of MnSO_4 reduces the performance of the ZIBs, possibly due to the reduced pH accelerates the Zn corrosion reaction. Due to the remarkable effectiveness, this strategy has become a widely adopted technology for the construction of high performance $\text{Zn}-\text{MnO}_2$ ZIBs.^[2,18] However, it is worth noting that even in the addition of Mn^{2+} -containing electrolytes, Mn^{2+} dissolution-deposition still intensively occurs on the cathode side, which can still leads to dramatic structural degradation and capacity fading in long term running.^[28,56] At the same time, the $\text{MnSO}_4 + \text{ZnSO}_4$ electrolyte, even mild (pH 3–5 depending on the ZnSO_4 ^[197] and MnSO_4 concentration),^[21] may still cause the dissolution of cathodes^[197] and the corrosion of Zn anodes.^[21,190] For ZIBs with low acid-resistance cathodes, more neutral $\text{Zn}(\text{CH}_3\text{COO})_2$ electrolytes (pH 5.5–6.5^[197]) maybe a reasonable choice.^[10,40,143]

In 2016, Zhang, Cheng and Chen et al.^[12] investigated the performances of three typical aqueous electrolytes, ZnCl_2 , $\text{Zn}(\text{NO}_3)_2$, ZnSO_4 , along with a novel bulky-anion zinc salt $\text{Zn}(\text{CF}_3\text{SO}_3)_2$ (zinc trifluoromethanesulfonate). Cyclic voltammetry tests indicate the higher stability and much wider operational voltage windows (2.3–2.4 V, Figure 13a–b) of ZnSO_4 and $\text{Zn}(\text{CF}_3\text{SO}_3)_2$ than ZnCl_2 and $\text{Zn}(\text{NO}_3)_2$ (<0.6 V), due to the better electrochemical stability of SO_4^{2-} and CF_3SO_3^- . Wu and Zhang's work^[143] further revealed the extremely low reversibility of Zn stripping/plating (average Coulombic efficiency $\sim 0\%$, Figure 13c) in the $\text{Zn}(\text{NO}_3)_2$ electrolytes, implying rapid oxidation of Zn metal anodes in this strongly oxidizing electrolytes. Galvanostatic charge-discharge tests further reveal the better Zn striping/plating kinetics of $\text{Zn}(\text{CF}_3\text{SO}_3)_2$ and $\text{Zn}(\text{CH}_3\text{COO})_2$ over ZnSO_4 ,^[143] probably because the bulky CF_3SO_3^- and

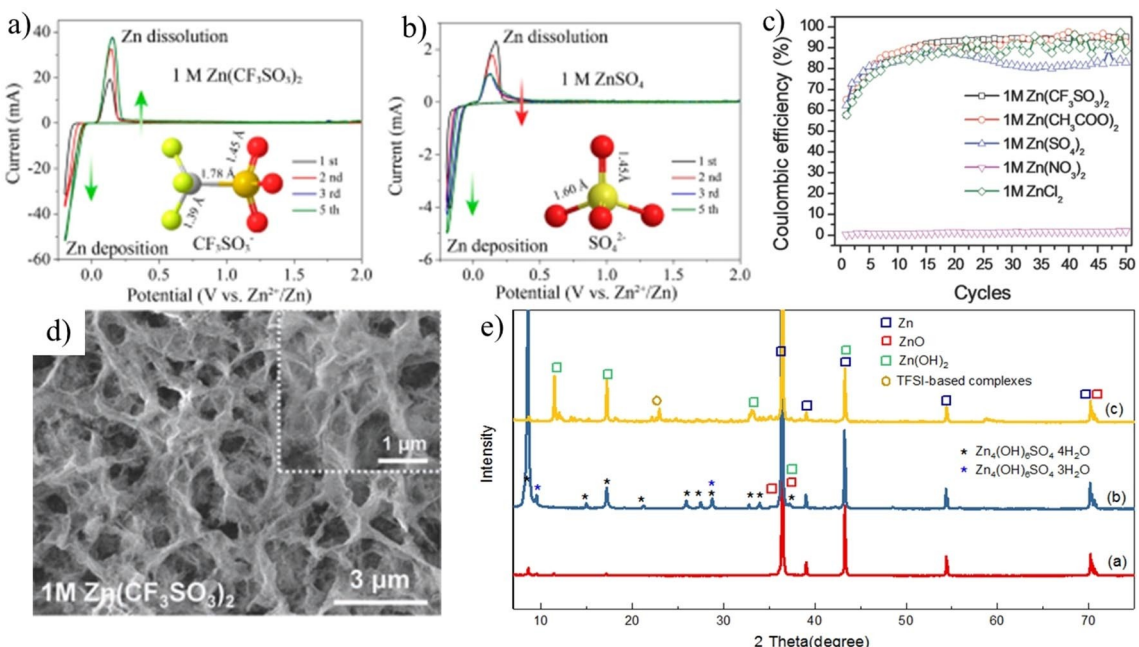


Figure 13. a-b) Cyclic voltammograms of Zn electrode in $\text{Zn}(\text{CF}_3\text{SO}_3)_2$ and ZnSO_4 electrolytes. Reproduced with permission from Ref. [12]. Copyright 2016, American Chemical Society. c) Coulombic efficiency of Zn stripping/plating on Ti foils in different electrolytes. d) Typical SEM images of the Zn deposits from the $\text{Zn}(\text{CF}_3\text{SO}_3)_2$ electrolyte. Reproduced with permission from Ref. [143]. Copyright 2019, Wiley-VCH. e) XRD patterns of the Zn foils after immersion in: a) water-in-deep eutectic solvent ($\text{LiTFSI} + \text{Zn}(\text{TFSI})_2 + \text{urea} + \text{H}_2\text{O}$), b) 0.25 M Li_2SO_4 + 0.5 M ZnSO_4 and c) 0.5 M $\text{LiTFSI} + 0.5$ M $\text{Zn}(\text{TFSI})_2$ electrolytes at room temperature for 15 days. Reproduced with permission from Ref. [204]. Copyright 2019, Elsevier.

CH_3COO^- anions decrease the solvation effect of Zn^{2+} and facilitate Zn^{2+} charge transfer and even deposition (Figure 13d).^[12,143]

Increase electrolyte concentration can further improve the cycling stability of both Zn anode and MnO_2 cathode, due to the depression of water-induced side reaction and Mn dissolution,^[132,202] but on the expense of cost. In these works, the authors suggested 3 M $\text{Zn}(\text{CF}_3\text{SO}_3)_2$ as the optimized electrolyte ($\text{pH}=3.55^{[4]}$) to balance performance and cost.^[12,143] In this electrolyte, introduction of Mn^{2+} ($\text{Mn}(\text{CF}_3\text{SO}_3)_2$) benefit also the cycling stability of Zn– MnO_2 ZIBs.^[18] Besides $\text{Zn}(\text{CF}_3\text{SO}_3)_2$, zinc bis(trifluoromethylsulfonyl)imide ($\text{Zn}(\text{TFSI})_2$), $\text{Zn}(\text{NS}_2\text{O}_4\text{C}_2\text{F}_6)_2$ represents other important bulky-anion electrolyte for ZIBs.^[132]

Very recently, Wang and sun et al.^[203] further discovered that $\text{Zn}(\text{ClO}_4)_2$ -based aqueous electrolyte should be also a good choice for ZIBs. In this electrolyte, the Zn stripping/plating process is much more reversible than in conventional ZnSO_4 electrolyte, possibly due to dendrite free deposition process and also the formation of a Cl^- containing layer on the Zn anode surface. The layer is thought able to limit continuous side reactions between Zn and the aqueous electrolyte, retaining smooth charge transfer process across the anode/electrolyte interfaces. This electrolyte can provide a working potential window up to 2.4 V, comparable to the ZnSO_4 and $\text{Zn}(\text{CF}_3\text{SO}_3)_2$ electrolytes.

Even though various aqueous electrolytes have been established, these electrolytes are still suffering from Zn corrosion reactions by free water. In these aqueous electrolytes, the H_2 evolution reaction (HER) between Zn metal and free

water molecules inevitably occurs, because of the low Zn/Zn^{2+} potential (-0.76 V vs. SHE).^[173,204] In 3 M ZnSO_4 electrolyte, for example, Zn corrosion results in the formation of $\text{Zn}_4(\text{OH})_6\text{SO}_4$ micro-sheets by hydrogen evolution reactions (Figure 13e).^[173,204] Impressively, the deepest corrosion pit of Zn metal can reach 132.2 μm after 30 days immersion, accompanied by dramatic increase of Zn striping/plating overpotentials.^[173] At the same time, the strong interactions between Zn^{2+} and water molecules makes it difficult to desolvate and deposit, increasing the possibility of water decomposition during each charging cycles. This decomposition reaction produces hydroxyl ions (OH^-) and electrochemically inactive $\text{Zn}(\text{OH})_2$, ZnO , etc., resulting in low Coulombic efficiency and fast dendrite growth.^[132,204] Finally, degassing the electrolyte should also be helpful to eliminate the oxidation and corrosion of Zn caused by dissolved oxygen.

Table 3 outlines the advantages and disadvantages of the various aqueous electrolytes used in ZIBs. Significantly, it seems that the zinc salts with bulky anions always exhibit superior reaction kinetics, possibly because these anions benefit the charge transfer and Zn deposition by changing the composition and structure of solvation shell surrounding Zn^{2+} . Especially, the long-ignored $\text{Zn}(\text{ClO}_4)_2$ and $\text{Zn}(\text{CH}_3\text{COO})_2$ aqueous solutions are attractive electrolyte candidates for ZIBs, due to their advantages of low cost, environmental benignity, and high compatibility with Zn. Turning the aqueous electrolytes into hydrogel can further reduced the free water content and depress corrosion rate and dendrite growth.

Table 3. Comparison of various aqueous electrolytes used in ZIBs.

	Cost	Solubility	Compatibility with Zn	Voltage window [V]	Environmental impact
ZnSO ₄	Low	Moderate	Fair	2.3–2.4	Low
ZnCl ₂	Low	High	Fair	0.6	Low
Zn(NO ₃) ₂	Low	Moderate	Very Poor	N/A	Low
Zn(CF ₃ SO ₃) ₂	High	High	Good	2.3–2.4	Low
Zn(CH ₃ COO) ₂	Low	Low	Good	>1.8	Low
Zn(TFSI) ₂	High	High	Good	2.3–2.4	Low
Zn(ClO ₄) ₂	Moderate	High	Good	2.3–2.4	Low

5.2. Functional Additives for Liquid Electrolytes

For further performance improvement, numerous functional additives are introduced into the aqueous electrolytes of ZIBs. For example, Huang and Liu et al.^[181] developed a 1 M ZnSO₄ + 0.1 M MnSO₄ electrolyte with two additives, which show synergistic effects on suppressing the corrosion reaction and dendrite growth of Zn anodes (Figure 14a). One additive is non-ionic low foaming surfactant-fatty methyl ester ethoxylate (FMEE) to homogenize the electrolyte, reduce the activation energy, and suppress Zn dendrite formation. Another additive, fumed silica (SiO₂), shows shear-thickening effect, leading to remarkable enhancement of mechanical strength of the electrolyte to resist the dendrite growth.^[192] The Zn/Zn symmetric cells in this electrolyte achieve a long cycling stability of 1500 h. Compared with the basic electrolyte, the SiO₂/FMEE-containing electrolyte alleviates the Zn corrosion rate by ten times (19.65 to 1.96 $\mu\text{A cm}^{-2}$) and increased the initial Coulombic efficiency from 92.3 to 99.5%. A Zn–MnO₂

battery with this modified electrolyte exhibits excellent cycling stability with low capacity loss of 0.002% per cycle.

According to electrostatic shield mechanism,^[205] the metal dendrite formation during charge process could be suppressed by adding other positive ions with lower reduction potential into electrolyte (Figure 14b). As we all know, Na⁺ has a lower reduction potential than Zn²⁺, and thus could be added into ZnSO₄ electrolyte to effectively avoid the growth of Zn dendrites. Chen et al.^[206] compared the electrochemical performance of the ZnSO₄ electrolyte with or without Na₂SO₄ additive, based on the same NaV₃O₈·1.5H₂O nano-belts (NVO) cathode and Zn anode. The Na₂SO₄ additive not only prevents the dissolution of NVO cathode by changing the dissolution equilibrium of Na⁺, but also synchronously restricts the growth of Zn dendrites. Interestingly, some other metal ions with more positive redox potentials, like bismuth ions (Bi³⁺)^[207] and lead ions (Pd²⁺)^[208] also shows impressive Zn-dendrite depressing ability. During charging of the batteries, these ions are reduced and deposited prior to Zn. The deposited tiny metal crystals in

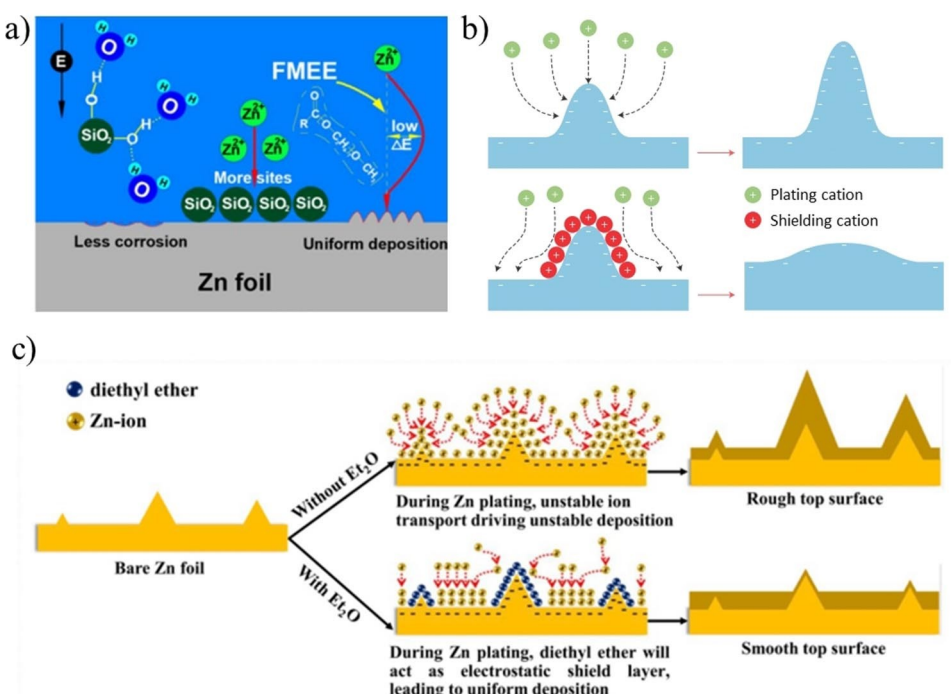


Figure 14. a) Illustration of the schemes of the electrochemical processes of Zn metal in the ZnSO₄ + FS + FMEE electrolyte. Reproduced with permission from Ref. [181]. Copyright 2019, the Electrochemical Society. Schematic illustration of the metal deposition process based on the self-healing electrostatic shield mechanism (b) (reproduced with permission from Ref. [205], Copyright 2013 American Chemical Society), and with/without Et₂O additives (c) (reproduced with permission from Ref. [180], Copyright 2019, Elsevier).

advance can serve as heterogeneous nuclei for uniform Zn plating, alike the case of Au-nano-particle modified Zn anodes.^[176] The uniform Zn deposits are denser and more conductive than the untreated ones, demonstrating lower interfacial impedances.

Adding various inorganic materials in the electroplating solution has been successfully implemented to control the Zn electroplating behaviors. Chen and co-workers^[209] investigated the effects of inorganic additives, like indium sulfate, tin oxide, and boric acid, on the Zn electroplating. Without additive, the Zn deposit mainly grew along [103] direction, representing the growth of Zn dendrites. The presence of inorganic additives changed the preferred Zn deposition orientation from [103] to [002] or, [103] implying a basal morphology and high resistance to dendrite growth. In addition, the corrosion rates of electroplated Zn with inorganic additives decrease as much as 11 times compared to the one deposited without additives. The enhanced cycling stability and low float charge current of these anodes can be readily inherited by ZIBs.

Apart from the inorganic compounds, the organic molecules are the other most widely used additives for ZIBs' electrolytes, including alcohols, aldehydes, organic acids, ammonium compounds, carbohydrates, surfactants, etc.^[177] The Zn dendrite inhibiting mechanism of these additives stems from their preferential adsorption on the surface of Zn anode as a prohibitive layer. The moderate adsorption of polymers can manipulate the local current distribution near the adsorbing Zn tip, but too strong adhesion of polymers will cause remarkable increase of interfacial impedance, adverse to the electrochemical performances of ZIBs.

Mitha and Chen et al.^[210] reported that poly-ethylene glycol polymers (PEG-200) can regulate Zn dendrite growth and improve the cycling stability of Zn²⁺/Li⁺ dual-cation batteries. With various microscopy and spectroscopy characterizations, the authors comprehensively elucidated the mechanism of PEG on inhibiting Zn dendrites growth. Without the addition of PEG-200, Zn²⁺ ions on the surface of the electrode tend to accumulate at the salient sites due to the high local electric field and the lack of transfer resistance. After PEG-200 addition, the adsorption of the polymer chain on the Zn anode depresses the lateral diffusion and gathering of Zn²⁺ toward the salient sites. Therefore, the growth of Zn dendrites (including Li dendrites in fact^[211]) is effectively restricted. Furthermore, this strategy can reduce the corrosion and chronoamperometric current density of the Zn anode by ~80%, possibly because the absorbed PEG200 layers can also retard H⁺ from adsorption and reduction on the electrode.^[212] The PEG200 additive seems provides persistent dendrite inhibiting functions, because it can even improve the ZIBs' performances with dendrite pre-grown Zn anodes.

Furthermore, Hu and Wang et al.^[180] discovered the strong Zn-dendrite depressing ability of diethyl ether (Et₂O, 2 vol %) as additives for both Zn(CF₃SO₃)₂-based and ZnSO₄-based electrolytes. The authors believe that highly-polarized diethyl ether can be preferably adsorbed on the Zn dendrite tips with strongly enhanced local electric field, persistently hinder the growth of these tips (Figure 14c), similar with the case of for

LIBs.^[213] The ZIBs with Et₂O modified Zn(CF₃SO₃)₂-based electrolyte demonstrated an outstanding cycling performance with a high capacity retention of 97.7% for 4000 cycles at 5 A g⁻¹.

In the electroplating industry, brightener is commonly used as additive to obtain a bright and smooth electroplated surface.^[214] Generally, most of these brighteners are ketone or aromatic aldehyde compounds. As a typical low-cost polymer containing ketone unit, polyacrylamide (PAM) had been verified an effective electrolyte additive to suppress the formation of dendrites during the electrodeposited Zn.^[215] Density functional theory (DFT) calculations that the acyl groups on PAM can selectively adsorb Zn²⁺ ions, enabling the transfer of Zn²⁺ ions along the polymer chains. Based on this understanding, Zhang and Wang et al.^[216] further developed a synergistic method combining the Cu-Zn solid solution interface on a copper mesh skeleton with good zinc affinity and a polyacrylamide electrolyte additive to modify the zinc anode, which can greatly reduce the over-potential of the zinc nucleation and increase the stability of zinc deposition. This design supports Zn anodes being continuously charged-discharged at 80% discharge depth (4 mAh cm⁻²) for 280 h in a ZnSO₄ based aqueous electrolyte.

Recently researches indicate that some organic molecules, such as ethanol and dicyanamide, can coordinate or complex with Zn²⁺ to regulate the Zn electroplating process. For example, DFT calculations demonstrate that the oxygen in ethanol can bind with the Zn cations through its lone-pair electrons, and replace a water molecule of Zn²⁺'s primary solvation shell.^[217] This is the reason why this additive can mitigate the growth of zinc dendrites in a zinc-polyiodide flow battery.

5.3. 'Water-in-Salt' Electrolytes

Following their famous concept of 'water in salt' electrolyte,^[202] Wang and Xu et al.^[132] extended the bulky-anion electrolyte concentration to >20 M, and developed a 1 M Zn(TFSI)₂+20 M LiTFSI electrolyte to tame the detrimental dendrite growth and corrosion reactions on Zn anodes. In this electrolyte, the neutral and high concentration LiTFSI was used to depress hydrolysis of water molecules while providing enough TFSI⁻ anions. Meanwhile, the small water content is important for the achievement of high liquidity for the electrolyte. The extremely high population of TFSI⁻ anions promotes the formation of close (Zn-TFSI)⁺ ion pairs instead of (Zn-(H₂O)₆)²⁺ (Figure 15a-b), enabling dendrite-free Zn striping/plating processes with excellent reversibility (nearly 100% Coulombic efficiency, Figure 15c-d) comparable with ionic liquid-based electrolytes.^[218] XPS analyses suggest the formation of a protective interface layer containing zinc-based fluoride, sulfide, sulfate, oxide and carbonate on the cycled Zn anodes in this electrolyte, which should be also favorable for the dendrite-free striping/plating of Zn.^[170] This design is efficient to retain water even in the open atmosphere, making hermetic cell configurations optional. To show their potential applications, Zn/LiMn₂O₄ and Zn/air batteries were demonstrated with this electrolyte.

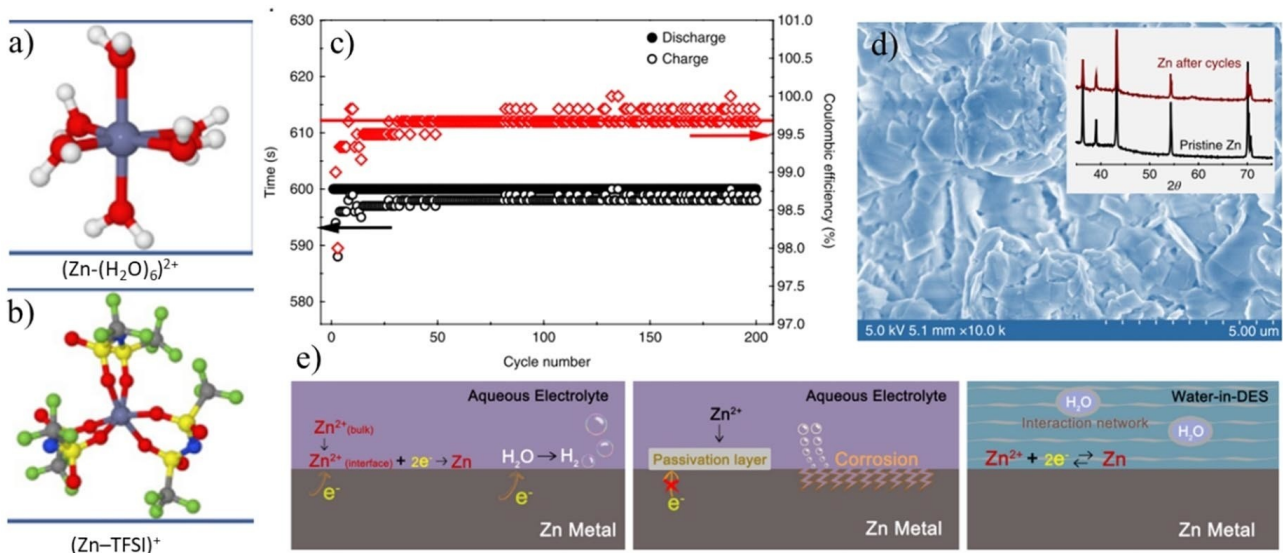


Figure 15. Representative Zn^{2+} -solvation structures in the electrolytes with 1 M $\text{Zn}(\text{TFSI})_2$ (a) and concentrations of LiTFSI (20 M, b). c) The Zn plating/stripping Coulombic efficiency on the Pt working electrode, d) SEM image and XRD pattern (inset) of a Zn anode after 500 stripping/plating cycles. Reproduced with permission from Ref. [132]. Copyright 2018, Springer Nature. e) Schematic diagrams of interfacial reactions on Zn anodes in the traditional aqueous electrolytes and the water-in-DES electrolyte. Reproduced with permission from Ref. [204]. Copyright 2019, Elsevier.

To depress the content of expensive TFSI salts in the ‘water-in-salt’ electrolyte, Zhao and Cui et al.^[204] further developed a new ‘water-in-deep eutectic solvent (water-in-DES)’ electrolyte (Figure 15e). The DES, as attractive alternatives to ionic liquids, is an eutectic mixture of Lewis acids and bases in proper molar ratios.^[219] In this work, the DES part of the electrolytes were simple formed by mixing and mildly heating the three components (LiTFSI, $\text{Zn}(\text{TFSI})_2$ and urea). The coordinating and H-bonding species (ions or molecules) within DESs make them strongly water-miscible and highly hygroscopic.^[220] Below an upper limited, all water molecules participate into the DES’s internal interaction (H-bonding and coordinating) network; remarkably depress the free-water-induced side reactions. At the same time, adding proper amount of water can effectively improve the viscosity and conductivity of the electrolyte. In this electrolyte, Zn anodes are chemically robust and highly reversible in striping/plating, realizing a 0.11 V upward shift in the operating voltage for $\text{Zn}/\text{LiMn}_2\text{O}_4$ batteries.^[204] A 2-Ah pouch battery based on this water-in-DES electrolyte achieves an energy density of 52 Wh kg^{-1} (based on the total device mass) and a long lifespan with acceptable capacity retention (84.8% after 150 cycles). The electrolyte design benefits the energy density of batteries by increasing the utilization and reversibility of Zn anodes, but discounting the cost advantage of aqueous ZIBs.^[170]

To further expand the “water-in-salt” electrolyte system, Yang and Zhi et al.^[170] comprehensively investigated the effect of electrolyte concentration (0.2 M-saturated ZnSO_4) on Zn dendrite formation behavior at different current densities ($1\text{--}10 \text{ mA cm}^{-2}$). Experimental results indicate that the lifespan of Zn electrode can be slightly widened by the electrolyte concentration increase. However, the solubility of ZnSO_4 in aqueous electrolyte is limited, preventing the development of

ZnSO_4 -based “water-in-salt” electrolyte. On the other hand, other cheap yet high solubility Zn salts, such as ZnCl_2 ,^[221] and ZnI_2 ^[222] etc., have also been proposed to prepare “water-in-salts” electrolytes for long-life ZIBs. One should be aware that the effects of these “water-in-salt” electrolytes are double sides: the lack of free-water slows down detrimental corrosion reaction and dendrite growth speed, but may also eliminate the beneficial influence of free-water on electrochemical reactions.^[52,55,223]

5.4. Hydrogel Electrolytes

With the rapid development of wearable electronics, flexible ZIBs begin to attract numerous attentions.^[198] The construction of flexible ZIBs is a systemic project that requires the redesign of all battery components, including of cause the electrolytes. Generally, ideal flexible ZIBs not only require mechanically flexible, stability and durability, but also safety. Therefore, transforming conventional rigid/fragile ZIBs’ materials/structures into soft/flexible ones is vitally important. Usually, the electrode active layers of flexible ZIBs are strongly bonded to the soft/flexible current collectors, in order to avoid interfacial separation under various flexibility tests and application conditions. At the same time, achieving highly flexible and Zn^{2+} -ion conductive electrolytes is also a key step towards high-performance flexible ZIBs.^[224] Recently, gel electrolytes are widely explored in the configurations of flexible ZIBs. In this section, we will focus on some important progress on this issue. One can also refer to Lu’s^[5] and Xia’s^[225] impressive reviews for more details.

The gel electrolytes are formed by introducing stretchable and compressible 3D gelation skeletons into the aqueous Zn

salt electrolytes,^[226] sometimes even combining with other functions such as self-healing,^[227] anti-freezing,^[228,229] etc. Comparing with the traditional aqueous electrolytes, the attractive features of the gel electrolytes lie in the following aspects: 1) the gel electrolytes can avoid electrolyte leakage, increasing the user friendliness;^[225] 2) the gel electrolytes can maintain the structural integrity and electrochemical performances of the device, even under the application scenarios with dynamic external forces;^[230] 3) the gel electrolytes simultaneously play the role of separators, remarkably simplifying the configurations of flexible ZIBs;^[231] 4) the gel electrolytes can alleviate the dissolution of cathode active materials while impeding the dendrite growth and corrosion reaction on anode side.^[232] Currently, various polymers, such as gelatin,^[233] sodium alginate (SA),^[234,235] xanthan gum (XG),^[236] polyvinyl alcohol (PVA),^[87] polyacrylamide (PAM),^[237] poly(acrylonitrile) (PAN),^[238] poly(ethylene glycol) diacrylate (PEGDA)^[239] and polyacrylic acid^[144] have been studied to prepare gel electrolytes for ZIBs.

Gelatin, a biocompatible, hydrophilic polymer widely used in food and pharmaceutical industries, shows an interesting transformation between melt and gelation states. Gelatin possesses laudable environmental benignity, high salt tolerance, and thereby is regard as an important gelling agent for gel electrolytes. Recently, Chi and Liu et al.^[233] developed a facile self-standing gelatin-based hydrogel electrolyte (GHE) for

solid-state ZIBs. For assembly, the gelatin was thermally dissolved into the $0.5\text{ M Li}_2\text{SO}_4 + 0.5\text{ M ZnSO}_4$ electrolytes to firstly obtain the melting GHE solution, which was then casted onto electrode surfaces before gelation transformation. The high porosity and high aqueous electrolyte reservation capability of the GHE give a high ionic conductivity of 6.15 mS cm^{-1} , even though the mechanical strength is relatively low (compressive strength $\sim 100\text{ kPa}$). This GHE can suppress the dendrite growth and corrosion reactions on Zn anodes, achieving low self-discharge rate and high cycling stability in the flexible Zn–LiMn₂O₄ ZIBs. Treating the electrolyte in high concentration inorganic salt solution can further reinforce the GHE due to dehydration effects and enhancement of polymer chain bundling, resulting in effectively enhanced mechanical strength (2.78 MPa)^[240] comparable to the composite electrolyte systems like gelatin-g-PAM.^[230]

Another commonly used polymer matrix for gel electrolytes is algin, a carbohydrate product extracted from brown seaweed. The gelation of algin solution can be easily triggered by multivalent cation assistant crosslinking by Ca, Cu, Pb, Cd, Ba, etc. in ambient temperature.^[241] Accordingly, Zhou and Liang et al.^[234] prepared an Algin-Zn gel electrolyte with high ionic conductivity ($1.83 \times 10^{-2}\text{ Scm}^{-1}$), based on the interaction between carboxylate groups of algin and Zn²⁺ (Figure 16a). Within this electrolyte, the migration of Zn²⁺ is guided and

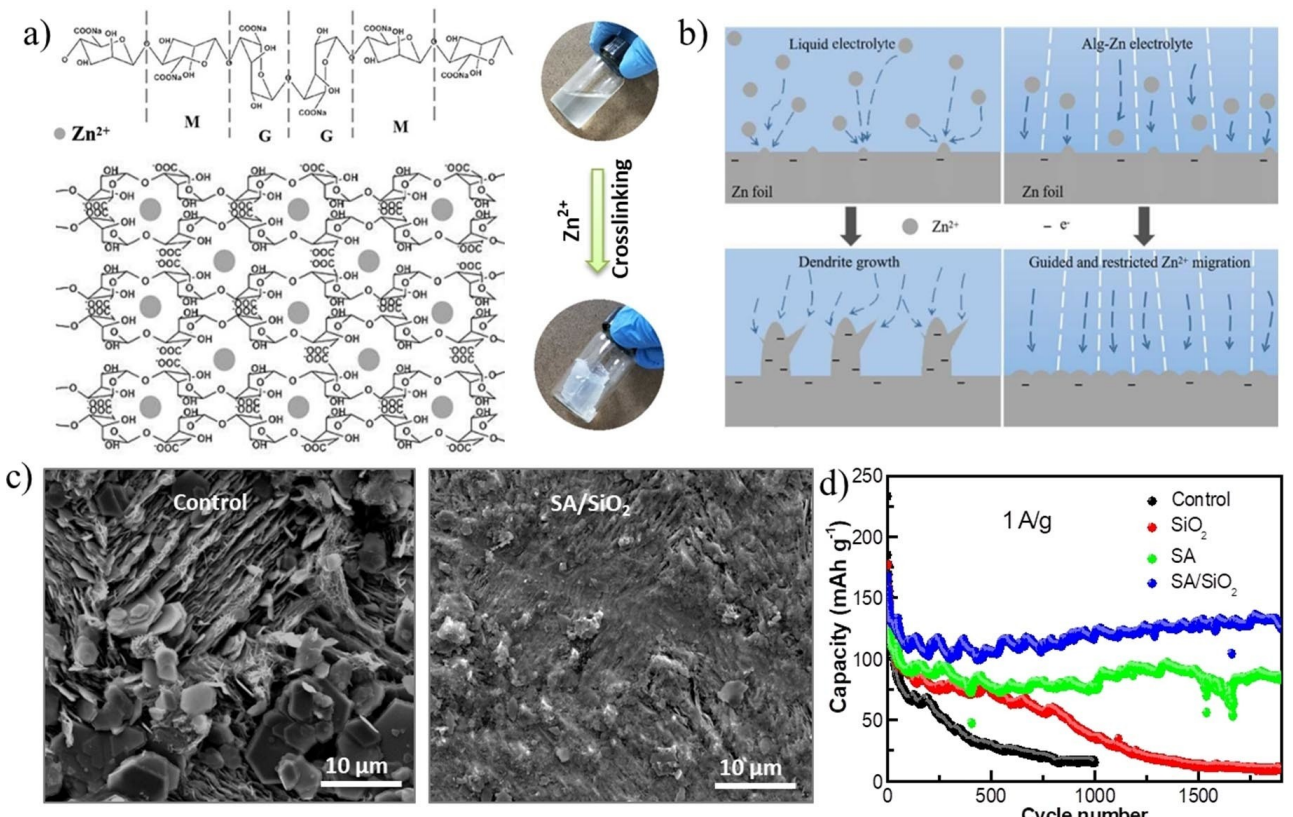


Figure 16. a) Schematic diagram and photographs showing the Zn²⁺ assistance crosslinking of Alg-Zn gel electrolyte, b) Zn plating in $\text{ZnSO}_4 + \text{MnSO}_4$ aqueous electrolyte and Alg-Zn gel electrolyte. Reproduced with permission from Ref. [234]. Copyright 2020, Elsevier. c) SEM images of cycled Zn anodes in the ZnSO_4 control electrolyte and the SA/SiO₂ quasi-gel electrolyte, d) Capacity evolution of Zn–MnO₂ batteries using different electrolytes. Reproduced with permission from Ref. [235]. Copyright 2020, Journal of Inorganic Materials.

restricted by the carboxylate groups,^[56] arising a remarkably suppressing ability to dendrite growth and side reactions on Zn anodes (Figure 16b). Combining the 3D gelation skeletons of cation-linked alginate and gelatin can further improve the mechanical strength, cycling performance and even operational windows of the electrolytes.^[242] As expected, the Zn/Algin-Zn/Zn cell displayed a stable and low voltage polarization over 270 h cycling without any short circuits. The relatively flat and dendrite-free morphology of the cycled Zn anodes confirms the uniform striping/plating behavior of Zn anode in this electrolyte.

At almost the same time, we also developed a SiO₂-reinforced sodium alginate-based (SA/SiO₂) gel electrolytes for long-life ZIBs,^[235] thanks to the strong polymer/oxide interactions and Zn²⁺-induced gelation. The 3D enhanced gel skeletons by SiO₂ nano-particles should be able to homogenize the migration of Zn²⁺, effectively depressing rapid evolution of Zn dendrites by avoiding Zn²⁺ gathering on tips (Figure 16c). Implementation of this gel electrolyte remarkably improved cycle stability of the Zn–MnO₂ batteries even with filter paper separators that are unevenly porous(Figure 16d).

Xanthan gum (XG) and cyclodextrin (CD) are also eco-friendly, highly soluble and salt tolerant biomass gelling agent for aqueous electrolytes. XG is a complex exopolysaccharide consisted of α , β -1,4-linked glucan backbone and trisaccharide side chains attaching on the alternating d-glucosyl residues.^[225] In the XG-based gel, water molecules are attracted on the hydroxyl groups of polymer, rendering high ionic conductivity and viscosity.^[236] Flexible Zn–MnO₂ batteries employing XG-based gel electrolytes have been reported by Di and Li et al.^[243] The optimized sticky gel electrolyte achieves high ionic conductivity of 2.5×10^{-3} S cm⁻¹, which can amazingly remain unchanged at -8°C or yearlong storage at 5°C . This electrolyte holds also the ability to depress Zn dendrite growth and corrosion, guaranteeing the flexible Zn–MnO₂ battery high cycling stability, rate capability, and durability. By adding thixotropic fumed silica (FS) and non-thixotropic β -cyclodextrin (CD) into ZnSO₄+Li₂SO₄ liquid electrolyte, Hoang and Chen et al.^[244] developed a FS+CD composite gel electrolyte for hybrid aqueous batteries. This gel electrolyte can also enhance the specific capacity and cycling stability of the batteries, due to the suppression of Zn dendrite growth.

Besides aqueous gel electrolytes with biomass gelling agents, their industrial counterparts are also attracting numerous attentions.^[225] PVA, a non-toxic, mechanically strong, hydrophilic and cheap synthetic resin commonly used in the textiles and paper industries, has been widely used in various aqueous electrolytes.^[245] For example, Zeng and Lu et al.^[246] reported a flexible Zn–MnO₂@PEDOT battery based on PVA/LiCl–ZnCl₂–MnSO₄ gel electrolyte. The flexible Zn–MnO₂ battery achieved an admirable energy density of 504.9 Wh kg⁻¹ (33.95 mWh cm⁻³) together with a peak power density of 8.6 kW kg⁻¹, and maintained \sim 83.7% of its initial capacity after 300 cycles. In addition, PVA can also be used to produce alkaline gel electrolytes (such as PVA-KOH saturated by Zn²⁺) for the construction of alkaline ZnO-NiO and Zn–Co₃O₄ batteries.^[20,247] For PVA-based gel electrolyte, achievement of

high ionic conductivity and stretching ability are two important issues that should been well addressed.^[225]

PAM (Polyacrylamide) is a high performance gelling agent with numerous hydrophilic amide groups, which can construct gel electrolytes with high conductivity, salt tolerance, mechanical strength and stretching ability.^[248] Recently, Li and Zhi's group^[249] successfully developed a cross-linked PAM-based gel electrolyte for ZIBs by both covalent cross-links and hydrogen bonds, which provided high stretching ability (3000% strain), excellent tensile strength (273 kPa) along with high ionic conductivity (Figure 17a). With a double-helix yarn configuration, a high performance, waterproof, tailorable and stretchable yarn-shape Zn–MnO₂ battery was successfully fabricated (Figure 17b). In addition, the researchers further developed a novel hierarchical composite gel electrolyte (gelatin-g-PAM) via in situ grafting PAM onto gelatin chains.^[230] The introduction of PAM onto the gelatin hydrogel significantly enhances the mechanical strength and ionic conductivity of this composite electrolyte (Figure 17c). The flexible, package-free Zn–MnO₂ battery based on this gel electrolyte achieves highly safety and wearability, and can work under severe application conditions, including cutting, bending, hammering, puncturing, firing, sewing and even washing.

For aqueous batteries, performance deterioration resulting from electrolytes' freezing and fluidity/elasticity loss is another huge fundamental challenge waiting for solving. To solve this problem, Zhi et al. further designed a novel ethylene glycol (EG) based waterborne anionic polyurethane acrylates/PAM (EG-waPUA/PAM) composite hydrogel electrolytes,^[228] achieving excellent freeze-resistance, stability, ionic conductivity and mechanical robustness even at -20°C (Figure 17d). The freeze-resistance is ascribed to the strong cooperative hydrogen bonding between the polymer skeleton and the firmly anchored water molecules inside the polymer matrix. On the other hand, the dual cross-linked structure between EG-waPUA and PAM endows the hydrogel electrolyte flexibly and durability. The flexible Zn–MnO₂ battery based on this gel electrolyte still performs well, electrochemically and mechanically, even at -20°C within 600 cycles.

Pay attention that PAM hydrogels will lose their mechanical robustness in strong alkaline environments. Therefore, solid-state alkaline batteries require further chemical design on electrolytes.^[229,250,251] The salt-tolerant polyacrylic acid (PAA) hydrogel can work in both alkaline and neutral electrolytes, and is therefore adoptable for both ZIBs and Zn-Air batteries.^[144,252] For example, Pei et al.^[229] recently developed a solid state Zn-Air battery that can work at -20°C , by rationally designing the anti-freezing polyacrylic acid (PAA) electrolyte and cold-tolerant noble-metal free catalyst. Moreover, Pei and Chen et al.^[144] further developed a flexible zinc-ion hybrid fiber capacitor based on a ZnSO₄-filled PAA electrolyte, fibrous rGO/CNT positive electrode and Zn/graphite negative electrode (Figure 18). The resulting high ionic conductive hydrogel enables efficient Zn²⁺ adsorption/desorption on positive electrodes and the fast reversible Zn plating/stripping on negative electrodes.

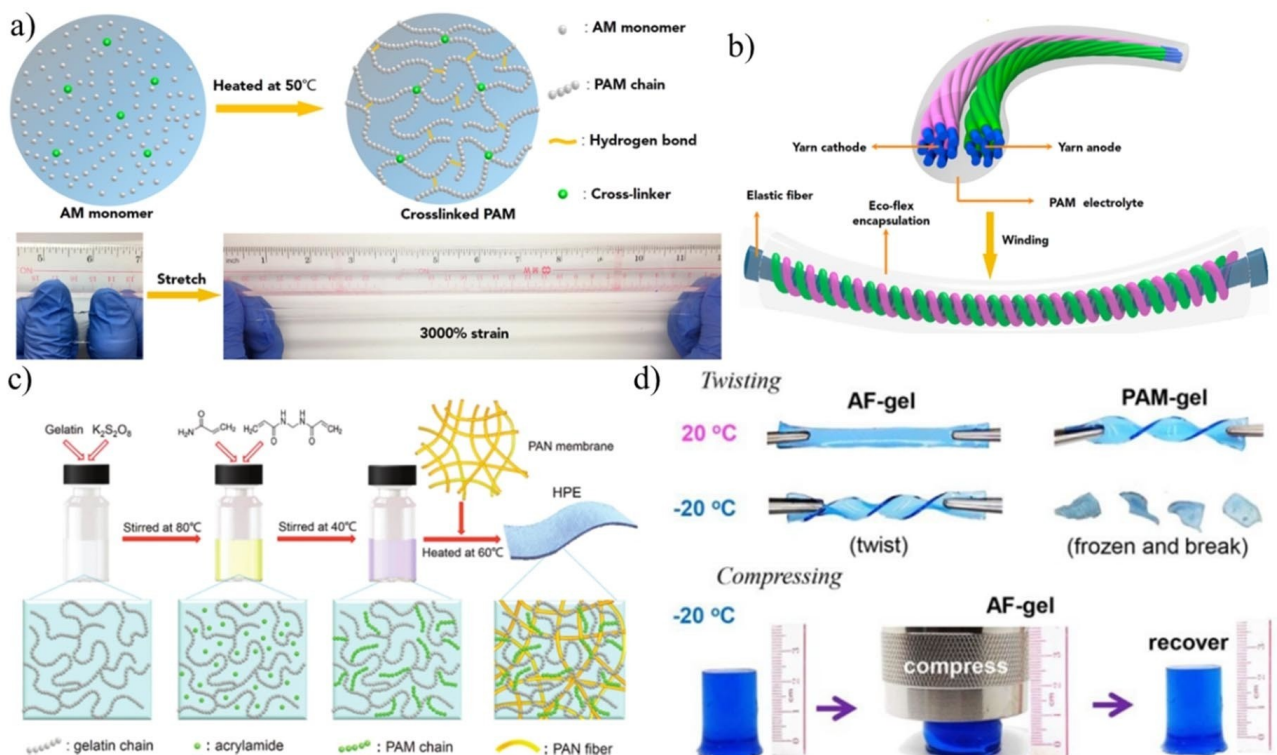


Figure 17. a) Schematic diagram for the fabrication of the cross-linked PAM-based electrolyte and relaxed and elongated states of the cross-linked PAM, showing good stretching ability (3000% strain), b) Schematic encapsulation diagram of the yarn Zn–MnO₂ battery. Reproduced with permission from Ref. [249] Copyright 2018, American Chemical Society. c) Schematic illustration for the synthesis of gelatin-g-PAM gel electrolyte. Reproduced with permission from Ref. [230]. Copyright 2018, the Royal Society of Chemistry. d) Twisting and compressing tests of the anti-freezing EG-waPUA/PAM electrolyte. Reproduced with permission from Ref. [228]. Copyright 2019, the Royal Society of Chemistry.

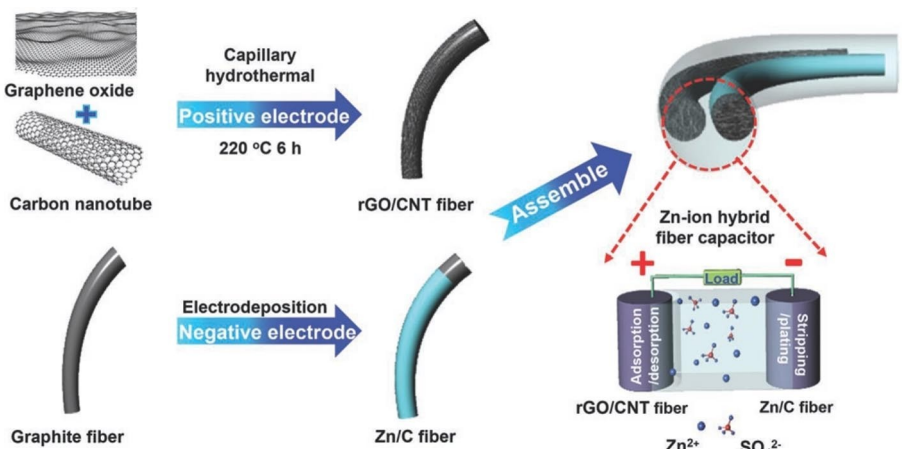


Figure 18. Schematic illustration of the synthesis of rGO/CNT and Zn-coated graphite fibers for assembling a Zn-ion hybrid fiber capacitor and its energy storage mechanism. Reproduced with permission from Ref. [144]. Copyright 2019, Wiley-VCH.

6. Current Collectors for ZIBs

On one hand, the hostless Zn metal anode design can remarkably boost energy densities of ZIBs via maximizing the anodes' capacities and the batteries' operation voltages.^[56] On the other hand, the pure Zn anodes tend to fail rapidly due to the corrosion reaction, infinite relative volume change and randomly grown of dendrites during cycling.^[185,216] Therefore,

the "hostless" anodes actually still need the support of electric conductive current collectors as plating hosts.^[253] Many works indicate that the properties and microstructures of current collectors can even manipulate the plating/stripping behaviors of metal anodes.^[162,177] Generally, this manipulating ability originates from two important facts: 1) current collectors with large specific surface areas can reduce surficial current density and Zn deposit thickness, promoting the uniform deposition of

Zn metal.^[183] 2) Surface structures or high zincophilicity of some current collectors help the uniform and dense heterogeneous nucleation of Zn metals, which then further guide the subsequent Zn plating.^[179] For ZIBs, the proposed current collectors include Cu,^[253] Ti,^[119,150,160,254] Ni,^[255] stainless steel,^[21,256] and a variety of carbon materials (carbon cloth/felt,^[257,258] carbon fiber,^[182,259] graphite paper^[260,261] and graphene foam^[67,192] etc.).

Cu foils are the standard current collectors of commercial LIBs' graphite anodes. It is further suggested that nanostructured Cu is suitable to host Li metal anode due to the large surface area.^[262,263] Generally, the Cu nano-structures are obtained by either chemical de-alloying method,^[262] reducing nanostructured copper oxides,^[263] or simply chemical etching.^[253] In the study of ZIBs, Cu foils are also a widely used current collector, in both half cells and full cells.^[55,176] Indeed, it is reported that Cu hold good Zn affinity and can promote uniform nucleation of Zn through in situ formation of Cu-Zn solid solution.^[173,216] Recently, Xu et al.^[253] demonstrated a stable 3D Zn anode by electrodepositing Zn onto a facile NH₃-H₂O etched nano-porous Cu skeleton (Figure 19a). The Zn on the Cu

skeleton is uniform and compact, can reversibly plating/stripping with fast electrochemical kinetics and high Coulombic efficiency almost 100% for 350 h. In addition, commercially available Cu,^[264–266] Ni^[255] foams and Cu meshes^[216] are also feasible alternatives of nanostructured Cu skeleton to stabilize Zn metal anodes, in both neutral and alkaline electrolytes.

Although the applications of metallic current collectors in ZIBs have been well demonstrated, the selection of current collectors for potential commercial ZIBs should still be cautious, regarding their chemical/electrochemical stability, cost, environmental impact, and potential influence on side reactions (for example, catalyzing hydrogen evolution reactions).^[267] In addition, the corrosion and dissolution of metallic current collectors may become severe in low-pH aqueous electrolytes or abused conditions.^[268,269] Therefore, specific studies are still urgently needed to establish high performance and long-term stable current collectors for ZIBs. In this field, relative design concepts of strongly acid/alkaline batteries should be worth learning from.^[6,270]

Compared to metallic ones, carbon materials with high specific surface areas are also attractive current collectors for

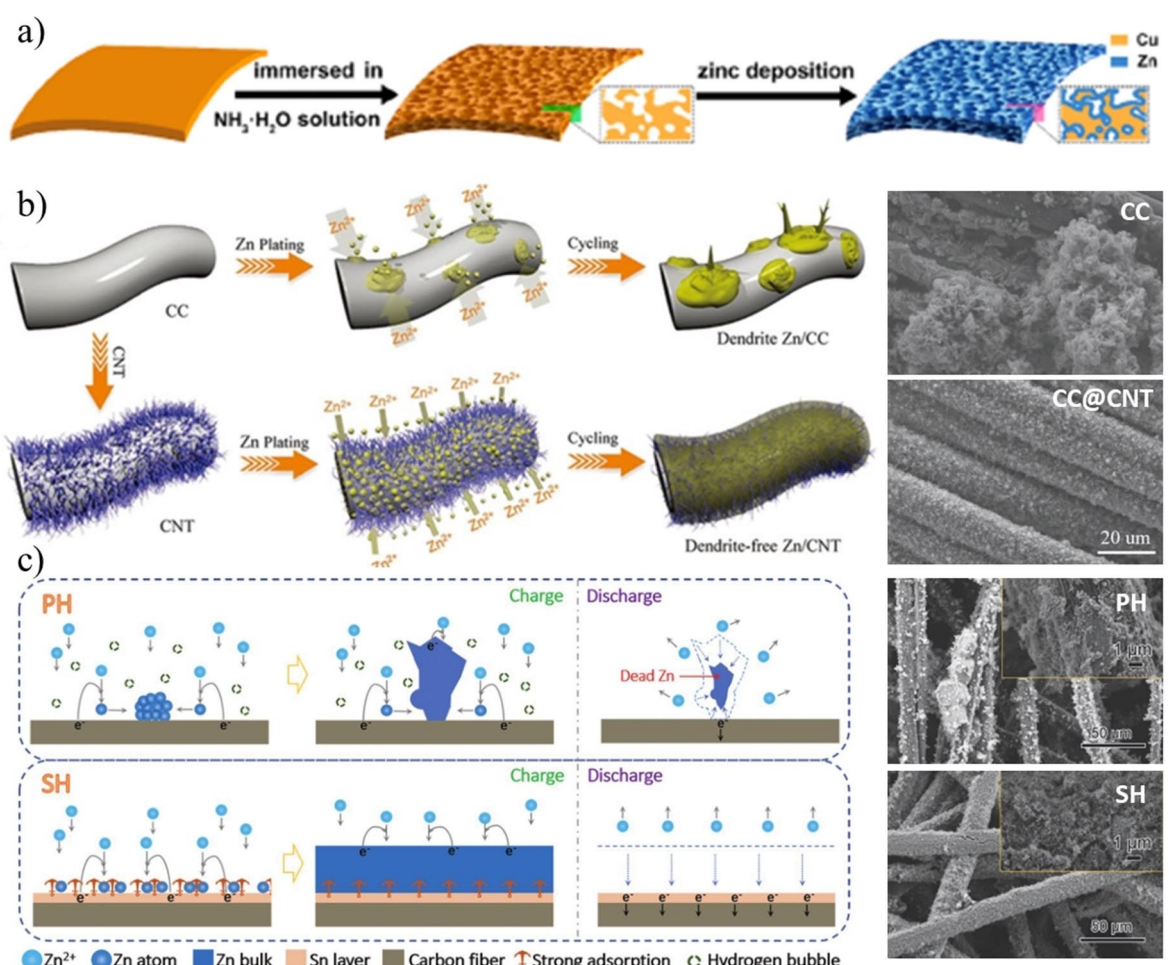


Figure 19. a) Fabricating process of 3D Zn anodes supported by nano-porous Cu skeleton. Reproduced with permission from Ref. [253]. Copyright 2019, American Chemical Society. b-c) Schematic illustration and SEM images of the zinc deposition on carbon cloth (CC), carbon nanotube modified carbon cloth (CC@CNT) (reproduced with permission from Ref. [191], Copyright 2019, Wiley-VCH), carbon felt (PH) and Sn nano-particle modified carbon felt (SH) (Reproduced with permission from Ref. [193], Copyright © 2020, Wiley-VCH).

ZIBs, due to their conductivity, abundance, and chemical stability. As in the cases of ZIBs,^[271,272] modifications of the carbon materials by doping or depositing can further increase hydro- and zincophilicity of the current collectors, affiliating the uniform electro-plating of Zn metals.^[184] For example, Zang and Lu et al.^[191] developed a flexible CNT@CC current collectors by growing carbon nanotube arrays onto flexible carbon clothes (CC). This CNT@CC substrates show large specific surface areas, high zincophilicity and homogeneous electric field distribution, endowing a low-barrier, compact, dendrite-free, and reversible Zn plating process (Figure 19b). This rationally designed collector can also boost the performance of cathodes in ZIBs.^[65]

Decorating carbon current collectors with zincophilic nanomaterials is also an effective approach to stabilize Zn metal anodes. Li and Mai et al.^[183] reported a trilayer 3D CC-ZnO@C current collector by *In situ* growing ZIFs (zeolitic-imidazolate frameworks) derived ZnO@C core-shell nano-rod array on a carbon cloth. This hierarchical-structured collector combine the high flexibility of the carbon cloth and high surface area and zincophilicity of the ZnO@C array, achieving a high anti-dendrite ability.

Recently, Yin and Li et al.^[193] developed a Sn-modified 3D carbon felt current collectors for aqueous zinc-based flow batteries (Figure 19c). The Sn modification layer was deposited by a magnetron sputtering method. Different from the weak physical adsorption by van der Waals interaction between Zn and carbon,^[185] density functional theoretical (DFT) calculation suggests the existence of stronger electronic interactions

between Zn and Sn.^[193] These interactions can effectively alleviate the aggregation and peeling off of plated Zn deposits. As a result, uniform and reversible Zn plating/stripping processes are achieved, resulting in compact and flat Zn deposits without obvious dendrites.

As a remarkable and fresh breakthrough in the field of current collectors, Zheng and Archer et al.^[179] innovated an epitaxial mechanism to regulate nucleation, growth, and reversibility of metal anodes, including Zn (Figure 20a–d). The main idea of this strategy is to lock crystallographic orientation of the electro-deposited metals with specific current collectors. For the sake of clear demonstration, the researchers developed a rheological method to enable parallel arrange of graphene sheets on the stainless steel surface. The graphene, holding a low lattice mismatch with Zn, can drive the planar epitaxial electro-deposition of Zn, and achieves exceptional reversibility for the metal anodes. With this method, the utilization efficiency of Zn anode can be promoted up to 50% in a long-life battery, a unprecedented level for ZIBs. The researchers also concluded the crystallographic, surface texturing, and electrochemical criteria for the achievement of this reversible epitaxial electro-deposition. Almost at the same time, Li and Wei et al.^[273] reported the similar impacts of graphene on Li plating, confirming the wide applicability of this pathway toward energy-dense metal batteries (Figure 20e–q).

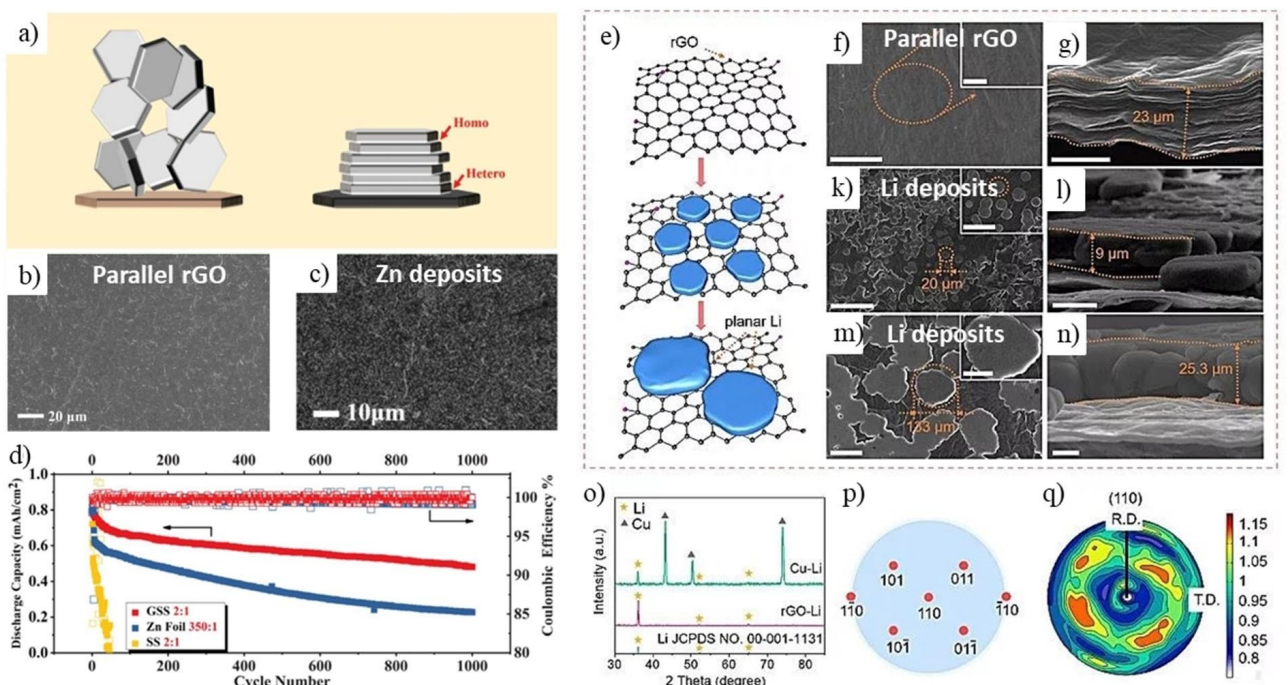


Figure 20. (a–c, e–n) Scheme illustrating and Typical SEM images showing the epitaxial metal electro-deposition process (c, k–n) on graphenes (b, f–g). (d) Cycling performance of Zn– α -MnO₂ full cells with and without the graphene epitaxial mechanism, with controlled anode:cathode capacity ratios (the red numbers). (o) XRD patterns of standard Li, Li on Cu foil and Li on the rGO substrate. (p) Standard projection figure of (110) plane and (q) orientation characterization of the deposited Li on the rGO substrate. Panels (a–d) and (e–q) are reproduced from with permission from Ref. [179] (Copyright 2019, American Association for the Advancement of Science) and Ref. [273] (Copyright 2020, Wiley-VCH), respectively.

7. Separators for ZIBs

In common cases, a separator is an electrically insulating but electrolyte-permeable membrane sandwiched between the anode and cathode of a battery. It can prevent the electrodes (anode and cathode laminates) from electrical short circuits by blocking physical contact, while allowing the smooth transport of ionic charge carriers that are dispersible for the battery's chemistry. If the electrodes have already been well isolated from each other by structure design, separators are eliminable, for example in some electrochromic batteries.^[113,114,274] For solid-state batteries, the gel or solid-state electrolytes can be regarded as an integration of separators and electrolytes.^[88] In this configuration, individual separators may also become unnecessary.^[5] In this section, we mainly focus on the traditional porous and freestanding separators for ZIBs with liquid electrolytes.

Different from the diverse cathode and electrolyte materials, there are only a few choices of separators for ZIBs, even though they may have significant influence on batteries performance.^[164] For instance, rational-designed smart separators can address fire risk of LIBs, which melts into dense sheets and cut off ionic transport in accidental short circuit situations and block the out of control charge/discharge processes.^[275] However, the commercial LIBs' polyolefin separators (e.g., polyethylene (PE) or polypropylene (PP) porous membranes) are not suitable for aqueous ZIBs, due to their hydrophobic nature and low ability to protect dendrite piercing. In fact, developing of an adequate separator for specific battery is far from easy, since its requirements include thickness (in micron

scale), areal weight, uniformity, mechanical strength, chemical/electrochemical stability, electrolyte uptake ability, etc.^[276]

Figure 21 compares the morphology and performance of three typical ZIBs' separators. Among them, glass fiber paper (GFPs, Figure 21a) is the first reported and widely used separator for ZIBs.^[17,24,197] This separator is made from randomly distributed or weaved glass fibers with 0.2–2 µm diameters, leaving plenty of interconnected micron pores for electrolyte permeation. Their high porosity ensures uniform electrolyte flux within the separators, which is very favorable for the achievement of dendrite-free Zn plating/stripping.^[56] Indeed, similar dendrite-growth depression by GFPs is also detectable in the plating/stripping processes of Li anodes, where the interactions between surface groups (e.g., Si–O and O–H) and Li⁺ may further homogenize Li⁺ distribution on the anode surfaces.^[164] With advantages of high chemical stability, reasonable cost, and stiffness, applications of this versatile material extend from batteries' separators, filter papers to polymeric resins' reinforcement. As batteries' separators, the main disadvantage of GFPs is their large thickness and heavy areal weight.

Airlaid^[38] and filter papers^[56,150] made from wood pulp are also attractive separator materials for ZIBs. The typical SEM image of filter paper clearly shows its wood fabric and inhomogeneous pore structure (Figure 21b). There are tens-micron pores in some parts of the filter paper, while the rest parts are much denser. In ZIBs, the dense parts of filter papers can limit local electrolyte transport and there increases the over-potentials of Zn plating/stripping, due to microscopic pore-deficiency (Figure 21b). On the other hand, the pore parts, as

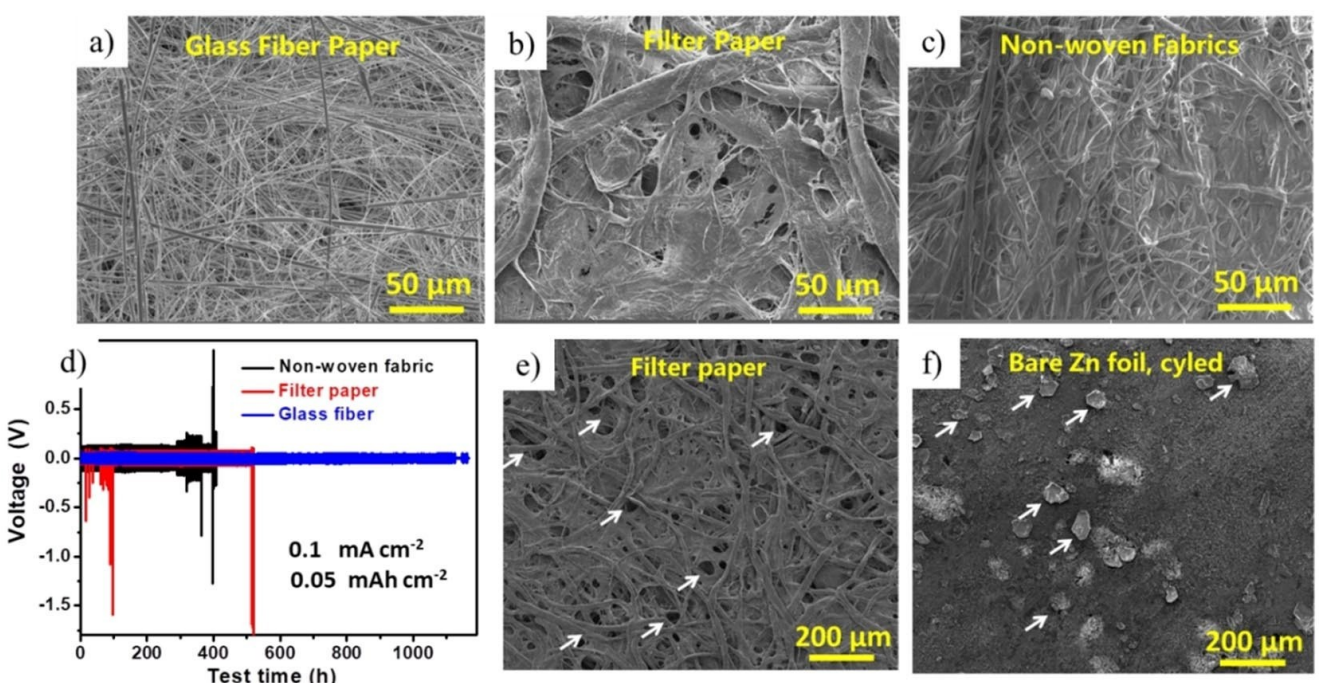


Figure 21. a–c, e) Typical SEM images of different separators, and d) their influences on cycling stability of Zn–Zn symmetric cells in ZnSO₄ electrolyte. e–f) Morphology comparison of a filter paper and a cycled Zn anode cling to the filter paper. The white arrows in panel (e–f) highlight the shape, size and distribution similarity between the separator pores and the Zn dendrites' protuberances, implying a close relationship between them. Panels (a–b) and (e–f) were redrew with data from Ref. [56] (Copyright 2018, Wiley-VCH).

electrolyte transport "highways", kinetically accelerate the growth and detachment of Zn dendrites on local anode surface. Therefore, Zn dendrites' protuberances with shape, size and density highly similar to the filter paper separator's pores formed after cycling (Figure 21e-f). These continuously accumulating dendrites can easily pierce the separator and cause internal short circuits.^[56] Electrolyte wetting can significantly weaken the mechanical strength of this separator, which may decrease the batteries' reliability and lifetime.

Compared to GFPs and filter papers, non-woven fabrics (NWFs) hold uniform morphology and deliver a moderate Zn plating/stripping cycling stability. However, their low porosity gives rise to high over-potentials of Zn plating/stripping, which is obviously disadvantageous for practical applications (Figure 21c-d). In general, the advantages of filter/airlaid papers and NWFs separators stems from their environmental-friendly, light-weight and cost-efficient nature, and the GFPs' from their high performances.

Besides porous electrolyte-permeable separators, some ZIBs employ cation or anion exchanging membranes as separators,^[24] analogous to redox flow batteries.^[277] These separators can connect different electrolyte without shuttle effects, making the ZIBs design more flexible.^[278] The use of ion-selective membrane separators can further suppress the dissolution of cathode materials and protect the Zn anode from poisoning by the dissolved cathode materials.^[150] For these separators, the high cost and low ionic conductivity are two big obstacles for practical applications.^[279]

8. Conclusions and Outlook

In the past three decades, the rise of high-energy-density lithium ion batteries (LIBs) brings numerous technology visions into reality. At the same time, survival of the Pb-acid batteries and the many unsuccessful implementation efforts of LIBs remind us the necessity of diverse battery technologies. As one number of the rich aqueous battery family, zinc ion batteries (ZIBs) hold the precious balance of energy density, cycling life, cost and safety. The intensive studies of ZIBs after 2012 make tremendous progresses on both the understanding of battery chemistry and the development of battery materials. These works clearly show ZIBs' possibility to evolve into an attractive energy-safety-balanced alternative of LIBs, but also highlight the existence of tremendous challenges that impede their practical applications.^[7,280] In our opinion, there are at least 4 issues and challenges that should be considered for the development or even commercialization of ZIBs.

1. The achievement of stable and high areal capacity on cathode side is very important for practical application, since it is closely related with the cell-level energy density. Up to date, there are only a few works regarding this aspects,^[97,281] while the other works tested cathode materials at mass loadings less than 5 mg cm^{-2} . Special attentions should be paid on the scalable preparation and proper evaluation of high performance cathode materials. Therefore, standard test systems are urgently needed and highly

desired for the sake of objectively evaluating the performances of Zn anodes.

2. Mass production of stable and high utilization rate Zn anodes is a prerequisite for the commercialization of ZIBs, which means effective depression of the dendritic deposition and corrosion reaction. Considering the fact that all these detrimental side reactions are interfacial processes, surface modification of Zn anodes and current collectors associating with the buffer layer and epitaxial electrodeposition strategies is worthy of attention. Moreover, development of non-aqueous electrolytes that are thermodynamically stable with Zn anodes represents a more radical approach for the construction of stable ZIBs. However, this methodology is not widely applicable because water is indispensable for a wide range of cathodic reactions.
3. The important influence of separators on ZIBs' performances has been long neglected. In fact, the few separator choices make the lightweight while high performance separators of ZIBs currently unavailable. High ionic conductive hydrogel electrolytes are important for ZIBs, since they can eliminate the needs of separators without performance and safety deterioration.
4. The design of multi-functional ZIBs is a valuable subject deserving to be explored. For instance, flexible ZIBs are important power source for wearable devices due to their safe, non-corrosive and $\text{H}_2\text{O}/\text{O}_2$ -tolerant natures. The combination of electrochromic and ZIBs' technology leads to the emergence of color-changeable batteries and energy-storable smart window. The latter not only turns windows into batteries, but also dynamically manages the indoor-entering solar energy of the installed buildings.

After the overwhelming development and implementation of LIBs for decades, it is the time to rediscover the importance and diverse potential of aqueous batteries. The recent rapid development of ZIBs is an extraordinary story of activating these ancient batteries with powerful nanotechnologies. These nanotechnologies provide chances to understand chemical mechanisms behind performances, but many of them are facing cost problems. It means that the commercialization of ZIBs still requires considerable traditional technologies. To promote the process, we should confront and solve these problems and challenges with innovative strategies.

Acknowledgements

The authors thank the National Natural Science Foundation of China (51502194, 51772257), Major Basic Research Projects of Shandong Natural Science Foundation (ZR2018ZC1459) for financial support.

Conflict of Interest

The authors declare no conflict of interest.

Keywords: zinc-ion battery • aqueous battery • aqueous electrolyte • Zn anode

- [1] J. B. Goodenough, Y. Kim, *Chem. Mater.* **2010**, *22*, 587–603.
- [2] H. Pan, Y. Shao, P. Yan, Y. Cheng, K. S. Han, Z. Nie, C. Wang, J. Yang, X. Li, P. Bhattacharya, K. T. Mueller, J. Liu, *Nat. Energy.* **2016**, *1*, 16039.
- [3] W. Li, J. R. Dahn, D. S. Wainwright, *Science.* **1994**, *264*, 1115–1118.
- [4] Q. Pang, C. Sun, Y. Yu, K. Zhao, Z. Zhang, P. M. Voyles, G. Chen, Y. Wei, X. Wang, *Adv. Energy Mater.* **2018**, *8*, 1800144.
- [5] P. Yu, Y. Zeng, H. Zhang, M. Yu, Y. Tong, X. Lu, *Small.* **2019**, *15*, 1804760.
- [6] X. Zeng, J. Hao, Z. Wang, J. Mao, Z. Guo, *Energy Storage Mater.* **2019**, *20*, 410–437.
- [7] G. Fang, J. Zhou, A. Pan, S. Liang, *ACS Energy Lett.* **2018**, *3*, 2480–2501.
- [8] D. Kundu, B. D. Adams, V. Duffort, S. H. Vajargah, L. F. Nazar, *Nat. Energy.* **2016**, *1*, 16119.
- [9] C. Xia, J. Guo, Y. Lei, H. Liang, C. Zhao, H. N. Alshareef, *Adv. Mater.* **2018**, *30*, 1705580.
- [10] G. Li, Z. Yang, Y. Jiang, C. Jin, W. Huang, X. Ding, Y. Huang, *Nano Energy.* **2016**, *25*, 211–217.
- [11] J. F. Parker, C. N. Chervin, I. R. Pala, M. Machler, M. F. Burz, J. W. Long, D. R. Rolison, *Science.* **2017**, *356*, 415–418.
- [12] N. Zhang, F. Cheng, Y. Liu, Q. Zhao, K. Lei, C. Chen, X. Liu, J. Chen, *J. Am. Chem. Soc.* **2016**, *138*, 12894–12901.
- [13] C. Xu, B. Li, H. Du, F. Kang, *Angew. Chem. Int. Ed.* **2012**, *51*, 933–935; *Angew. Chem.* **2012**, *124*, 957–959.
- [14] L.-N. Chen, M.-Y. Yan, Z.-W. Mei, L.-Q. Mai, *J. Inorg. Mater.* **2017**, *32*, 225–234.
- [15] C. Xia, J. Guo, P. Li, X. Zhang, H. N. Alshareef, *Angew. Chem.* **2018**, *130*, 4007–4012; *Angew. Chem. Int. Ed.* **2018**, *57*, 3943–3948.
- [16] M. Winter, R. J. Brodd, *Chem. Rev.* **2004**, *104*, 4245–4270.
- [17] T. Yamamoto, T. Shoji, *Inorg. Chim. Acta.* **1986**, *117*, L27–L28.
- [18] N. Zhang, F. Cheng, J. Liu, L. Wang, X. Long, X. Liu, F. Li, J. Chen, *Nat. Commun.* **2017**, *8*, 405.
- [19] A. J. Gibson, B. Johannessen, Y. Beyad, J. Allen, S. W. Donne, *J. Electrochem. Soc.* **2016**, *163*, H305–H312.
- [20] X. W. Wang, F. X. Wang, L. Y. Wang, M. X. Li, Y. F. Wang, B. W. Chen, Y. S. Zhu, L. J. Fu, L. S. Zha, L. X. Zhang, Y. P. Wu, W. Huang, *Adv. Mater.* **2016**, *28*, 4904–4911.
- [21] S. H. Kim, S. M. Oh, *J. Power Sources.* **1998**, *72*, 150–158.
- [22] J. F. Parker, C. N. Chervin, E. S. Nelson, D. R. Rolison, J. W. Long, *Energy Environ. Sci.* **2014**, *7*, 1117–1124.
- [23] X. Cao, H. Xia, X. Zhao, *Funct. Mater. Lett.* **2019**, *12*, 1930004.
- [24] T. Shoji, M. Hishinuma, T. Yamamoto, *J. Appl. Electrochem.* **1988**, *18*, 521–526.
- [25] R. Trócoli, F. La Mantia, *ChemSusChem.* **2015**, *8*, 481–485.
- [26] Y. Shen, K. Kordeschi, *J. Power Sources.* **2000**, *87*, 162–166.
- [27] J. W. Gallaway, D. Desai, A. Gaikwad, C. Corredor, S. Banerjee, D. Steingart, *J. Electrochem. Soc.* **2010**, *157*, A1279–A1286.
- [28] W. Sun, F. Wang, S. Hou, C. Yang, X. Fan, Z. Ma, T. Gao, F. Han, R. Hu, M. Zhu, C. Wang, *J. Am. Chem. Soc.* **2017**, *139*, 9775–9778.
- [29] D. Xu, B. Li, C. Wei, Y.-B. He, H. Du, X. Chu, X. Qin, Q.-H. Yang, F. Kang, *Electrochim. Acta.* **2014**, *133*, 254–261.
- [30] S. Higashi, S. W. Lee, J. S. Lee, K. Takechi, Y. Cui, *Nat. Commun.* **2016**, *7*, 11801.
- [31] X. Guo, J. Zhou, C. Bai, X. Li, G. Fang, S. Liang, *Mater. Today* **2020**, *16*, 100396.
- [32] B. Lee, C. S. Yoon, H. R. Lee, K. Y. Chung, B. W. Cho, S. H. Oh, *Sci. Rep.* **2014**, *4*, 6066.
- [33] C. Xu, Y. Chen, S. Shi, J. Li, F. Kang, D. Su, *Sci. Rep.* **2015**, *5*, 14120.
- [34] P. Senguttuvan, S. D. Han, S. Kim, A. L. Lipson, S. Tepavcevic, T. T. Fister, I. D. Bloom, A. K. Burrell, C. S. Johnson, *Adv. Energy Mater.* **2016**, *6*, 1600826.
- [35] C. Xu, H. Du, B. Li, F. Kang, Y. Zeng, *Electrochim. Solid-State Lett.* **2009**, *12*, A61–A65.
- [36] R. Y. Wang, C. D. Wessells, R. A. Huggins, Y. Cui, *Nano Lett.* **2013**, *13*, 5748–5752.
- [37] M. Song, H. Tan, D. Chao, H. J. Fan, *Adv. Funct. Mater.* **2018**, *28*, 1802564.
- [38] B. Jiang, C. Xu, C. Wu, L. Dong, J. Li, F. Kang, *Electrochim. Acta.* **2017**, *229*, 422–428.
- [39] X. Zhu, X. Wu, T. N. L. Doan, Y. Tian, H. Zhao, P. Chen, *J. Power Sources.* **2016**, *326*, 498–504.
- [40] B. Zhang, Y. Liu, X. Wu, Y. Yang, Z. Chang, Z. Wen, Y. Wu, *Chem. Commun.* **2014**, *50*, 1209–1211.
- [41] P. Hu, T. Zhu, X. Wang, X. Wei, M. Yan, J. Li, W. Luo, W. Yang, W. Zhang, L. Zhou, Z. Zhou, L. Mai, *Nano Lett.* **2018**, *18*, 1758–1763.
- [42] P. He, G. Zhang, X. Liao, M. Yan, X. Xu, Q. An, J. Liu, L. Mai, *Adv. Energy Mater.* **2018**, *8*, 1702463.
- [43] P. He, M. Yan, G. Zhang, R. Sun, L. Chen, Q. An, L. Mai, *Adv. Energy Mater.* **2017**, *7*, 1601920.
- [44] Z. Liu, G. Pulletkurthi, F. Endres, *ACS Appl. Mater. Interfaces.* **2016**, *8*, 12158–12164.
- [45] L. Zhang, L. Chen, X. Zhou, Z. Liu, *Sci. Rep.* **2015**, *5*, 18263.
- [46] Q. Yang, F. Mo, Z. Liu, L. Ma, X. Li, D. Fang, S. Chen, S. Zhang, C. Zhi, *Adv. Mater.* **2019**, *31*, 1901521.
- [47] N. Zhang, Y. Dong, M. Jia, X. Bian, Y. Wang, M. Qiu, J. Xu, Y. Liu, L. Jiao, F. Cheng, *ACS Energy Lett.* **2018**, *3*, 1366–1372.
- [48] M. H. Alfaruqi, V. Mathew, J. Gim, S. Kim, J. Song, J. P. Baboo, S. H. Choi, J. Kim, *Chem. Mater.* **2015**, *27*, 3609–3620.
- [49] O. Ghodbane, J.-L. Pascal, F. Favier, *ACS Appl. Mater. Interfaces.* **2009**, *1*, 1130–1139.
- [50] J. Lee, J. B. Ju, W. I. Cho, B. W. Cho, S. H. Oh, *Electrochim. Acta.* **2013**, *112*, 138–143.
- [51] D. Wang, L. Wang, G. Liang, H. Li, Z. Liu, Z. Tang, J. Liang, C. Zhi, *ACS Nano.* **2019**, *13*, 10643–10652.
- [52] K. W. Nam, H. Kim, J. H. Choi, J. W. Choi, *Energy Environ. Sci.* **2019**, *12*, 1999–2009.
- [53] M. H. Alfaruqi, J. Gim, S. Kim, J. Song, D. T. Pham, J. Jo, Z. Xiu, V. Mathew, J. Kim, *Electrochim. Commun.* **2015**, *60*, 121–125.
- [54] N. Qiu, H. Chen, Z. Yang, S. Sun, Y. Wang, *Electrochim. Acta.* **2018**, *272*, 154–160.
- [55] A. Naveed, H. Yang, J. Yang, Y. Nuli, J. Wang, *Angew. Chem. Int. Ed.* **2019**, *58*, 2760–2764.
- [56] L. Kang, M. Cui, F. Jiang, Y. Gao, H. Luo, J. Liu, W. Liang, C. Zhi, *Adv. Energy Mater.* **2018**, *8*, 1801090.
- [57] M. H. Alfaruqi, S. Islam, J. Gim, J. Song, S. Kim, D. T. Pham, J. Jo, Z. Xiu, V. Mathew, J. Kim, *Chem. Phys. Lett.* **2016**, *650*, 64–68.
- [58] D. Chao, W. Zhou, C. Ye, Q. Zhang, Y. Chen, L. Gu, K. Davey, S.-Z. Qiao, *Angew. Chem. Int. Ed.* **2019**, *58*, 7823–7828.
- [59] C. Zhong, B. Liu, J. Ding, X. Liu, Y. Zhong, Y. Li, C. Sun, X. Han, Y. Deng, N. Zhao, W. Hu, *Nat. Energy.* **2020**, *10*, 10.1038/s41560-41020-40584-y.
- [60] W. Chen, G. Li, A. Pei, Y. Li, L. Liao, H. Wang, J. Wan, Z. Liang, G. Chen, H. Zhang, J. Wang, Y. Cui, *Nat. Energy.* **2018**, *3*, 428–435.
- [61] C. Liu, X. Chi, Q. Han, Y. Liu, *Adv. Energy Mater.* **2020**, *10*, 1903589.
- [62] Y. Zhang, S. Deng, G. Pan, H. Zhang, B. Liu, X.-L. Wang, X. Zheng, Q. Liu, X. Wang, X. Xia, J. Tu, *Small Methods.* **2020**, 1900828.
- [63] Z. Hu, X. Xiao, C. Chen, T. Li, L. Huang, C. Zhang, J. Su, L. Miao, J. Jiang, Y. Zhang, J. Zhou, *Nano Energy.* **2015**, *11*, 226–234.
- [64] L. Kang, P. Li, K. Tao, X. Wang, W. Liang, Y. Gao, *J. Power Sources.* **2016**, *302*, 352–360.
- [65] X. Zhang, S. Wu, S. Deng, W. Wu, Y. Zeng, X. Xia, G. Pan, Y. Tong, X. Lu, *Small Methods.* **2019**, 1900525.
- [66] B. Wu, G. Zhang, M. Yan, T. Xiong, P. He, L. He, X. Xu, L. Mai, *Small.* **2018**, *14*, 1703850.
- [67] C. Wang, M. Wang, Z. He, L. Liu, Y. Huang, *ACS Appl. Energy Mater.* **2020**, *3*, 1742–1748.
- [68] L. Ma, L. Li, Y. Liu, J. Zhu, T. Meng, H. Zhang, J. Jiang, C. M. Li, *Chem. Commun.* **2018**, *54*, 10835–10838.
- [69] Y. Fu, Q. Wei, G. Zhang, X. Wang, J. Zhang, Y. Hu, D. Wang, L. Zuin, T. Zhou, Y. Wu, S. Sun, *Adv. Energy Mater.* **2018**, *8*, 1801445.
- [70] Z. Yang, L. Trahey, Y. Ren, M. K. Y. Chan, C. Lin, J. Okasinski, M. M. Thackeray, *J. Mater. Chem. A.* **2015**, *3*, 7389–7398.
- [71] J. Shin, D. Shin, H. Hwang, T. Yeo, S. Park, W. Choi, *J. Mater. Chem. A.* **2017**, *5*, 13488–13498.
- [72] J. J. Duan, S. Chen, S. Dai, S. Z. Qiao, *Adv. Funct. Mater.* **2014**, *24*, 2072–2078.
- [73] E. Levi, Y. Gofer, D. Aurbach, *Chem. Mater.* **2010**, *22*, 860–868.
- [74] M. Yan, P. He, Y. Chen, S. Wang, Q. Wei, K. Zhao, X. Xu, Q. An, Y. Shuang, Y. Shao, K. T. Mueller, L. Mai, J. Liu, J. Yang, *Adv. Mater.* **2018**, *30*, 1703725.
- [75] Y. Zhu, C. Wang, *J. Phys. Chem. C.* **2010**, *114*, 2830–2841.
- [76] B. Li, C. Han, Y.-B. He, C. Yang, H. Du, Q.-H. Yang, F. Kang, *Energy Environ. Sci.* **2012**, *5*, 9595–9602.
- [77] M. Park, X. Zhang, M. Chung, G. B. Less, A. M. Sastry, *J. Power Sources.* **2010**, *195*, 7904–7929.

- [78] M. H. Alfaruqi, V. Mathew, J. Song, S. Kim, S. Islam, D. T. Pham, J. Jo, S. Kim, J. P. Baboo, Z. Xiu, K.-S. Lee, Y.-K. Sun, J. Kim, *Chem. Mater.* **2017**, *29*, 1684–1694.
- [79] J. H. Jo, Y. K. Sun, S. T. Myung, *J. Mater. Chem. A* **2017**, *5*, 8367–8375.
- [80] X. Dai, F. Wan, L. Zhang, H. Cao, Z. Niu, *Energy Storage Mater.* **2019**, *17*, 143–150.
- [81] B. Lan, C. Tang, L. Chen, W. Zhang, W. Tang, C. Zuo, X. Fu, S. Dong, Q. An, P. Luo, *J. Alloys Compd.* **2020**, *818*, 153372.
- [82] Y. Oka, T. Yao, N. Yamamoto, *J. Solid State Chem.* **1990**, *89*, 372–377.
- [83] H. Q. Li, T. Y. Zhai, P. He, Y. G. Wang, E. Hosono, H. S. Zhou, *J. Mater. Chem.* **2011**, *21*, 1780–1787.
- [84] M. M. Rahman, J. Z. Wang, N. H. Idris, Z. X. Chen, H. K. Liu, *Electrochim. Acta* **2010**, *56*, 693–699.
- [85] X. Rui, D. Sim, C. Xu, W. Liu, H. Tan, K. Wong, H. H. Hng, T. M. Lim, Q. Yan, *RSC Adv.* **2012**, *2*, 1174–1180.
- [86] K. Wang, X. Zhang, J. Han, X. Zhang, X. Sun, C. Li, W. Liu, Q. Li, Y. Ma, *ACS Appl. Mater. Interfaces* **2018**, *10*, 24573–24582.
- [87] W. Qiu, Y. Li, A. You, Z. Zhang, G. Li, X. Lu, Y. Tong, *J. Mater. Chem. A* **2017**, *5*, 14838–14846.
- [88] P. Liu, R. Lv, Y. He, B. Na, B. Wang, H. Liu, *J. Power Sources* **2019**, *410*, 411, 137–142.
- [89] L. Ma, N. Li, C. Long, B. Dong, D. Fang, Z. Liu, Y. Zhao, X. Li, J. Fan, S. Chen, S. Zhang, C. Zhi, *Adv. Funct. Mater.* **2019**, *29*, 1906142.
- [90] W. Xu, C. Sun, K. Zhao, X. Cheng, S. Rawal, Y. Xu, Y. Wang, *Energy Storage Mater.* **2019**, *16*, 527–534.
- [91] Y. Lei, K. Fujisawa, F. Zhang, N. Briggs, A. R. Aref, Y.-T. Yeh, Z. Lin, J. A. Robinson, R. Rajagopalan, M. Terrones, *ACS Appl. Energy Mater.* **2019**, *2*, 8625–8632.
- [92] C. Zhao, C. Yu, M. Zhang, Q. Sun, S. Li, M. Norouzi Banis, X. Han, Q. Dong, J. Yang, G. Wang, X. Sun, J. Qiu, *Nano Energy* **2017**, *41*, 66–74.
- [93] J. Zhou, Y. Liu, S. Zhang, T. Zhou, Z. Guo, *InfoMat.* **2020**, *2*, 437–465.
- [94] H. Liang, Z. Cao, F. Ming, W. Zhang, D. H. Anjum, Y. Cui, L. Cavallo, H. N. Alshareef, *Nano Lett.* **2019**, *19*, 3199–3206.
- [95] H. Li, Q. Yang, F. Mo, G. Liang, Z. Liu, Z. Tang, L. Ma, J. Liu, Z. Shi, C. Zhi, *Energy Storage Mater.* **2019**, *19*, 94–101.
- [96] J. Xie, J. Zhang, S. Li, F. Grote, X. Zhang, H. Zhang, R. Wang, Y. Lei, B. Pan, Y. Xie, *J. Am. Chem. Soc.* **2013**, *135*, 17881–17888.
- [97] T. Jiao, Q. Yang, S. Wu, Z. Wang, D. Chen, D. Shen, B. Liu, J. Cheng, H. Li, L. Ma, C. Zhi, W. Zhang, *J. Mater. Chem. A* **2019**, *7*, 16330–16338.
- [98] H. Qin, Z. Yang, L. Chen, X. Chen, L. Wang, *J. Mater. Chem. A* **2018**, *6*, 23757–23765.
- [99] T. Xiong, Y. Wang, B. Yin, W. Shi, W. S. V. Lee, J. Xue, *Nano-Micro Lett.* **2019**, *12*, 8.
- [100] L. Zhang, Q. Wei, D. Sun, N. Li, H. Ju, J. Feng, J. Zhu, L. Mai, E. J. Cairns, J. Guo, *Nano Energy* **2018**, *51*, 391–399.
- [101] C. D. Wessells, S. V. Peddada, R. A. Huggins, Y. Cui, *Nano Lett.* **2011**, *11*, 5421–5425.
- [102] A. A. Karyakin, *Electroanalysis* **2001**, *13*, 813–819.
- [103] Q. Zhang, Z. Wang, S. Zhang, T. Zhou, J. Mao, Z. Guo, *Electrochem. Energy Rev.* **2018**, *1*, 625–658.
- [104] C. D. Wessells, S. V. Peddada, M. T. McDowell, R. A. Huggins, Y. Cui, *J. Electrochem. Soc.* **2011**, *159*, A98–A103.
- [105] M. Pasta, C. D. Wessells, R. A. Huggins, Y. Cui, *Nat. Commun.* **2012**, *3*, 1149.
- [106] F. Herran, P. Fischer, A. Ludi, W. Haelg, *Inorg. Chem.* **1980**, *19*, 956–959.
- [107] H. Lee, Y.-I. Kim, J.-K. Park, J. W. Choi, *Chem. Commun.* **2012**, *48*, 8416–8418.
- [108] P. Novák, R. Imhof, O. Haas, *Electrochim. Acta* **1999**, *45*, 351–367.
- [109] Y. Moritomo, K. Igarashi, J. Kim, H. Tanaka, *Appl. Phys. Express* **2009**, *2*, 085001.
- [110] L. Zhang, L. Chen, X. Zhou, Z. Liu, *Adv. Energy Mater.* **2015**, *5*, 1400930.
- [111] Z. Jia, B. Wang, Y. Wang, *Mater. Chem. Phys.* **2015**, *149*–*150*, 601–606.
- [112] M. S. Chae, S.-T. Hong, *Batteries* **2019**, *5*, 3.
- [113] B. Wang, M. Cui, Y. Gao, F. Jiang, W. Du, F. Gao, L. Kang, C. Zhi, H. Luo, *Solar RRL* **2020**, *4*, 1900425.
- [114] H. Li, C. J. Firby, A. Y. Elezzabi, *Joule* **2019**, *3*, 2268–2278.
- [115] H. Li, L. McRae, C. J. Firby, A. Y. Elezzabi, *Adv. Mater.* **2019**, *31*, 1807065.
- [116] W. Zhang, H. Li, M. Al-Hussein, A. Y. Elezzabi, *Adv. Opt. Mater.* **2019**, *8*, 1901224.
- [117] Y. X. Huang, M. Xie, J. T. Zhang, Z. H. Wang, Y. Jiang, G. H. Xiao, S. J. Li, L. Li, F. Wu, R. J. Chen, *Nano Energy* **2017**, *39*, 273–283.
- [118] L. Ma, S. Chen, C. Long, X. Li, Y. Zhao, Z. Liu, Z. Huang, B. Dong, J. A. Zapien, C. Zhi, *Adv. Energy Mater.* **2019**, *9*, 1902446.
- [119] W. Li, K. Wang, S. Cheng, K. Jiang, *Energy Storage Mater.* **2018**, *15*, 14–21.
- [120] Z. Jian, C. Yuan, W. Han, X. Lu, L. Gu, X. Xi, Y.-S. Hu, H. Li, W. Chen, D. Chen, Y. Ikuhara, L. Chen, *Adv. Funct. Mater.* **2014**, *24*, 4265–4272.
- [121] Q. An, F. Xiong, Q. Wei, J. Sheng, L. He, D. Ma, Y. Yao, L. Mai, *Adv. Energy Mater.* **2015**, *5*, 1401963.
- [122] K. Saravanan, C. W. Mason, A. Rudola, K. H. Wong, P. Balaya, *Adv. Energy Mater.* **2013**, *3*, 444–450.
- [123] Y. Jiang, Z. Yang, W. Li, L. Zeng, F. Pan, M. Wang, X. Wei, G. Hu, L. Gu, Y. Yu, *Adv. Energy Mater.* **2015**, *5*, 1402104.
- [124] C. Masquelier, L. Croguennec, *Chem. Rev.* **2013**, *113*, 6552–6591.
- [125] G. Li, Z. Yang, Y. Jiang, W. Zhang, Y. Huang, *J. Power Sources* **2016**, *308*, 52–57.
- [126] P. Hu, T. Zhu, X. Wang, X. Zhou, X. Wei, X. Yao, W. Luo, C. Shi, K. A. Owusu, L. Zhou, L. Mai, *Nano Energy* **2019**, *58*, 492–498.
- [127] W. Song, Z. Wu, J. Chen, Q. Lan, Y. Zhu, Y. Yang, C. Pan, H. Hou, M. Jing, X. Ji, *Electrochim. Acta* **2014**, *146*, 142–150.
- [128] L. Ma, S. Chen, H. Li, Z. Ruan, Z. Tang, Z. Liu, Z. Wang, Y. Huang, Z. Pei, J. A. Zapien, C. Zhi, *Energy Environ. Sci.* **2018**, *11*, 2521–2530.
- [129] K. Takegami, N. Furuya, *Electrochim. Commun.* **2006**, *74*, 825–827.
- [130] H. Zhang, Q. Du, C. Li, X. Sun, *J. Electrochem. Soc.* **2012**, *159*, A2001–A2004.
- [131] N. Yesibolati, N. Umirov, A. Koishbay, M. Omarova, I. Kurmanbayeva, Y. Zhang, Y. Zhao, Z. Bakenov, *Electrochim. Acta* **2015**, *152*, 505–511.
- [132] F. Wang, O. Borodin, T. Gao, X. Fan, W. Sun, F. Han, A. Faraone, J. A. Dura, K. Xu, C. Wang, *Nat. Mater.* **2018**, *17*, 543–549.
- [133] J. Yan, J. Wang, H. Liu, Z. Bakenov, D. Gosselink, P. Chen, *J. Power Sources* **2012**, *216*, 222–226.
- [134] Y.-g. Wang, J.-y. Luo, C.-x. Wang, Y.-y. Xia, *J. Electrochem. Soc.* **2006**, *153*, A1425–A1431.
- [135] R. J. Gummow, A. de Kock, M. M. Thackeray, *Solid State Ionics* **1994**, *69*, 59–67.
- [136] X. Wu, M. Shao, C. Wu, J. Qian, Y. Cao, X. Ai, H. Yang, *ACS Appl. Mater. Interfaces* **2016**, *8*, 23706–23712.
- [137] H. Li, A. Y. Elezzabi, *Nanoscale Horiz.* **2020**, *5*, 691–695.
- [138] S. Zhang, S. Cao, T. Zhang, A. Fisher, J. Y. Lee, *Energy Environ. Sci.* **2018**, *11*, 2884–2892.
- [139] F. Wang, F. Yu, X. Wang, Z. Chang, L. Fu, Y. Zhu, Z. Wen, Y. Wu, W. Huang, *ACS Appl. Mater. Interfaces* **2016**, *8*, 9022–9029.
- [140] K. Parvez, Z.-S. Wu, R. Li, X. Liu, R. Graf, X. Feng, K. Müllen, *J. Am. Chem. Soc.* **2014**, *136*, 6083–6091.
- [141] L. Dong, X. Ma, Y. Li, L. Zhao, W. Liu, J. Cheng, C. Xu, B. Li, Q.-H. Yang, F. Kang, *Energy Storage Mater.* **2018**, *13*, 96–102.
- [142] H. Wang, M. Wang, Y. Tang, *Energy Storage Mater.* **2018**, *13*, 1–7.
- [143] S. Wu, Y. Chen, T. Jiao, J. Zhou, J. Cheng, B. Liu, S. Yang, K. Zhang, W. Zhang, *Adv. Energy Mater.* **2019**, *9*, 1902915.
- [144] X. Zhang, Z. Pei, C. Wang, Z. Yuan, L. Wei, Y. Pan, A. mAhmood, Q. Shao, Y. Chen, *Small* **2019**, *15*, 1903817.
- [145] H. Zhang, Q. Liu, Y. Fang, C. Teng, X. Liu, P. Fang, Y. Tong, X. Lu, *Adv. Mater.* **2019**, *31*, 1904948.
- [146] Y. Huang, J. Liu, J. Wang, M. Hu, F. Mo, G. Liang, C. Zhi, *Angew. Chem. Int. Ed.* **2018**, *57*, 9810–9813; *Angew. Chem.* **2018**, *130*, 9958–9961.
- [147] X. Zhao, W. Qiu, C. Ma, Y. Zhao, K. Wang, W. Zhang, L. Kang, J. Liu, *ACS Appl. Mater. Interfaces* **2018**, *10*, 2496–2503.
- [148] Y. Liu, X. Zhao, C. Fang, Z. Ye, Y.-B. He, D. Lei, J. Yang, Y. Zhang, Y. Li, Q. Liu, Y. Huang, R. Zeng, L. Kang, J. Liu, Y.-H. Huang, *Chem.* **2018**, *4*, 2463–2478.
- [149] Z. P. Song, H. S. Zhou, *Energy Environ. Sci.* **2013**, *6*, 2280–2301.
- [150] Q. Zhao, W. W. Huang, Z. Q. Luo, L. J. Liu, Y. Lu, Y. X. Li, L. Li, J. Y. Hu, H. Ma, J. Chen, *Sci. Adv.* **2018**, *4*, 10.
- [151] H. Alt, H. Binder, A. Köhling, G. Sandstede, *Electrochim. Acta* **1972**, *17*, 873–887.
- [152] K. X. Lin, Q. Chen, M. R. Gerhardt, L. C. Tong, S. B. Kim, L. Eisenach, A. W. Valle, D. Hardee, R. G. Gordon, M. J. Aziz, M. P. Marshak, *Science* **2015**, *349*, 1529–1532.
- [153] J. Steuber, G. Vohl, M. S. Casutt, T. Vorburger, K. Diederichs, G. Fritz, *Nature* **2014**, *516*, 62.
- [154] Y. Liang, Y. Jing, S. Gheytani, K.-Y. Lee, P. Liu, A. Facchetti, Y. Yao, *Nat. Mater.* **2017**, *16*, 841.
- [155] B. Yang, L. Hooper-Burkhardt, F. Wang, G. K. Surya Prakash, S. R. Narayanan, *J. Electrochem. Soc.* **2014**, *161*, A1371–A1380.
- [156] T. B. Schon, B. T. McAllister, P.-F. Li, D. S. Seferos, *Chem. Soc. Rev.* **2016**, *45*, 6345–6404.
- [157] S. Er, C. Suh, M. P. Marshak, A. Aspuru-Guzik, *Chem. Sci.* **2015**, *6*, 885–893.
- [158] S. Bai, X. Liu, K. Zhu, S. Wu, H. Zhou, *Nat. Energy* **2016**, *1*, 16094.

- [159] T. Zhao, Y. Ye, X. Peng, G. Divitini, H.-K. Kim, C.-Y. Lao, P. R. Coxon, K. Xi, Y. Liu, C. Ducati, R. Chen, R. V. Kumar, *Adv. Funct. Mater.* **2016**, *26*, 8418–8426.
- [160] Z. Guo, Y. Ma, X. Dong, J. Huang, Y. Wang, Y. Xia, *Angew. Chem. Int. Ed.* **2018**, *57*, 11737–11741; *Angew. Chem.* **2018**, *130*, 11911–11915.
- [161] Z. Tie, L. Liu, S. Deng, D. Zhao, Z. Niu, *Angew. Chem. Int. Ed.* **2020**, *59*, 4920–4924.
- [162] D. Lin, Y. Liu, Y. Cui, *Nat. Nanotechnol.* **2017**, *12*, 194–206.
- [163] Y. Zhao, L. V. Goncharova, A. Lushington, Q. Sun, H. Yadegari, B. Wang, W. Xiao, R. Li, X. Sun, *Adv. Mater.* **2017**, *29*, 1606663.
- [164] X.-B. Cheng, T.-Z. Hou, R. Zhang, H.-J. Peng, C.-Z. Zhao, J.-Q. Huang, Q. Zhang, *Adv. Mater.* **2016**, *28*, 2888–2895.
- [165] X.-B. Cheng, R. Zhang, C.-Z. Zhao, Q. Zhang, *Chem. Rev.* **2017**, *117*, 10403–10473.
- [166] X.-Q. Zhang, X. Chen, X.-B. Cheng, B.-Q. Li, X. Shen, C. Yan, J.-Q. Huang, Q. Zhang, *Angew. Chem. Int. Ed.* **2018**, *57*, 5301–5305; *Angew. Chem.* **2018**, *130*, 5399–5403.
- [167] K. N. Wood, E. Kazyak, A. F. Chadwick, K.-H. Chen, J.-G. Zhang, K. Thornton, N. P. Dasgupta, *ACS Cent. Sci.* **2016**, *2*, 790–801.
- [168] K. Wang, Y. Xiao, P. Pei, X. Liu, Y. Wang, *J. Electrochem. Soc.* **2019**, *166*, D389–D394.
- [169] J. W. Diggle, A. R. Despic, J. O. M. Bockris, *J. Electrochem. Soc.* **1969**, *116*, 1503–1514.
- [170] Q. Yang, G. Liang, Y. Guo, Z. Liu, B. Yan, D. Wang, Z. Huang, X. Li, J. Fan, C. Zhi, *Adv. Mater.* **2019**, *31*, 1903778.
- [171] Z. Wang, J. Huang, Z. Guo, X. Dong, Y. Liu, Y. Wang, Y. Xia, *Joule* **2019**, *3*, 1289–1300.
- [172] M. A. González, R. Trócoli, I. Pavlovic, C. Barriga, F. La Mantia, *Electrochim. Commun.* **2016**, *68*, 1–4.
- [173] Z. Cai, Y. Ou, J. Wang, R. Xiao, L. Fu, Z. Yuan, R. Zhan, Y. Sun, *Energy Storage Mater.* **2020**, *27*, 205–211.
- [174] W. Li, K. Wang, S. Cheng, K. Jiang, *Adv. Energy Mater.* **2019**, *9*, 1900993.
- [175] M. S. Chae, J. W. Heo, S.-C. Lim, S.-T. Hong, *Inorg. Chem.* **2016**, *55*, 3294–3301.
- [176] M. Cui, Y. Xiao, L. Kang, W. Du, Y. Gao, X. Sun, Y. Zhou, X. Li, H. Li, F. Jiang, C. Zhi, *ACS Appl. Energy Mater.* **2019**, *2*, 6490–6496.
- [177] W. Lu, C. Xie, H. Zhang, X. Li, *ChemSusChem* **2018**, *11*, 3996–4006.
- [178] H. Li, C. Xu, C. Han, Y. Chen, C. Wei, B. Li, F. Kang, *J. Electrochem. Soc.* **2015**, *162*, A1439–A1444.
- [179] J. Zheng, Q. Zhao, T. Tang, J. Yin, C. D. Quilty, G. D. Renderos, X. Liu, Y. Deng, L. Wang, D. C. Bock, C. Jaye, D. Zhang, E. S. Takeuchi, K. J. Takeuchi, A. C. Marschilok, L. A. Archer, *Science* **2019**, *366*, 645–648.
- [180] W. Xu, K. Zhao, W. Huo, Y. Wang, G. Yao, X. Gu, H. Cheng, L. Mai, C. Hu, X. Wang, *Nano Energy* **2019**, *62*, 275–281.
- [181] J. Q. Huang, X. W. Chi, Q. Han, Y. Z. Liu, Y. X. Du, J. H. Yang, Y. Liu, *J. Electrochem. Soc.* **2019**, *166*, A1211–A1216.
- [182] L.-P. Wang, N.-W. Li, T.-S. Wang, Y.-X. Yin, Y.-G. Guo, C.-R. Wang, *Electrochim. Acta* **2017**, *244*, 172–177.
- [183] M. Li, J. Meng, Q. Li, M. Huang, X. Liu, K. A. Owusu, Z. Liu, L. Mai, *Adv. Funct. Mater.* **2018**, *28*, 1802016.
- [184] C. Li, X. Xie, S. Liang, J. Zhou, *Energy Environ. Sci.* **2020**, *10*.1002/eem1002.12067.
- [185] Q. Zhang, J. Luan, Y. Tang, X. Ji, H.-Y. Wang, *Angew. Chem. Int. Ed.* **2020**, *10*.1002/anie.202000162.
- [186] H. Wei, X. Hu, X. Zhang, Z. Yu, T. Zhou, Y. Liu, Y. Liu, Y. Wang, J. Xie, L. Sun, M. Liang, P. Jiang, *Energy Technol.* **2019**, *7*, 1800912.
- [187] X. Xie, S. Liang, J. Gao, S. Guo, J. Guo, C. Wang, G. Xu, X. Wu, G. Chen, J. Zhou, *Energy Environ. Sci.* **2020**, *13*, 503–510.
- [188] C. Deng, X. Xie, J. Han, Y. Tang, J. Gao, C. Liu, X. Shi, J. Zhou, S. Liang, *Adv. Funct. Mater.* **2020**, *2000599*.
- [189] P. Liang, J. Yi, X. Liu, K. Wu, Z. Wang, J. Cui, Y. Liu, Y. Wang, Y. Xia, J. Zhang, *Adv. Funct. Mater.* **2020**, *19098528*.
- [190] Z. Zhao, J. Zhao, Z. Hu, J. Li, J. Li, Y. Zhang, C. Wang, G. Cui, *Energy Environ. Sci.* **2019**, *12*, 1938–1949.
- [191] Y. Zeng, X. Zhang, R. Qin, X. Liu, P. Fang, D. Zheng, Y. Tong, X. Lu, *Adv. Mater.* **2019**, *31*, 1903675.
- [192] D. Chao, C. Zhu, M. Song, P. Liang, X. Zhang, N. H. Tiep, H. Zhao, J. Wang, R. Wang, H. Zhang, H. J. Fan, *Adv. Mater.* **2018**, *30*, 1803181.
- [193] Y. Yin, S. Wang, Q. Zhang, Y. Song, N. Chang, Y. Pan, H. Zhang, X. Li, *Adv. Mater.* **2020**, *32*, 1906803.
- [194] X. Q. Sun, P. Bonnick, L. F. Nazar, *ACS Energy Lett.* **2016**, *1*, 297–301.
- [195] Y. Cheng, L. Luo, L. Zhong, J. Chen, B. Li, W. Wang, S. X. Mao, C. Wang, V. L. Sprenkle, G. Li, J. Liu, *ACS Appl. Mater. Interfaces* **2016**, *8*, 13673–13677.
- [196] E. Levi, G. Gershinsky, D. Aurbach, O. Isnard, G. Ceder, *Chem. Mater.* **2009**, *21*, 1390–1399.
- [197] W. Kaveevivitchai, A. Manthiram, *J. Mater. Chem. A* **2016**, *4*, 18737–18741.
- [198] H. Li, Z. Tang, Z. Liu, C. Zhi, *Joule* **2019**, *3*, 613–619.
- [199] T. Shoji, T. Yamamoto, *Inorg. Chim. Acta* **1987**, *129*, L21–L22.
- [200] T. Shoji, T. Yamamoto, *J. Electroanal. Chem.* **1993**, *362*, 153–157.
- [201] W. P. Hagan, R. J. Latham, R. G. Linford, S. L. Vickers, *Solid State Ionics* **1994**, *70*–*71*, 666–669.
- [202] L. Suo, O. Borodin, T. Gao, M. Olguin, J. Ho, X. Fan, C. Luo, C. Wang, K. Xu, *Science* **2015**, *350*, 938–943.
- [203] L. Wang, Y. Zhang, H. Hu, H.-Y. Shi, Y. Song, D. Guo, X.-X. Liu, X. Sun, *ACS Appl. Mater. Interfaces* **2019**, *11*, 42000–42005.
- [204] J. Zhao, J. Zhang, W. Yang, B. Chen, Z. Zhao, H. Qiu, S. Dong, X. Zhou, G. Cui, L. Chen, *Nano Energy* **2019**, *57*, 625–634.
- [205] F. Ding, W. Xu, G. L. Graff, J. Zhang, M. L. Sushko, X. Chen, Y. Shao, M. H. Engelhard, Z. Nie, J. Xiao, X. Liu, P. V. Sushko, J. Liu, J.-G. Zhang, *J. Am. Chem. Soc.* **2013**, *135*, 4450–4456.
- [206] F. Wan, L. Zhang, X. Dai, X. Wang, Z. Niu, J. Chen, *Nat. Commun.* **2018**, *9*, 1656.
- [207] C. Yang, Z. J. Zhang, Z. L. Tian, K. Zhang, J. Li, Y. Q. Lai, *J. Electrochem. Soc.* **2018**, *165*, A86–A88.
- [208] T. Otani, Y. Fukunaka, T. Homma, *Electrochim. Acta* **2017**, *242*, 364–372.
- [209] K. E. K. Sun, T. K. A. Hoang, T. N. L. Doan, Y. Yu, P. Chen, *Chem. Eur. J.* **2018**, *24*, 1667–1673.
- [210] A. Mitha, A. Z. Yazdi, M. Ahmed, P. Chen, *ChemElectroChem* **2018**, *5*, 2409–2418.
- [211] Q. Wang, C. Yang, Y. Zhang, J. Yang, K. Wu, C. Hu, J. Lu, W. Liu, H. Zhou, *ACS Appl. Energy Mater.* **2019**, *2*, 4602–4608.
- [212] D. S. Baik, D. J. Fray, *J. Appl. Electrochem.* **2001**, *31*, 1141–1147.
- [213] K. M. Abraham, J. L. Goldman, D. L. Natwig, *J. Electrochem. Soc.* **1982**, *129*, 2404–2409.
- [214] B. G. Miller, T. W. Traut, Wolfenden, *J. Am. Chem. Soc.* **1998**, *120*, 2666–2667.
- [215] Q. Li, W. Ge, P. Yang, J. Zhang, M. An, *J. Electrochem. Soc.* **2016**, *163*, D127–D132.
- [216] Q. Zhang, J. Luan, L. Fu, S. Wu, Y. Tang, X. Ji, H.-Y. Wang, *Angew. Chem. Int. Ed.* **2019**, *131*, 15988–15994.
- [217] B. Li, Z. Nie, M. Vijayakumar, G. Li, J. Liu, V. Sprenkle, W. Wang, *Nat. Commun.* **2015**, *6*, 6303.
- [218] Z. Liu, T. Cui, G. Pulletikurthi, A. Lahiri, T. Carstens, M. Olschewski, F. Endres, *Angew. Chem. Int. Ed.* **2016**, *55*, 2889–2893; *Angew. Chem.* **2016**, *128*, 2939–2943.
- [219] Q. Zhang, K. De Oliveira Vigier, S. Royer, F. Jérôme, *Chem. Soc. Rev.* **2012**, *41*, 7108–7146.
- [220] D. Shah, F. S. Mjalli, *Phys. Chem. Chem. Phys.* **2014**, *16*, 23900–23907.
- [221] C. Zhang, J. Holoubek, X. Wu, A. Daniyar, L. Zhu, C. Chen, D. P. Leonard, I. A. Rodríguez-Pérez, J.-X. Jiang, C. Fang, X. Ji, *Chem. Commun.* **2018**, *54*, 14097–14099.
- [222] J. J. Hong, L. Zhu, C. Chen, L. Tang, H. Jiang, B. Jin, T. C. Gallagher, Q. Guo, C. Fang, X. Ji, *Angew. Chem. Int. Ed.* **2019**, *58*, 15910–15915.
- [223] F. Wang, W. Sun, Z. Shadike, E. Hu, X. Ji, T. Gao, X.-Q. Yang, K. Xu, C. Wang, *Angew. Chem. Int. Ed.* **2018**, *57*, 11978–11981; *Angew. Chem.* **2018**, *130*, 12154–12157.
- [224] H. Li, L. Ma, C. Han, Z. Wang, Z. Liu, Z. Tang, C. Zhi, *Nano Energy* **2019**, *62*, 550–587.
- [225] K. Wu, J. Huang, J. Yi, X. Liu, Y. Liu, Y. Wang, J. Zhang, Y. Xia, *Adv. Energy Mater.* **2020**, *10*, 1903977.
- [226] J. Liu, M. Hu, J. Wang, N. Nie, Y. Wang, Y. Wang, J. Zhang, Y. Huang, *Nano Energy* **2019**, *58*, 338–346.
- [227] Z. Liu, D. Wang, Z. Tang, G. Liang, Q. Yang, H. Li, L. Ma, F. Mo, C. Zhi, *Energy Storage Mater.* **2019**, *23*, 636–645.
- [228] F. Mo, G. Liang, Q. Meng, Z. Liu, H. Li, J. Fan, C. Zhi, *Energy Environ. Sci.* **2019**, *12*, 706–715.
- [229] Z. Pei, Z. Yuan, C. Wang, S. Zhao, J. Fei, L. Wei, J. Chen, C. Wang, R. Qi, Z. Liu, Y. Chen, *Angew. Chem. Int. Ed.* **2020**, *59*, 4793–4799.
- [230] H. Li, C. Han, Y. Huang, Y. Huang, M. Zhu, Z. Pei, Q. Xue, Z. Wang, Z. Liu, Z. Tang, Y. Wang, F. Kang, B. Li, C. Zhi, *Energy Environ. Sci.* **2018**, *11*, 941–951.
- [231] Z. Liu, F. Mo, H. Li, M. Zhu, Z. Wang, G. Liang, C. Zhi, *Small Methods* **2018**, *2*, 1800124.
- [232] Y. Cui, Q. Zhao, X. Wu, Z. Wang, R. Qin, Y. Wang, M. Liu, Y. Song, G. Qian, Z. Song, L. Yang, F. Pan, *Energy Storage Mater.* **2020**, *27*, 1–8.

- [233] Q. Han, X. Chi, S. Zhang, Y. Liu, B. Zhou, J. Yang, Y. Liu, *J. Mater. Chem. A*. **2018**, *6*, 23046–23054.
- [234] Y. Tang, C. Liu, H. Zhu, X. Xie, J. Gao, C. Deng, M. Han, S. Liang, J. Zhou, *Energy Storage Mater.* **2020**, *27*, 109–116.
- [235] X. Y. Li, H.-G. Wang, Z. Tian, J. -H. Zhu, Y. Liu, L. Jia, D.-J. You, X.-M. Li, L.-T. Kang, *J. Inorg. Mater.* **2020**, *10.15541/jim20190473*.
- [236] S. Ghorai, A. Sarkar, M. Raoufi, A. B. Panda, H. Schönherr, S. Pal, *ACS Appl. Mater. Interfaces*. **2014**, *6*, 4766–4777.
- [237] D. Wang, H. Li, Z. Liu, Z. Tang, G. Liang, F. Mo, Q. Yang, L. Ma, C. Zhi, *Small*. **2018**, *14*, 1803978.
- [238] M. Watanabe, M. Kanba, K. Nagaoka, I. Shinohara, *J. Appl. Polym. Sci.* **1982**, *27*, 4191–4198.
- [239] S. Ikeda, Y. Mori, Y. Furuhashi, H. Masuda, O. Yamamoto, *J. Power Sources*. **1999**, *81–82*, 720–723.
- [240] Q. Han, X. Chi, Y. Liu, L. Wang, Y. Du, Y. Ren, Y. Liu, *J. Mater. Chem. A*. **2019**, *7*, 22287–22295.
- [241] C. H. Yang, M. X. Wang, H. Haider, J. H. Yang, J.-Y. Sun, Y. M. Chen, J. Zhou, Z. Suo, *ACS Appl. Mater. Interfaces*. **2013**, *5*, 10418–10422.
- [242] Y. Lu, T. Zhu, N. Xu, K. Huang, *ACS Appl. Energy Mater.* **2019**, *2*, 6904–6910.
- [243] S. Zhang, N. Yu, S. Zeng, S. Zhou, M. Chen, J. Di, Q. Li, *J. Mater. Chem. A*. **2018**, *6*, 12237–12243.
- [244] T. K. A. Hoang, T. N. L. Doan, C. Lu, M. Ghaznavi, H. Zhao, P. Chen, *ACS Sustainable Chem. Eng.* **2016**, *5*, 1804–1811.
- [245] D. P. Dubal, N. R. Chodankar, D.-H. Kim, P. Gomez-Romero, *Chem. Soc. Rev.* **2018**, *47*, 2065–2129.
- [246] Y. Zeng, X. Zhang, Y. Meng, M. Yu, J. Yi, Y. Wu, X. Lu, Y. Tong, *Adv. Mater.* **2017**, *29*, 1700274.
- [247] J. Liu, C. Guan, C. Zhou, Z. Fan, Q. Ke, G. Zhang, C. Liu, J. Wang, *Adv. Mater.* **2016**, *28*, 8732–8739.
- [248] L. Ma, S. Chen, Z. Pei, H. Li, Z. Wang, Z. Liu, Z. Tang, J. A. Zapien, C. Zhi, *ACS Nano*. **2018**, *12*, 8597–8605.
- [249] H. Li, Z. Liu, G. Liang, Y. Huang, Y. Huang, M. Zhu, Z. Pei, Q. Xue, Z. Tang, Y. Wang, B. Li, C. Zhi, *ACS Nano*. **2018**, *12*, 3140–3148.
- [250] Y. Huang, Z. Li, Z. Pei, Z. Liu, H. Li, M. Zhu, J. Fan, Q. Dai, M. Zhang, L. Dai, C. Zhi, *Adv. Energy Mater.* **2018**, *8*, 1802288.
- [251] K. N. Dinh, Z. Pei, Z. Yuan, V. C. Hoang, L. Wei, Q. Huang, X. Liao, C. Liu, Y. Chen, Q. Yan, *J. Mater. Chem. A*. **2020**, *8*, 7297–7308.
- [252] Z. Pei, Y. Huang, Z. Tang, L. Ma, Z. Liu, Q. Xue, Z. Wang, H. Li, Y. Chen, C. Zhi, *Energy Storage Mater.* **2019**, *20*, 234–242.
- [253] Z. Kang, C. Wu, L. Dong, W. Liu, J. Mou, J. Zhang, Z. Chang, B. Jiang, G. Wang, F. Kang, C. Xu, *ACS Sustainable Chem. Eng.* **2019**, *7*, 3364–3371.
- [254] H. Qiu, X. Du, J. Zhao, Y. Wang, J. Ju, Z. Chen, Z. Hu, D. Yan, X. Zhou, G. Cui, *Nat. Commun.* **2019**, *10*, 5374.
- [255] Y. Cheng, H. Zhang, Q. Lai, X. Li, D. Shi, L. Zhang, *J. Power Sources*. **2013**, *241*, 196–202.
- [256] L. Ma, S. Chen, N. Li, Z. Liu, Z. Tang, J. A. Zapien, S. Chen, J. Fan, C. Zhi, *Adv. Mater.* **2020**, *32*, 1908121.
- [257] H. Zhang, J. Wang, Q. Liu, W. He, Z. Lai, X. Zhang, M. Yu, Y. Tong, X. Lu, *Energy Storage Mater.* **2018**, *21*, 154–161.
- [258] C. Wang, W. Lu, Q. Lai, P. Xu, H. Zhang, X. Li, *Adv. Mater.* **2019**, *31*, 1904690.
- [259] X. Yu, Y. Fu, X. Cai, H. Kafafy, H. Wu, M. Peng, S. Hou, Z. Lv, S. Ye, D. Zou, *Nano Energy*. **2013**, *2*, 1242–1248.
- [260] L. P. Wang, N. W. Li, T. S. Wang, Y. X. Yin, Y. G. Guo, C. R. Wang, *Electrochim. Acta*. **2017**, *244*, 172–177.
- [261] H. R. Jiang, M. C. Wu, Y. X. Ren, W. Shyy, T. S. Zhao, *Appl. Energy*. **2018**, *213*, 366–374.
- [262] Q. Yun, Y.-B. He, W. Lv, Y. Zhao, B. Li, F. Kang, Q.-H. Yang, *Adv. Mater.* **2016**, *28*, 6932–6939.
- [263] C.-P. Yang, Y.-X. Yin, S.-F. Zhang, N.-W. Li, Y.-G. Guo, *Nat. Commun.* **2015**, *6*, 8058.
- [264] X. Shi, G. Xu, S. Liang, C. Li, S. Guo, X. Xie, X. Ma, J. Zhou, *ACS Sustainable Chem. Eng.* **2019**, *7*, 17737–17746.
- [265] C. Li, X. Shi, S. Liang, X. Ma, M. Han, X. Wu, J. Zhou, *Chem. Eng. J.* **2020**, *379*, 122248.
- [266] Z. Yan, E. Wang, L. Jiang, G. Sun, *RSC Adv.* **2015**, *5*, 83781–83787.
- [267] Z. Liu, Y. Huang, Y. Huang, Q. Yang, X. Li, Z. Huang, C. Zhi, *Chem. Soc. Rev.* **2020**, *49*, 180–232.
- [268] G. Liang, F. Mo, Q. Yang, Z. Huang, X. Li, D. Wang, Z. Liu, H. Li, Q. Zhang, C. Zhi, *Adv. Mater.* **2019**, *31*, 1905873.
- [269] Q. Zhu, M. Cheng, B. Zhang, K. Jin, S. Chen, Z. Ren, Y. Yu, *Adv. Funct. Mater.* **2019**, *29*, 1905979.
- [270] G. J. May, A. Davidson, B. Monahov, *J. Energy Storage*. **2018**, *15*, 145–157.
- [271] C. Niu, H. Pan, W. Xu, J. Xiao, J.-G. Zhang, L. Luo, C. Wang, D. Mei, J. Meng, X. Wang, Z. Liu, L. Mai, J. Liu, *Nat. Nanotechnol.* **2019**.
- [272] R. Zhang, X.-R. Chen, X. Chen, X.-B. Cheng, X.-Q. Zhang, C. Yan, Q. Zhang, *Angew. Chem. Int. Ed.* **2017**, *56*, 7764–7768; *Angew. Chem.* **2017**, *129*, 5653–5656.
- [273] N. Li, K. Zhang, K. Xie, W. Wei, Y. Gao, M. Bai, Y. Gao, Q. Hou, C. Shen, Z. Xia, B. Wei, *Adv. Mater.* **2020**, *32*, 1907079.
- [274] J. Wang, L. Zhang, L. Yu, Z. Jiao, H. Xie, X. W. Lou, X. Wei Sun, *Nat. Commun.* **2014**, *5*, 4921.
- [275] H. Lee, M. Yanilmaz, O. Toprakci, K. Fu, X. Zhang, *Energy Environ. Sci.* **2014**, *7*, 3857–3886.
- [276] X. Huang, *J. Solid State Electrochem.* **2011**, *15*, 649–662.
- [277] N. Yun, J. J. Park, O. O. Park, K. B. Lee, J. H. Yang, *Electrochim. Acta*. **2018**, *278*, 226–235.
- [278] C. Xie, Y. Liu, W. Lu, H. Zhang, X. Li, *Energy Environ. Sci.* **2019**.
- [279] C. Xie, H. Zhang, W. Xu, W. Wang, X. Li, *Angew. Chem. Int. Ed.* **2018**, *57*, 11171–11176; *Angew. Chem.* **2018**, *130*, 11341–11346.
- [280] L. E. Blanc, D. Kundu, L. F. Nazar, *Joule*. **2020**, *4*, 771–799.
- [281] W. Zhang, S. Liang, G. Fang, Y. Yang, J. Zhou, *Nano-Micro Lett.* **2019**, *11*, 69.

Manuscript received: March 19, 2020

Revised manuscript received: May 17, 2020

Accepted manuscript online: June 1, 2020

Version of record online: July 7, 2020